THESIS

MEASUREMENTS OF THE MOTIONS OF ATOMS: FLOW VELOCITIES AND DIFFUSION CONSTANTS

Submitted by

John V. Prodan

Department of Physics

In partial fulfillment of the requirements

for the Degree of Doctor of Philosophy of Science

Colorado State University

Fort Collins, Colorado

Fall 1981

COLORADO STATE UNIVERSITY

November , 1981

WE HEREBY RECOMMEND THAT THE THESIS PREPARED UNDER OUR SUPERVISION BY JOHN V. PRODAN ENTITLED MEASUREMENTS OF THE MOTIONS OF ATOMS: FLOW VELOCITIES AND DIFFUSION CONSTANTS BE ACCEPTED AS FULFILLING IN PART REQUIREMENTS FOR THE DEGREE OF DOCTOR OF PHILOSOPHY OF SCIENCE.

Committee on Graduate Work

George Collins

Edward-yan Byre

J. C. Raich

William M. Fairbank, Jr.

Adviser

ABSTRACT OF THESIS

MEASUREMENTS OF THE MOTIONS OF ATOMS:
FLOW VELOCITIES AND DIFFUSION CONSTANTS

Using Fluorescence Correlation Spectroscopy (FCS), the motion of atoms have been measured in real time. Single sodium atoms have been detected with this method and their flow velocity crudely measured. By averaging over many atoms, very clear signals were obtained and velocities up to 85 m/sec were measured. These velocities were determined by measuring the transit time of atoms across two resonantly tuned laser beams.

Diffusion constants, D, of sodium in helium, neon and argon buffer gases were also measured using FCS. The products, Dp, where p is the pressure of the buffer gas, for these three cases were determined to be 427 ± 7 Torr cm^2/sec, 277 ± 10 Torr cm^2/sec and 200 ± 9 Torr cm^2/sec, respectively. These numbers were obtained from measuring the average duration of the fluorescence burst from individual sodium atoms diffusing through the laser beam. Also measured was the diffusion constant for the excited sodium atom ($^2P_{3/2}$) in a helium buffer gas at 200 Torr pressure, with a result of 598 ± 84 Torr cm^2/sec.

John V. Prodan
Physics Department
Colorado State University
Fort Collins, Colorado 80523
Fall 1981

DEDICATION

To experimentalists everywhere

"Everything that exists exists in some degree,
and if it exists in some degree it ought to be
measured"

- Mathematicians' Bill of Rights

ACKNOWLEDGMENTS

I wish to thank my adviser, Dr. William M. Fairbank, Jr., for his patience, suggestions and many informative discussions throughout the course of this project. I would also like to express my sincere appreciation to his wife, Donna, for her friendship, understanding and encouragement. I am indebted to Dr. Chiao-Yao She, my co-adviser, (in all but formal title!) for his much appreciated help. Ci-Ling Pan, my initial mentor for this project, also helped me considerably while I worked with him in the initial stages of this experiment.

I am grateful for the extensive help I received from James Buckley on the somewhat unusual machining requirements involved in this project. I thank Louis Hlousek, my office mate for four years, and Greg Herring for the many helpful discussions and ideas which aided me in completing this work. I also appreciate the help that Richard Kelley gave me in developing a program to allow microprocessor control of the experiment.

To my good friends and my folks, I am indebted for the encouragement received during the "dismal" hours involved in the preparation of this thesis. I also thank Tawana Maynard and Leona Woeber for typing this manuscript so quickly.

Last, but certainly not least, I acknowledge Johnny Hart, Brant Parker, Bill Rechin, Mort Walker, Jim Davis, Tom Ryan, Charles Schulz, Don Martin and Sergio Aragones, whose wits and talents have allowed me to keep a reasonable perspective on life, even through graduate school!

This work was funded by NASA.

TABLE OF CONTENTS

LIST OF FIGURES

List of Figures (continued)

LIST OF TABLES

I. INTRODUCTION

The availability of tunable dye lasers in recent years has led to the development of several highly sensitive spectroscopic techniques. These spectroscopic techniques have, in turn, provided the means by which very small concentrations of substances can be detected. Fairbank[1] et al, in 1974, were able to detect a concentration of sodium atoms of only 100 atoms/cc, an improvement of six orders of magnitude over previous measurements, by detecting the fluorescence from atoms in a resonantly tuned laser. In the past few years, several groups have reported schemes for the detection of single atomic events.[2-7] These methods all use the same first step. The laser is tuned to an atomic transition, to resonantly pump the atom to a particular excited state. Two of these methods, those of Hurst[2] and Bekov,[3] selectively ionize the atom from that state and detect the newly created electron or ion. These two schemes differ somewhat in the way the atom is ionized. In Hurst's method, the atom is directly photoionized with the same pulsed laser. Bekov, however, uses a different laser to excite that atom to highly excited stationary state just below the ionization limit. The ionization is then accomplished with a pulsed electric field. The other methods, that have been successfully used, monitor the fluorescence from the atom. Gelbwachs[4] et al, monitored fluorescence from sodium atoms at the $D_2(^2S_{1/2} - {}^2P_{3/2})$ line, while

exciting the atom with a laser tuned to the $D_1(^2S_{1/2} - {}^2P_{1/2})$ line. Their experiment was done in a high pressure (1 atm) environment and the $^2P_{3/2}$ level was populated by background atoms/molecules collisionally exciting the $^2P_{1/2}$ atoms. Balykin[6] et al, excited sodium atoms at the D_1 line and monitored the fluorescence with two photomultipliers. Coincidence between the signals from the two detectors was used to discriminate against background light. The method used by Greenlees[5] et al, was to look for bursts of photons as the atom traveled through a resonantly tuned laser. In their experiment, the conditions were such that on the average about 1 photon count per atom would be detected but because of the statistical nature of the processes involved, there was a significant probability that an atom would yield several detected photons. Thus looking for bursts of 3 to 6, they were able to effectively discriminate against the background which has a much lower average count. In these last two methods, those of Balykin and Greenlees, fluorescence was monitored at the frequency of the exciting laser. This type of method has an inherent difficulty in that the noise is also the same frequency as the signal, thus sophisticated detection schemes are necessary. The main advantage of this method, though, is that the signal that one can obtain from an atom is theoretically unlimited. As long as this "two-level" atom is in the laser, it is absorbing and spontaneously emitting photons.

The capability of detecting single atomic events opens up some interesting possibilities, including the direct measurement of an atom's motion. The object of our experiments was to measure this motion, due to either an imposed one-dimensional flow or due to

two-dimensional diffusion. Such measurements would lead to an experimental determination of flow speeds or diffusion constants, respectively. The method used to accomplish these measurements involves monitoring the spontaneous fluorescence from atoms traversing a resonantly tuned laser beam and determining the temporal distribution of the fluorescence emission. Similar to Greenlees' experiment, this technique uses the fact that the desired signal will occur only during the time the atom is residing in the laser beam, that is, the signal is bunched. However, unlike Greenlees, we wished to measure how this burst was distributed in time. This technique is called Fluorescence Correlation Spectroscopy (FCS).[9,10] The form of the temporal distribution of the burst depends on the type of motion being studied and will be derived in the next chapter.

We became interested in measuring the velocity of a single atom with the idea that if such a technique could be developed with enough sensitivity, direct measurement of the thermal velocity of a single atom would be possible. Such a measurement would be of fundamental interest in physics. Two other applications of such a tool might include the ability to measure high speed flows (e.g., in wind tunnels) or perhaps even flows occurring in turbulent boundary layers.[8] The advantages of developing a laser velocimetry technique to accomplish these last two tasks would include the following. First, as in other laser velocimeters (devices that use lasers to measure speeds) this method does not disturb the flow itself. Secondly, a small movable volume of space can be probed. Third, unlike standard laser velocimeters, this technique would measure the actual speed of the flow. The standard laser velocimeters rely on scattering from particles, which

can lag the actual flow in high speed conditions, whereas atoms make the flow.

In the experiments designed to measure flows, the sodium atoms were carried along in a flowing gas as tracers. During the initial experiments, with flows on the order of 1 m/sec or less, it was discovered that diffusive motion could also be measured using FCS. This type of motion is caused by random collisions with the surrounding gas atoms or molecules. Indeed, if the flow velocity is too slow, the diffusional motion will dominate and little or no information concerning the one-dimensional flow can be realized. It then became necessary to characterize this motion in order to determine the conditions under which the one-dimensional flow would dominate. The parameter that characterizes this random motion is the diffusion constant for the system being studied. Transport coefficients, like the diffusion constant, are important quantities in their own right and hence the scope of the research was broadened to include a study of diffusion.

These transport coefficients provide information concerning some of the details of the interactions that are occurring. In particular, from the diffusion constant for a binary mixture, it is possible to gain insight into the interaction potential between the two species. There were two types of diffusion constants that were measured. One describing the interaction of the buffer gas with the ground state of the sodium atoms, and the other describing the interaction of the buffer gas with the excited state ($^2P_{3/2}$) of the sodium atom. One would expect that the interactions of the sodium atom with the buffer gas would depend on the particular state that the sodium atom was in,

and therefore the diffusion constants for the two systems should be different.

Sodium was chosen as the tracer atom for the flow measurements. The basic reason is that, since the atom can be thought of as a two level system, there is no limit to its fluorescence yield.[8] The wavelength of this transition (D_2) is 5889.96 Å, which was within the range of our tunable dye laser/pump laser system, to be described later.

To measure the velocity of the atoms, two laser geometries were employed. First, a two-beam system was used (called Laser Time of Flight or LTV[16]), where the atom was moving in the plane that contained both lasers, perpendicular to those beams. The atom would spontaneously fluoresce as it went through each beam, giving two bursts of photons. Since the time between these bursts is equal to the distance between the beams divided by the atom's velocity, if the physical separation of the beams is known and the time can be measured, the velocity can be determined. A one beam system was also used to measure the atom's velocity. The velocity of the atom and the intensity distribution of the laser beam will determine the temporal distribution of the burst of photons. Therefore, analysis of the emitted photon distribution along with information about the beam will allow the velocity to be calculated. Since diffusion is random, undirected motion, only one laser beam need be used. Analysis of the temporal distribution of signals generated by this process, averaged over many atoms, gives the information needed to calculate the diffusion constant.

The organization of this thesis is as follows. Chapter II presents the basic theory needed to describe the processes being studied. It includes the spectroscopic relations necessary to determine the signal generated by the atoms. Also, the auto-correlation functions which describe the temporal distributions of the bursts of emitted fluorescence photons for a flowing atom or a diffusing atom will be derived. Chapter III contains a description of the experimental set-up and also describes the method used to collect the data. The analysis of the data is found in Chapter IV. Finally, a summary of results and possible further work needed will be presented in Chapter V.

II. THEORY

The basic relationships necessary to understand our experiment are developed in this chapter. First the rate equations describing the interaction of the atom with the laser beam are presented. These relations are needed in order to determine the amount signal that can be expected from a single atom. Next, the autocorrelation function which describes the temporal evolution of this signal is derived. The general form of this function will contain the contributions from both types of motion that were studied. Knowledge of this relationship is required because it contains the information needed to calculate either the velocity of the atom or the diffusion constant of the system. The particular form that describes the individual process will be distilled from the general function. Finally a short discussion of the formula for the diffusion constant as derived from kinetic theory will be given. Results of our experiments will be compared with those values predicted by this formula, which is applicable to sodium atoms in either the excited state or the ground state.

Section II-1. Evaluation of the Fluorescence Emission

The signal that a single atom can produce can be calculated by solving the rate equations for the atomic system being studied, taking into account the motion of that atom as well as the spatial distribution

of the exciting radiation. First the rate equations for a two level atom will be presented. From these, the rate of spontaneous emission as a function of the exciting intensity will be found. The corresponding rate for a three level system and a four level system will also be presented. The effect of the spatial distribution of the exciting intensity as well as the motion of the atom will then be considered.

II-1.1. Rate Equations. Consider the rate equations describing a two level system. An example of such a system is the $3^2S_{1/2}(F = 2)$ to $3^2P_{3/2}(F = 3)$ transition in atomic sodium (see Fig. II-1). If the sodium atom is in the F = 2 hyperfine level of the $3^2S_{1/2}$ ground state and a laser is tuned such that the F = 3 level of the $3^2P_{3/2}$ state is excited, the dipole selection rule $\Delta F = \pm 1,0$ indicates that the $3^2P_{3/2}(F = 3)$ state will decay back to the $3^2S_{1/2}(F = 2)$ state ($\Delta F = -1$ for this transition). Since the laser is already tuned to this particular transition, the atom can be excited once again. As long as the atom can be pumped to the $3^2P_{3/2}(F = 3)$ state, this cycle of absorption and re-emission can be continued indefinitely. The rate equations which describe time dependence of the population of these states are as follows:

$$\frac{dn_1}{dt} = A_{21}n_2 - w_{12}n_2 + w_{21}n_1 \qquad (1)$$

$$\frac{dn_2}{dt} = -A_{21}n_1 + w_{12}n_2 - w_{21}n_1 \qquad (2)$$

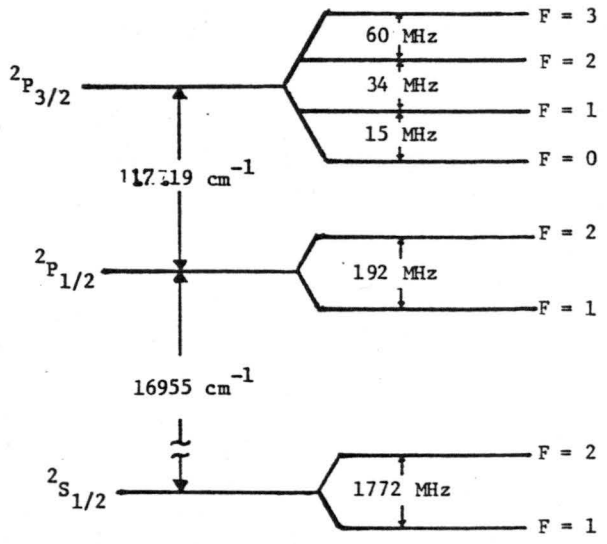

Fig. II-1. Partial energy level diagram for sodium.

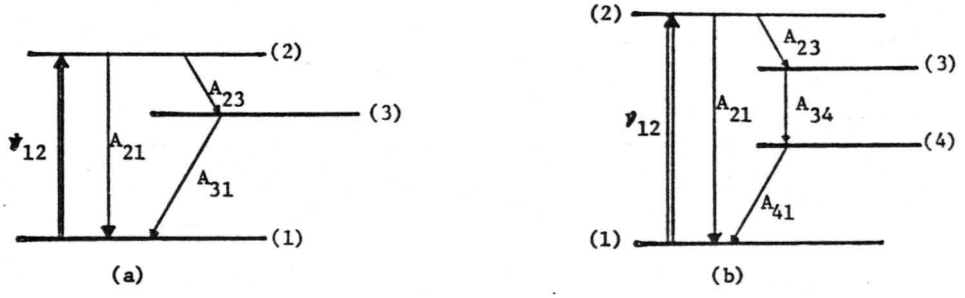

Fig. II-2(a). Three level atom system.
(b). Four level atom system.

where n_1 and n_2 are the number densities of the sodium atoms in level 1 and level 2 respectively, A_{21} is the spontaneous emission rate (the Einstein A coefficient), and w_{12} and w_{21} are the (stimulated) absorption rate and stimulated emission rate respectively. For a two level system for which level 2 has a degeneracy of g_2 and level 1 has a degeneracy of g_1, the stimulated rates are related by

$$\frac{w_{12}}{w_{21}} = \frac{g_2}{g_1} \quad . \tag{3}$$

With the further restriction that

$$n_1+n_2 = N \tag{4}$$

where N, the total density of atoms, is a constant, one can solve Eqs. (1) and (2). The result is

$$n_1 = N \frac{w_{21}+A_{21}}{A_{21}+(1+g_2/g_1)w_{21}} \tag{5}$$

$$n_2 = N(g_2/g_1) \frac{w_{21}}{A_{21}+(1+g_2/g_1)w_{21}} \quad . \tag{6}$$

The spontaneous emission rate (A_{21}) and the stimulated emission rate (w_{21}) are related by the following expression,

$$w_{21} = \frac{A_{21}c^2 Ig(\nu)}{8\pi h\nu^3 n^2} \quad , \tag{7}$$

where c/n is the speed of light in the surrounding medium, I is the

intensity of the exciting radiation, $g(\nu)$ is the normalized Lorentzian linewidth of the atomic transition, and ν is the frequency of that transition. Substitution of (7) into (6) and making the further designation of

$$I_s = \frac{8\pi hcn^2}{(1+g_2/g_1)\lambda^3 g(\nu)} \tag{8}$$

one obtains, for the population of level 2

$$n_2 = \frac{Ng_2}{g_1+g_2}\left(\frac{I}{I_s}\right)\left(1 + \frac{I}{I_s}\right)^{-1} \quad . \tag{9}$$

The meaning of I_s can now be seen; it is just the value of the intensity at which n_2 is one-half its maximum allowable value of $Ng_2/(g_1+g_2)$. The parameter I_s is called the saturation intensity at the particular frequency.

The total rate of spontaneous emission is, from Eqs. (2) and (9),

$$R \equiv n_2 A_{21} V = NV \frac{A_{21} g_2}{g_1+g_2}\left(\frac{I}{I_s}\right)\left(1 + \frac{I}{I_s}\right)^{-1} \quad , \tag{10}$$

where V is the volume under consideration. Defining a quantity R_s such that

$$R_s = \frac{A_{21} g_2}{g_1+g_2} \tag{11}$$

one can rewrite Eq. (10) as

$$R = NV\, R_s \left(\frac{I}{I_s}\right)\left(1 + \frac{I}{I_s}\right)^{-1} \quad . \qquad (12)$$

R_s is the maximum (saturated) rate of spontaneous emission per atom. To find the rate of spontaneous scattering of resonant photons for a single atom, one merely sets the total number of atoms (NV) equal to 1 in Eq. (12). For the vacuum case and using the sodium D_2 transition (the $F = 2 \rightarrow F = 3$ hyperfine component) $R_s = 3.6 \times 10^7$/sec and $I_s = 15.9$ mW/cm^2. For our experiments, we were normally operating at a background pressure of 200 Torr of helium. At this pressure, $\Delta\nu_L$ (the Lorenztian linewidth $\propto$ 3.4 GHz) and the degeneracies g_1 and g_2 are 8 and 16 respectively. Substituting these values into Eqs. (8) and (11) with $A_{21} = (1.62 \times 10^{-8}$ sec$)^{-1}$, one obtains $R_s = 4.1 \times 10^7$ sec^{-1} and $I_s = 6.5$ W/cm^2. For the values of g_1 and g_2 given above to be valid, one must assume that the pressure is sufficiently high to broaden the transition enough so that the hyperfine levels within each state, ($^2S_{1/2}$) and ($^2P_{3/2}$), are degenerate.

For a three level atomic system, as in Figure II-2(a), one can still use Eq. (12), with appropriate modifications to the quantities R_s and I_s where needed. Two types of these systems are worth considering. First one can consider the case where 3 is a metastable level (an example of this type of system is barium[8]). If a branching ratio of η (the ratio of the $2 \rightarrow 3$ transition probability to the $2 \rightarrow 1$ transition probability) is assumed, then the maximum number of emitted photons is given by $(1 - \eta)/\eta$ (for barium, $\eta = .04$, therefore $(1 - \eta)/\eta = 24$). The atom is then essentially in the metastable state and hence no longer in resonance with the laser. An example of a second

type of three level system would be to excite the D_1 transition in sodium, allow it to collisionally excite to the $^2P_{3/2}$ state and monitor the fluorescence at the D_2 frequency. A fast monochromator or a suitable narrow band optical filter could then be used to eliminate the stray light noise at the laser frequency. This technique was used by Gelbwachs[4] et al and has been given the name Saturated Optical Nonresonant Emission Spectroscopy (SONRES). In general, for a three level system, in which the $3 \rightarrow 1$ transition rate is monitored, R_s and I_s are given by

$$R_s = \frac{g_2 A_{31} \tau_{31}}{g_2 \tau_{31} + \tau_{23}(g_1+g_2)} \quad , \tag{13}$$

$$I_s = \frac{4\pi h\nu^3 n^2}{A_{21} g(\nu) c^2} \left(\frac{1}{\tau_{31}+\tau_{23}} + \frac{A_{21}}{\tau_{31}} \right) \frac{1}{\frac{1}{\tau_{23}} \frac{g_2}{g_1} + \frac{1}{\tau_{31}} \left(1 + \frac{g_2}{g_1} \right)} \tag{14}$$

where τ_{nm} is the lifetime of the state n with respect to the state m, including radiative and nonradiative terms. For the sodium case $\frac{1}{\tau_{23}} \simeq \frac{1}{\tau_c}$, the state changing collision rate and $\tau_{31} \simeq \frac{1}{A_{31}}$. Substituting these results into Eq. (14) one finds

$$R_s = \frac{g_2 A_{31}}{g_2 + A_{31} \tau_c (g_1+g_2)} \quad . \tag{15}$$

For a four level system such as shown in Figure II-2(b) and monitoring transition $4 \rightarrow 1$, the formulae for I_s and R_s are[8]

$$R_s = \frac{A_{23} g_2}{g_1 + g_2(1+\alpha_3+\alpha_4)} \tag{16}$$

$$I_s = \frac{8\pi hc}{\left[1 + \left(\frac{g_2}{g_1}\right)(1+\alpha_3+\alpha_4)\right]\lambda^3 g(\nu)\tau_2 A_{21}} \qquad (17)$$

The quantity A_{23} is the total transition rate to all of the states in 3, τ_2 is the lifetime of state 2, and the factor $\alpha_3 + \alpha_4$ takes into account the population buildup in the intermediate levels 3 and 4.

II-1.2. Calculation of the Number of Photons Emitted By One Atom Moving At A Constant Velocity. In the previous section, the rate at which the atom can resonantly scatter photons for a given, constant laser intensity has been calculated. The next step is to determine the number of photons which are scattered as a single atom passes through a real laser beam. For this calculation the knowledge of the intensity profile of the laser exciting the transition as well as the motion of the atom is necessary.

Let the direction of motion of the atom be defined as along the x axis which passes through the center of the laser beam. If the laser beam has a TEM_{oo} gaussian spatial intensity profile with the center of the beam at x = 0, then the intensity, as a function of x, can be written as

$$I(x) = I_o EXP[-2x^2/w^2] \quad . \qquad (18)$$

I_o is the intensity at the center of the beam and w is called the beam radius or waist and is the distance at which the intensity is down to $1/e^2$ of its peak intensity. Furthermore, if the atom is moving

perpendicular to the laser beam with a velocity v(x = vt), then the atom will see a time varying intensity distribution as it travels through the laser beam. This distribution will have the form

$$I(t) = I_o EXP[-2v^2t^2/w^2] \tag{19}$$

obtained by substituting x = vt into Eq. (18). The rate at which the atom will spontaneously scatter the photons (for a two level atom) is given by Eq. (12) (with NV = 1), with an incident intensity, I, given in Eq. (18). Therefore, for a moving atom the spontaneous fluorescence rate is also a function of time. By integrating the fluorescence rate over time, one obtains the total number of resonantly scattered photons by the atom as

$$F(o) = \int_{-\infty}^{\infty} R(t)dt \quad . \tag{20}$$

Substituting the time dependent intensity [Eq. (19)] into the formula for R [Eq. (12) with NV = 1] one finds[8]

$$F(o) = R_s \frac{w}{\sqrt{2}\,v} \sqrt{\frac{I_o}{I_s}}\; f\left(\frac{I_o}{I_s}\right) \quad . \tag{21}$$

[An error was made in the printing of this relation in reference (8) when the velocity, v, was included under the square root sign. The notation used here, that is F(o), is referring to the fact that the atom is assumed to go through the center of the beam.] The quantity $f(I_o/I_s)$ is a slowly varying function of I_o/I_s and is of the following form

$$f(x) = \sqrt{x} \int_{-\infty}^{\infty} [EXP(u^2) + x]^{-1} du \quad . \qquad (22)$$

This function is graphed in Figure II-3 and is tabulated in Appendix C. Equation (21) can be rewritten as

$$F(o) = R_s \frac{w_s}{\sqrt{2}\, v} \; f\left(\frac{I_o}{I_s}\right) \qquad (23)$$

where

$$w_s = w\left(\frac{I_o}{I_s}\right)^{1/2} = \left(\frac{2P_o}{\pi I_s}\right)^{1/2} \qquad (24)$$

and is called the saturation waist, that is the beam waist that produces an intensity of I_s at the center of the beam for a given laser power P_o. Assuming that the power remains a constant, one finds that F(o) has a maximum when w is adjusted to give the ratio of the intensities a value of 1.91 (see Figure II-3). This fact is somewhat obscured when F(o) is written in the form (21), but becomes clear when F(o) is written as in (23). At 200 Torr background pressure, a beam waist of 300 μm, an intensity ratio of 1.91 and a velocity of 20 m/sec, F(o) is equal to 668 photons. This is the fluorescence signal above any background present that must be detected. With an overall detection efficiency of 2% the signal detected is only 13 photons. Note that the preceding calculation assumes that that atom travels through the center of the beam, as evidenced by the notation F(o). This assumption is generally not valid, however, and a modification to

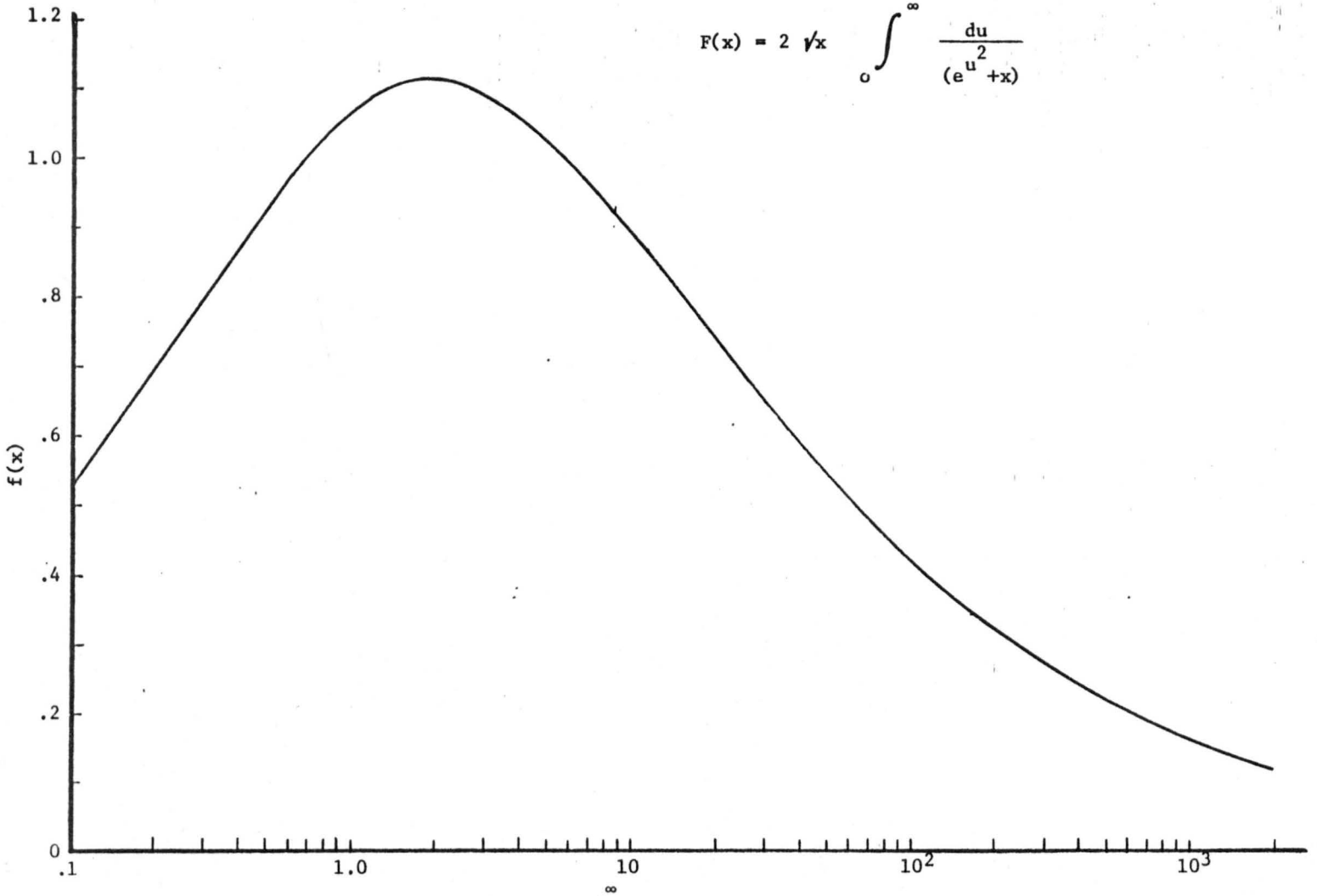

Fig. II-3. Graph of $2\sqrt{x}\int_0^\infty \frac{du}{e^{u^2}+x}$ vs. x

relations (19) and (21) [or (23)] must be made to account for atoms which don't pass through the center of the beam.

Consider a cartesian coordinate system in which there is an atom moving, as before with a speed v in the x direction toward a laser beam. Let the beam be propagating along and centered on the z axis. The two-dimensional intensity distribution of the laser beam perpendicular to its direction of propagation is, for a circular TEM_{oo} mode

$$I(x,y) = I_o EXP\left[\frac{-2(x^2+y^2)}{w^2}\right] . \qquad (25)$$

If at its closest approach to the origin, the atom is a distance y away, then the intensity that the atom would see would be I(o,y) in the notation of Eq. (25). Again making the substitution x = vt, the time varying intensity seen by the atom would then be

$$I(t,y) = I_o EXP\left(\frac{-2v^2t^2}{w^2}\right) EXP\left(\frac{-2y^2}{w^2}\right) , \qquad (26)$$

or letting $I_o EXP[-2y^2/w^2]$ be equal to I', one obtains

$$I(t,y) = I' \; EXP\left(\frac{-2v^2t^2}{w^2}\right) . \qquad (27)$$

Since Eq. (27) is the same form as (19) with I_o being replaced by I' (I' is independent of t), Eq. (21) will also remain unchanged in form. Let F(y/w) be the expression (21) with the substitution of I' for I_o. The ratio of F(y/w)/F(o) versus y/w is plotted in Figure II-4.[12] One can see that if y is within .5 w of the

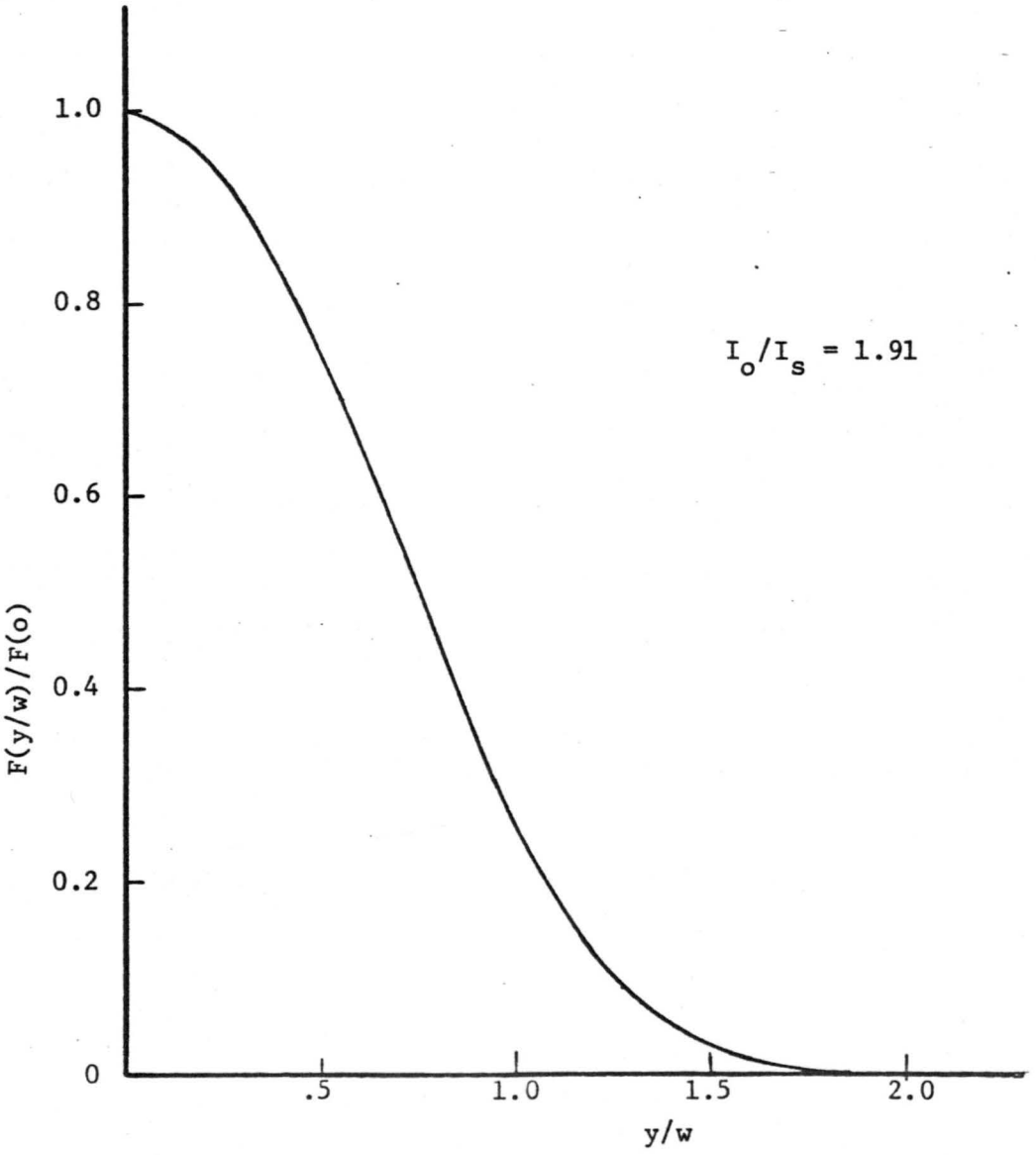

Fig. II-4. Graph of F(y/w)/F(o) vs. (y/w).

center, then one still obtains greater than 76% of the maximum possible number of scattered photons from an atom.

II-I.3. Determination of a Flux of Sodium Atoms From Their Total Fluorescence Rate. When trying to measure the velocity of a single atom, it is necessary to be able to determine the flux of atoms crossing the viewing volume. This is needed in order that the flux may be adjusted to insure that, during the observation time, there is a high probability of seeing, at most, one atom. Consider sodium atoms moving along and centered on the x axis of the coordinate system used above. Each atom passing through the laser beam will emit F(y/w) photons, y being the distance of closest approach, as before. The number of photons detected by our detection system is also a function of the emitting atom's position. Let this function be $\varepsilon\eta_o n(y,z)$, where ε is the quantum efficiency of our detector and $\eta_o n(y,z)$ is the efficiency of our optical collector [n(y,z) is a normalized function carrying the spatial dependence, with a value of 1 at (y,z) = (0,0)]. The number of detected photons, F_d, from a fluorescing atom is then

$$F_d = F\left(\frac{y}{w}\right)\varepsilon\eta_o n(y,z) \quad . \tag{28}$$

Let the total rate of detected fluorescence from a constant flux (ϕ) of atoms be T_r then

$$T_r = \int\int F_d \phi dydz = \iint \varepsilon\eta_o \phi F\left(\frac{y}{w}\right) n(y,z)dydz \tag{29}$$

or

$$\frac{T_r}{\varepsilon\eta_o}\left[\iint F\,\frac{y}{w}\,n(y,z)\,dydz\right]^{-1} = \phi \quad . \qquad (30)$$

The function n(y,z) will be discussed in detail in Chapter III and the double integral will then be approximated. The integral in (29) gives the fluorescence rate due to k atoms moving through the viewing volume per unit time, where k and ϕ are related by

$$k = \iint \phi n(y,z)\,dydz = A\phi \qquad (31)$$

and A is the double integral over n(y,z). The quantity A essentially defines the observable area for an averaged atom crossing the laser beam. Combining (30) and (31), one obtains

$$k = \frac{AT_r}{\varepsilon\eta_o}\left[\iint F\,\frac{y}{w}\,n(y,z)\,dydz\right]^{-1} \quad . \qquad (32)$$

Multiplying k by the observing time will give the total number of atoms that were present, on the average, in the viewing volume during that time. For single atom measurements this number should be less than one. This calculation will be returned to in Chapter III.

II-1.4. Calculation of the Expected Number of Photons Emitted By An Atom Diffusing Through a Laser Beam. For an atom moving in a high pressure environment, with a low flow speed, the trajectory of its motion is non-straight line. For a sufficiently slow speed, the atom's motion will be totally random. Under these conditions diffusion is

dominant and it is difficult to calculate the number of photons expected from this atom because of the random trajectory. In order to get an approximate answer, one possibility is to use Eq. (21), replacing the flow velocity, v, with an effective velocity, $v_{Eff} = w/\tau_D$. The parameter τ_D, represents the average time the atom takes to diffuse through a distance w (the laser beam waist) and is related to the diffusion constant, D, as shown below.

For an atom undergoing diffusion in two dimensions (diffusion along the laser beam will be shown to be insignificant later), the probability that in a time t, the position has changed a distance $r = (\sqrt{x^2+y^2})$ is

$$P(r,t\ |0,0) = \frac{1}{4\pi Dt}\ EXP\left[\frac{-r^2}{4Dt}\right] \qquad (33)$$

where D is the diffusion constant for the atom in the surrounding medium. For a laser beam propagating along the z axis, as before, the intensity distribution in the xy plane, for a TEM_{oo} gaussian beam is given by (25). The distance that the atom is from the center of the beam after a time t is $r(t) = [\sqrt{x^2(t) + y^2(t)}]$ or $r^2(t) = x^2(t) + y^2(t)$. Since Eq. (25) is a function of r^2, one needs to find the average value of r^2, $<r^2>$, as a function of time. To accomplish this, Eq. (33) must be multiplied by r^2 and integrated over the whole xy plane.

$$<r^2> = \frac{1}{4\pi Dt} \int_0^\infty r^2 EXP\left[\frac{-r^2}{(4Dt)}\right] 2\pi r dr = 4Dt \quad . \qquad (34)$$

We define a parameter τ_D, called the characteristic diffusion time, as the time at which the atom has traveled an average distance w, the laser beam waist, or from Eq. (34)

$$\tau_D = \frac{w^2}{4D} \quad . \tag{35a}$$

Therefore the effective velocity, from before, is

$$v_{eff} = \frac{w}{\tau_D} = \frac{4D}{w} \quad . \tag{35b}$$

The approximate number of photons can then be estimated from (21) with a velocity equal to v_{eff}. This result is[12]

$$F(o) = R_s \frac{w^2}{4\sqrt{2}D} \left(\frac{I_o}{I_s}\right)^{1/2} f\left(\frac{I_o}{I_s}\right) \tag{36a}$$

or using the definition of w_s, we get

$$F(o) = R_s \frac{w_s^2}{4\sqrt{2}D} \left(\frac{I_s}{I_o}\right)^{1/2} f\left(\frac{I_o}{I_s}\right) \quad . \tag{36b}$$

Even though Eq. (36) was derived from (21) and (23), Eq. (36) is a montonically decreasing function of $\frac{I_o}{I_s}$ for a constant power. Since diffusion is a random process, one would not expect an "optimum" value to exist.

An alternative method to estimate the number of photons a diffusing atom could emit would be to go back one step further than Eq. (21) and rewrite the time varying intensity that the atom sees using Eq. (34). Equation (19) then becomes

$$I(t) = I_o \text{ EXP}\left[\frac{-2\langle r^2\rangle}{w^2}\right] = I_o \text{ EXP}\left[\frac{-4Dt}{w^2}\right] \quad . \qquad (37)$$

Using expression (37) in the expression for the rate of spontaneous emission [Eq. (12) with NV = 1] and then integrating from the starting position, t = 0 (corresponding to the atom being at the center of the beam) to t = ∞, we get

$$F = R_s \frac{I_o}{I_s} \int_o^\infty \frac{\text{EXP}\left[-\frac{4D}{w^2} t\right]}{1 + \frac{I_o}{I_s} \text{EXP}\left[-\frac{4Dt}{w^2}\right]} dt$$

$$= R_s \frac{w^2}{4D} \ell n \left(1 + \frac{I_o}{I_s}\right) \quad . \qquad (38)$$

The basic motivation for the above formulation was to try to achieve a more reasonable derivation for estimating the number of photons emitted from a randomly moving atom. One of the basic premises used in the development of Eq. (21) was that the atom would see a particular time varying intensity distribution because of its rectilinear trajectory with the distance traveled being a linear function in time. Since the intensity distribution in space was a gaussian, these properties led to a gaussian (time-dependent) intensity profile as seen by the atom. However, for a diffusing atom, the trajectory is not a straight line and the average of square of the distance traveled is a linear function of time. Equation (37) is an attempt to take these two facts into account. The time varying intensity is linear in the time variable and hence is a pure exponentially decaying

intensity, which seems reasonable for a relaxation process like diffusion. Another item which lends credence to this type of intensity variation is that the atom will spend more time in the outer parts of the beam than the central region. From Eq. (35a), the average time the atom takes to travel a distance w is $\tau_D = \frac{w^2}{4D}$ and the average time to go a distance 2w is just $\tau(2w) = 4w^2/4D = W^2/D$. The difference between these two times is $3w^2/4D$. Therefore, the atom spends, on the average, three times as long in the region $2w > r > w$ than in the region $w > r > o$. Hence, even though the intensity of the beam is lower in the region $2w > r > w$, the increased time spent in this region partially compensates for this lower intensity.

If one substitutes the relation defining w_s [Eq. (24)] into Eq. (38), then the number of photons emitted becomes

$$F = R_s \frac{w_s^2}{4D} \left(\frac{I_s}{I_o}\right)^{1/2} \ell n \left(1 + \frac{I_o}{I_s}\right) \quad . \tag{39}$$

Like Eq. (36b), for a constant power, (39) is a monotonically decreasing function of $\frac{I_o}{I_s}$. This, again, is a quite reasonable result implying that no "optimization" is possible for the randomly moving atom. The two different intensity dependencies [Eqs. (36b) and (39)] are plotted in Fig. II-5, normalized to one at $\frac{I_o}{I_s} = 0$. As is evident from the graph, the variation of each distribution with respect to $\frac{I_o}{I_s}$ is quite similar. Also, even though both (36b) and (39) are both just approximations to the number of photons emitted by the atom, the derivation of the diffusion correlation function (below) will still be exact. This is because the random motions can be incorporated in the derivation of this function.

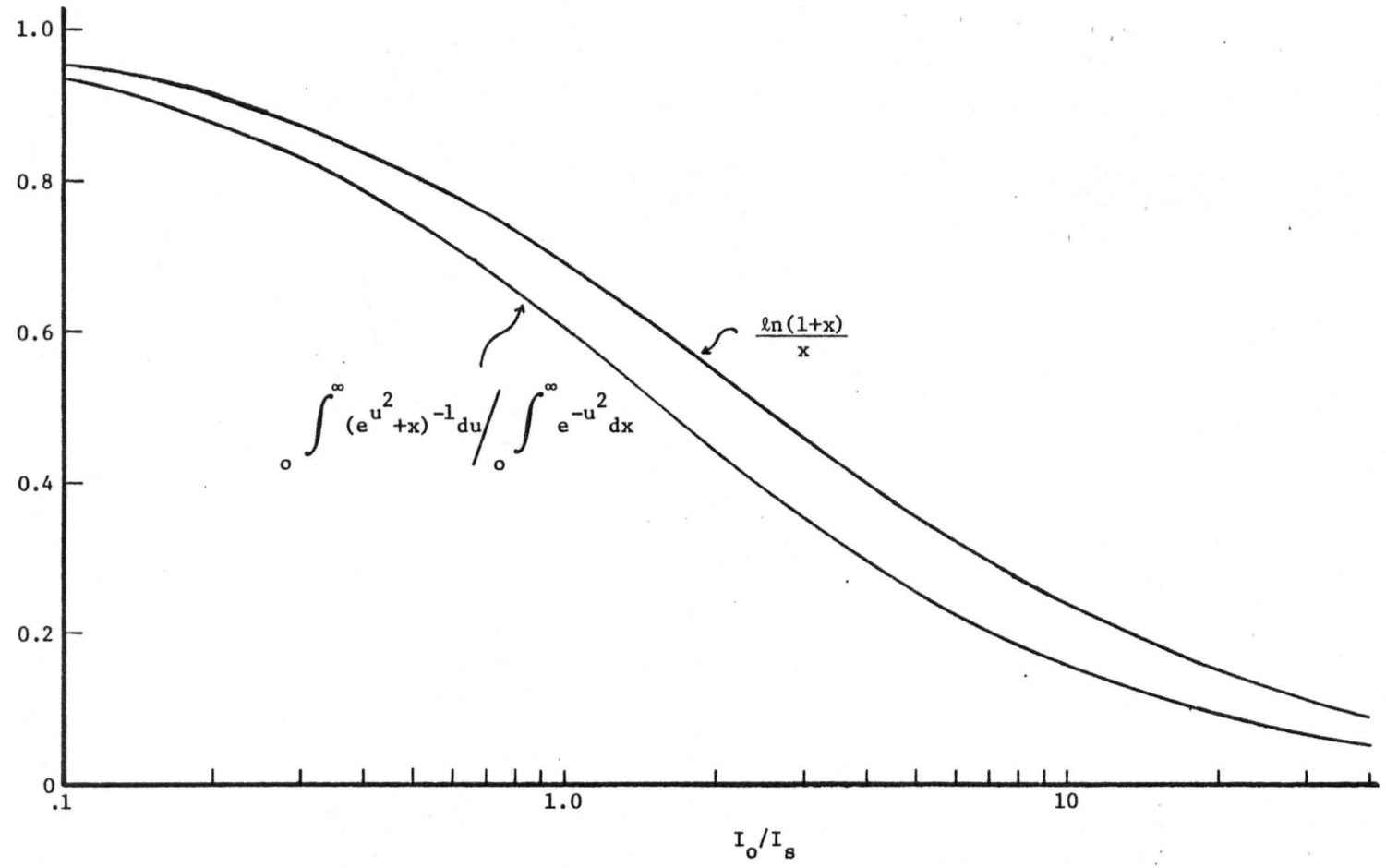
1.0
0.8
0.6
0.4
0.2
0
.1
1.0
10
I_o/I_s
$\frac{\ell n(1+x)}{x}$
$\int_o^\infty (e^{u^2}+x)^{-1}du \Big/ \int_o^\infty e^{-u^2}dx$

Fig. II-5.

II-2. Autocorrelation Functions

The signal that was generated by the atom, moving through the beam by diffusion or via an imposed constant flow, was processed by a real-time digital autocorrelator. In order to be able to use this processed signal, one must know the expected form for the autocorrelation function for this motion. Once the form of this function is known, then parameters such as the flow velocity and the diffusion constant can be determined from the observed correlation function. The next several sections deal with the derivation of the autocorrelation function.

II-2.1. Derivation of the Autocorrelation Function

The actual signal on which the autocorrelation function was generated was the observed count rate produced by the photon-counting section of our analyzing electronics (to be discussed in Chapter III). This count rate was proportional to the total rate of spontaneous emission, R(t), plus some randomly fluctuating background. The constant of proportionality was the total detection efficiency of our experimental set-up. The background contribution, since it was a random, uncorrelated function of time, only gave rise to an effective d.c. contribution to the count rate. On top of this d.c. level, was the burst contribution due to the atom. Therefore, the function needed is the autocorrelation function of the total rate of spontaneous emission, the bursts, as given by R(t) in Eq. (12).

By definition, the autocorrelation of R(t) for one atom is

$$C(\tau) = \langle R(t)R(t+\tau)\rangle = \lim_{T\to\infty} \frac{1}{T} \int_{-\frac{T}{2}}^{\frac{T}{2}} R(t)R(t+\tau)dt \quad . \qquad (40)$$

In order to calculate $C(\tau)$, it is convenient to first expand R(t) into a power series in the intensity ratio $\frac{I_o}{I_s}$. From Eq. (12), one can obtain, for one atom, the following

$$R(t) = R_s \frac{I(t)}{I_s}\left[1 - \frac{I(t)}{I_s} + \left(\frac{I(t)}{I_s}\right)^2 - \left(\frac{I(t)}{I_s}\right)^3 + \ldots\right]$$

$$= R_s \sum_{n=1}^{\infty} (-1)^{n-1}\left(\frac{I(t)}{I_s}\right)^n \quad . \qquad (41)$$

I(t) is the time varying intensity distribution as seen by the atom. The cartesian coordinate system to be used for the rest of this section is defined as follows: the z axis will be assumed colinear with the laser beam; if any imposed flow is considered, it will be one-dimensional and will be along the x axis; the origin of the xy plane will be at the center of the laser beam. The position of the atom at a time t is [x(t),y(t),z(t)]. Since the laser beam is colinear with the z axis, there will be no time dependence in I(t) corresponding to movement along this axis. Actually, for our uncollimated laser beam there is an intensity variation along its direction of propagation (about a 5% drop at ± 2 mm from the center), but it is insignificant compared to the intensity variation in the plane perpendicular to the propagation direction. The time dependent intensity as seen by the atom is then given by

$$I(t) = I_o EXP\{-2[(x(t)/w_x)^2 + (y(t)/w_y)^2]\} \quad , \qquad (42)$$

where w_x and w_y are the laser beam waists along the x and y directions, respectively. This added flexibility, of differing waists, is included to match the conditions under which the experiment was performed.

Consider an atom moving with a mean velocity v, in the x direction, superimposed on a random motion along the x, y and z directions. If the atom starts at a position $[x(t),y(t),z(t)]$ at a time t, then at a time, $t + \tau$, will be at a new position $[x(t+\tau),y(t+\tau),z(t+\tau)]$, where

$$x(t+\tau) = x(t) + \Delta x + v\tau \qquad (43a)$$

$$y(t+\tau) = y(t) + \Delta y \qquad (43b)$$

$$z(t+\tau) = z(t) + \Delta z \quad . \qquad (43c)$$

The quantities Δx, Δy and Δz are the random atomic position changes, in a time τ, due to diffusion, and $v\tau$ is the change in the atom's position due to the presence of the imposed flow. The probability that these diffusional changes occur in a time τ is given by the conditional probability

$$P(x+\Delta x,\ y+\Delta y,\ z+\Delta z,\ t+\tau \,|\, x,y,z,t)$$

$$= \left(\frac{1}{4\pi D\tau}\right)^{3/2} EXP[-(\Delta x^2+\Delta y^2+\Delta z^2)/4D\tau] \quad , \qquad (44)$$

where D is the diffusion constant for the system. Since Eq. (44) is

only a conditional probability, dependent on the fact that the position of the atom was (x,y,z) at the time t, one must determine the probability that the atom was at that position. For a uniformly seeded flowing gas, the density of resonant atoms is constant. In other words, the probability that atom will be at a position (x,y,z) at a time t is a constant depending on the density of atoms. Therefore

$$P(x,y,z,t)dxdydz = Ndxdydz \tag{45}$$

where N is the density of atoms. The correlation function, [Eq. (40)], can now be written as

$$C(\tau) = \lim_{T\to\infty} \frac{1}{T} \int_{-T/2}^{T/2} dt \int dx \int d(\Delta x) \int dy \int d(\Delta y) \int dz \int d(\Delta z)$$

$$E(t,\tau,x,y,z,\Delta x,\Delta y,\Delta z) \tag{46}$$

where

$$E = R(t)R(t+\tau)NP(x+\Delta x, y+\Delta y, z+\Delta z, t+\tau \,|\, x,y,z,t)$$

the spatial integrations over x, y and z are from -L/2 to L/2, where L/2 is a length large compared to w_x and w_y.

Using expression (41), the product $R(t)R(t+\tau)$ can be written in terms of increasing powers of $I(t)/I_s$. The result is

$$R(t)R(t+\tau) = R_s^2 \left[\sum_{n=1}^{\ell-1} (-1)^{n-1} \left(\frac{I(t)}{I_s} \right)^n \right] * \left[\sum_{m=1}^{\infty} (-1)^{m-1} \left(\frac{I(t+\tau)}{I_s} \right)^m \right] \quad . \tag{47}$$

Upon multiplication of the two sums, one finds that all of the terms are of the form

$$\frac{I^n(t) I^m(t+\tau)}{I_s^{n+m}} \quad .$$

Making the following definition,

$$\left\langle \frac{I^n(t) I^m(t+\tau)}{I_s^{n+m}} \right\rangle = \left(\frac{I_o}{I_s} \right)^{n+m} I_{nm} \tag{48}$$

then relation (46) reduces to

$$C(\tau) = N R_s^2 \sum_{\ell=2}^{\infty} \left(\frac{I_o}{I_s} \right)^{\ell} (-1)^{\ell} \sum_{n=1}^{\ell-1} I_{n,\ell-n} \tag{49}$$

where $\ell = n+m$. The generalized moment, I_{nm}, can be explicitly calculated, the integration limits on the integrals over $dx, d(\Delta x), dy, d\Delta y$ being allowed to go to $\pm \infty$ since L was large compared to w_x and w_y. The result of all the integrations being

$$I_{nm} = \frac{\pi w_x^2 w_y^2}{2(n+m)} \left\{ \left[w_x^2 + \frac{2nm}{n+m} 4D\tau \right] \left[w_y^2 + \frac{2nm}{n+m} 4D\tau \right] \right\}^{-1/2} * \text{EXP} \left\{ \frac{-2nmv^2\tau^2}{[2nm4D\tau + (n+m)w_x^2]} \right\} \left\{ L \text{ erf} [L/2\sqrt{4D\tau}\ ] \right\} \tag{50}$$

The last bracketed term in Eq. (50) represents the diffusional motion along the z axis. For a value of D of 2.2 cm^2/sec (experimtal value was 2.21 cm^2/sec, see Chapter IV) and L of 1 cm (typical laser beam waists were <400 μm, this term varies less than one part in 10^7 over four orders of magnitude in τ (ranging from .1 μs to 1 ms, typical for our experiments). Thus this last bracketed term will be treated as a constant in τ.

When the intensity ratio, I_o/I_s, is much less than 1, the first term in series (49) will dominate (ℓ=2,n=m=1). The correlation function is then

$$C(\tau) = R_s^2 N \left(\frac{I_o}{I_s}\right) \frac{2\pi w_x^2 w_y^2}{4} \left\{[w_x^2 + 4D\tau][w_y^2 + 4D\tau]\right\}^{-1/2} * \text{EXP}\left\{-v^2\tau^2/[4D\tau + w_x^2]\right\} \quad . \tag{51}$$

Equation (51) then describes the situation of an atom moving through the beam both by an imposed flow of velocity v and by diffusion.

In order to simplify the expressions in Eqs. (50) and (51) so that real experimental data can be analyzed, it is convenient to rewrite (50) and (51) to describe a single process, either one dimensional flow or diffusion. For a velocity dominant system, the time that the atom takes to cross the beam due to its one-dimensional velocity is much less than the characteristic diffusion time. This condition can be expressed as

$$\frac{2w}{v} << \frac{w^2}{4D} \quad . \tag{52a}$$

For a diffusion dominated system, the inequality in (52b) would be reversed,

$$\frac{w^2}{4D} << \frac{2w}{v} \quad . \tag{52b}$$

II-2.2. Correlation Function For A Velocity Dominated System. First, consider the case where the velocity is dominant, that is, the inequality in (52a) holds. For this system $4D\tau << w_x^2, w_y^2$ where τ is on the order of $2w_x/v$ (the atom's laser beam transit time due to the velocity, v.) The generalized moment, Eq. (50), reduces to

$$I_{nm} = \frac{\pi w_x^2 w_y^2}{2(n+m)} \; EXP\{-2nmv^2\tau^2/[(n+m)w_x^2]\} \tag{53}$$

and Eq. (51) becomes

$$C(\tau) = R_s^2 N \left(\frac{I_o}{I_s}\right)^2 \frac{\pi w_x^2 w_y^2}{4} \; EXP(-v^2\tau^2/w_x^2) \quad . \tag{54}$$

From Eq. (54), one can see that the correlation function describing the velocity dominant condition is a gaussian function in τ-space. The value of τ, call it τ_v (the width), such that $C(\tau_v)/C(o) = 1/e^2$ is given by

$$\tau_v = \frac{2\, w_x}{v} \quad , \tag{55}$$

or more importantly

$$v = \frac{2\, w_x}{\tau_v} \,. \qquad (56)$$

Therefore, since τ_v can be determined from the observed correlation function, the velocity of the atom can be determined.

When the intensity ratio, I_o/I_s, approaches 1, then many more terms in the expression (49) become significant. If the optimum intensity is used, that is $I_o/I_s = 1.91$ (as determined previously from Eq. (23) to attain the maximum signal from one atom for a fixed laser power), then the expansion derived for R(t) in Eq. (41) diverges and cannot be used to generate the correlation function. Instead, the form of R(t) given by (12) should be used in Eq. (40). Since the resulting integrals cannot all be carried out analytically, numerical integration techniques must be used.

Using (12) for R(t) and (19) for the time dependent intensity distribution for a velocity dominant system, the correlation function, as given by (40), was numerically evaluated for several values of I_o/I_s. The result for $I_o/I_s = 1.91$ is shown in Fig. II-6, and is labeled $C(\tau)$. We assumed, in our analysis, that the observed correlation would be of the form $C_1(\tau)$. Since the real correlation function (i.e., the observed function) should be of the form $C(\tau)$, a measurement of its width (using $C_1(\tau)$ as a model) would lead to an overestimation of the width to the $1/e^2$ point, as can be seen in Fig. II-6. An overestimation of the width of the correlation function will lead in turn to an underestimation of the velocity, since $v \propto 1/\tau_v$. The amount of underestimation depends primarily on the intensity ratio and will be discussed in the next chapter.

Fig. II-6. $C(\tau)$ and $C_1(\tau)$ vs. τ

$$C(\tau) = \int_{-\infty}^{\infty} \frac{(I_o/I_s)^2 EXP(-2x^2/w_y^2) EXP[-2(x+v\tau)^2/w_y^2]dx}{1+I_o/I_s\{EXP(-2x^2/w_x^2)+EXP[-2(x+v\tau)^2/w_x^2]\}+(I_o/I_s)^2 EXP(-2x^2/w_x^2) EXP[-2(x+D\tau)^2/w_x^2]}$$

$$C(\tau) \gtrsim EXP[-(v\tau/w_x)^2]$$

$I_o/I_s = 1.91$, $v = 30$ m/sec, $w_x = 300 \times 10^{-6}$ m

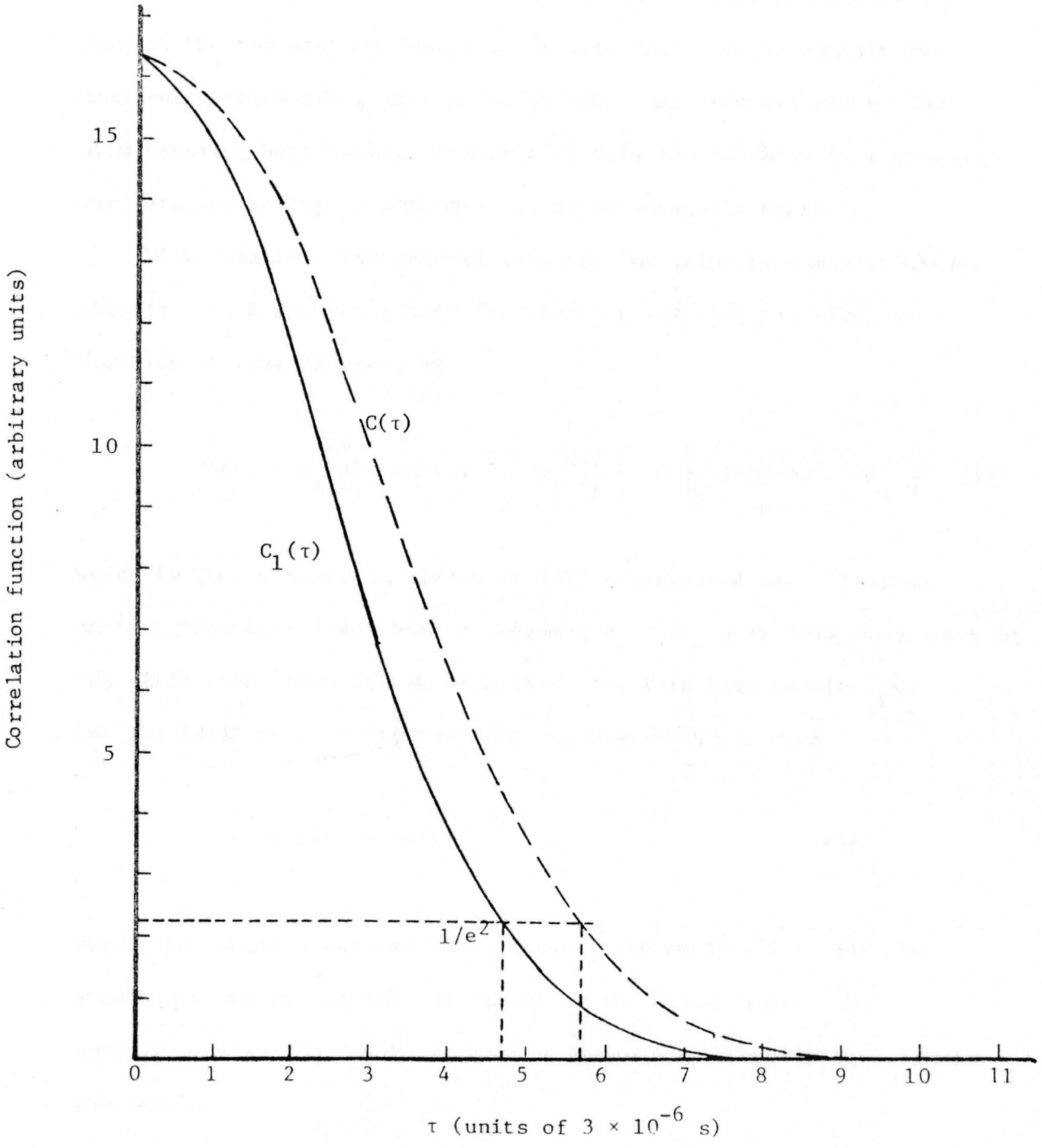
Correlation function (arbitrary units)
15
10
5
C(τ)
C1(τ)
1/e2
0
1
2
3
4
5
6
7
8
9
10
11
τ (units of 3 × 10-6 s)

II-2.3. Correlation Function For A Velocity Dominant System Using Two Laser Beams. The above generated correlation functions [(49) with (50) substituted in, (51) or (54)] were generated assuming a one beam geometry. We also want to consider the two beam system, on which velocity measurements were also made. We would expect the form of the correlation function, in this instance, to exhibit two maximums corresponding to the two bursts of photons emitted by the atom crossing both beams. Fortunately this can be shown in a general way, without having to evaluate the above integrals again.

If we consider the general case for the velocity dominant system, then for one beam, the atomic fluorescence rate for one atom, as a function of time is given by

$$R(t) = R_s\left(\frac{I_o}{I_s}\ \mathrm{EXP}[-2v^2t^2/w_x^2]\right)\left(1 + \frac{I_o}{I_s}\ \mathrm{EXP}[-2v^2t^2/w_x^2]\right)^{-1} \quad (57)$$

which is just expression (12) with (19) substituted in. If we set another identical laser beam a distance $d_o = vt_o$ away from the center of the first beam, then the emission rate for this beam is $R(t-t_o)$. Let the total rate of fluorescence emission be H(t), then

$$H(t) = R(t) + hR(t-t_o) \quad (58)$$

where the factor h can take into account the possibility that the atom might not go through the center of the second beam. The autocorrelation [Eq. (40)] is carried out on the function H(t), with the result

$$C(\tau) = \langle H(t)H(t+\tau)\rangle = \langle [R(t) + hR(t-t_o)][R(t+\tau) + hR(t-t_o+\tau)]\rangle \tag{59}$$

The products involved in (59) can be worked out term by term generating four different contributions to the correlation function. This can be written as

$$\begin{aligned} C(\tau) = {} & \langle R(t)R(t+\tau)\rangle + h^2\langle R(t-t_o)R(t-t_o+\tau)\rangle \\ & + h\langle R(t)R(t-t_o+\tau)\rangle \\ & + h\langle R(t+\tau)R(t-t_o)\rangle \quad . \end{aligned} \tag{60}$$

The difference of the arguments in the first two brackets are the same ($t+\tau-t = t-t_o+\tau-(t-t_o) = \tau$), therefore these terms are identical (except for h) since the autocorrelation function depends only on the difference of the arguments. This term has its maximum when $\tau = 0$, since it corresponds to the integral of a squared function (the correlation function being a measure of the overlap of two functions). The difference between the arguments in the third term is $\tau-t_o$, corresponding to a peak at $\tau-t_o = 0$ or $\tau = t_o$ with amplitude factor h. Similar reasoning shows that the fourth term peaks at $\tau = -t_o$ with amplitude factor h. Since we only look at positive values of τ with our correlator, we will see a peak at $\tau = 0$ and another at $\tau = t_o$ with the height of the second peak $h/(1+h^2)$ times the height of the first peak. For h = 1 (equal scattering by both beams) then the second peak will be one-half the size of the first peak. Since the beam separation can be measured accurately (to less than 1%) and the time τ_o between the two "humps" measured from the observed correlation function, the velocity can be easily calculated

$$v = \frac{d_o}{\tau_o} \quad . \tag{61}$$

The velocity calculated in (61) is actually just the perpendicular component (with respect to the beam) of the real velocity.

II-2.3. Correlation Function For A Diffusion Dominated System. We will now consider the case in which the diffusional motion dominates any imposed flow. For this situation, Eq. (52b) holds and $v\tau << w_x, w_y$ where τ is on the order of the characteristic diffusion time, τ_D. Under these conditions, the exponential term in the generalized moment is essentially a constant for all values of τ of concern and I_{nm} can be written as

$$I_{nm} = \frac{\pi w_x^2 w_y^2}{2(n+m)} \left\{ \left[w_x^2 + \frac{2nm}{n+m} 4D\tau \right] \left[w_y^2 + \frac{2nm}{n+m} 4D\tau \right] \right\}^{-1/2} \tag{62}$$

and for $I_o/I_s << 1$, Eq. (51) becomes

$$C(\tau) = R_s^2 N \frac{\pi w_x^2 w_y^2}{4} \left\{ \left[w_x^2 + 4D\tau \right] \left[w_y^2 + 4D\tau \right] \right\}^{-1/2} \quad . \tag{63}$$

For a circular gaussian beam, $w_x = w_y \equiv w$. Substituting the expression for the characteristic diffusion time τ_D, as given in Eq. (35), into Eq. (63), with $w_x = w_y = w$, we get

$$C(\tau) \propto \frac{1}{1 + \tau/\tau_D} \quad . \tag{64}$$

At $\tau = \tau_D$, $C(\tau_D)$ is down to one-half of its original value at $\tau = 0$. From the experimentally observed correlation function, one can estimate the value of τ_D. If in addition, we know the laser beam waist, w, then from Eq. (35) we can calculate the value of the diffusion constant. A more accurate method of obtaining a value for τ_D is to perform a least squares fit to the entire observed correlation function using (64) as the form of the fitting function. For our situation, that is $w_x \neq w_y$, a least square fit, using an expression similar to Eq. (63) was used to determine the characteristic diffusion time for the long dimension of the laser beam. This exact form for the fitting routine will be discussed in detail in Chapter III.

As stated in the Introduction, we wish to measure the diffusion constant for both the He+Na($^2S_{1/2}$) system and the He+Na($^2P_{3/2}$) system. In order to do this, it is convenient to look at the gas mixture as a ternary system in which there are two trace gases being monitored. The three components are He (the dominant component), Na($^2S_{1/2}$) and Na($^2P_{3/2}$). The diffusion constant determined from the observed correlation function actually contains contributions from each of those states. The effective (measured) diffusion constant for such a system is given by[13,14,15]

$$\frac{1}{D} = f_1 \frac{1}{D_{grd}} + f_2 \frac{1}{D_{exc}} \qquad (65)$$

where D is the effective diffusion constant, f_1 and f_2 are the fractional densities of sodium atoms in the ground and excited states respectively, and D_{grd} and D_{exc} are the respective diffusion constants for those states.

If (65) is multiplied by $w^2/4$ then from the definition of the characteristic diffusion time, (65) can be rewritten as

$$\tau_D = f_1\tau_{D_{grd}} + f_2\tau_{D_{exc}} \quad . \tag{66}$$

The meaning of (66) is clear, the measured diffusion time, τ_D, is just the weighted sum of the individual diffusion times. The values of f_1 and f_2 can be obtained directly from Eqs. (4) and (9). Equation (9) can be rewritten as

$$f_2 = \frac{n_2}{N} = \frac{g_2}{g_1+g_2}\,(I/I_s)(1 + I/I_s)^{-1} \quad . \tag{67a}$$

Substituting this expression into Eq. (4) and solving for n_1/N, we get

$$f_1 = \frac{n_1}{N} = \left\{1 + \left[\left(1 - \frac{g_2}{g_1+g_2}\right)\right]\frac{I}{I_s}\right\}\left(1 + \frac{I}{I_s}\right)^{-1} \quad . \tag{67b}$$

With the further substitution for the values of g_2 (= 16) and g_1 (= 8), we obtain

$$f_1 = \left(1 + \frac{1}{3}\frac{I}{I_s}\right)\left(1 + \frac{I}{I_s}\right)^{-1} \tag{68a}$$

$$f_2 = \frac{2}{3}\frac{I}{I_s}\left(1 + \frac{I}{I_s}\right)^{-1} \quad . \tag{68b}$$

It is evident from Eqs. (65) and (68) or (67) that the diffusion constant and diffusion time are functions of the intensity of the laser beam. For low laser intensities, (66) reduces to $\tau_D \doteq \tau_{D_{grd}}$ and the derivation of the autocorrelation function given in the last section

remains valid. However for intensities where f_2 becomes appreciable, the diffusion constant becomes a function of the intensity which, in turn, is a function of the coordinates. This fact must now be taken into account in the derivation of the autocorrelation function.

Since we are interested in the case where I_o/I_s is no longer small compared to 1, that is $I_o/I_s \gtrsim 1$, the expansion (47) is no longer appropriate, the expression given in (46) will be returned to as the starting point. The z-integral can still be carried out as before with the same result. Technically, this contribution should be included since it has a dependence on the diffusion constant. But, since at most, D can equal $3D_{grd}$ (if $I_o/I_s >> 1$ and $D_{exc} >> D_{grd}$) and at this value the error function [Eq. (50)] is still very near one (and gets closer as D decreases) the term corresponding to the z and Δz integrations is still essentially a constant. The correlation function was then given by

$$C(\tau)=R_s^2 N\left(\frac{I_o}{I_s}\right)^2 \int dx \int d(\Delta x) \int dy \int d(\Delta y) \quad \frac{1}{4\pi D\tau} \text{ EXP } -\left[\frac{\Delta x^2+ y^2}{4D\tau}\right] *$$

$$\text{EXP}\left[-\frac{2}{w_x^2}\left(2x^2+2x\Delta x+\Delta x^2\right)\right] * \quad .$$

$$\left[\frac{\text{EXP}\left\{-\frac{2}{w_y^2}\left(2y^2+2y\Delta y+\Delta y^2\right)\right\}}{1+\frac{I_o}{I_s}\text{ EXP}\left\{-2\left(\frac{x^2}{w_x^2}+\frac{y^2}{w_y^2}\right)\right\}+\frac{I_o}{I_s}\text{ EXP}\left\{-2\left(\frac{(x+\Delta x)^2}{w_x^2}+\frac{(y+\Delta y)^2}{w_y^2}\right)\right\}+}\right.$$

$$\left.\frac{}{\left(\frac{I_o}{I_s}\right)^2 \text{ EXP}\left\{-2\left(\frac{x^2}{w_x^2}+\frac{y^2}{w_y^2}\right)\right\} \text{ EXP}\left\{-2\left(\frac{(x+\Delta x)^2}{w_x^2}+\left(\frac{(y+\Delta y)^2}{w_y^2}\right)\right)\right\}}\right] \tag{69}$$

In order to evaluate the above, rather complicated, integral it was assumed that the diffusion constant D was only a function of the space variables x and y (through the intensity distribution). This seems to be a reasonable assumption based on the meaning of the conditional diffusion probability distribution [Eq. (44)]. Another step which was taken to evaluate the integrals was to suppress the Δx and Δy dependence in the denominator. With these two assumptions, the integrals over Δx and Δy could be carried out analytically with the following result

$$C(\tau)=R_s^2 N\left(\frac{I_o}{I_s}\right)^2 \int dx \int dy \; \frac{\text{EXP}\left\{-4x^2\left[\frac{1}{w_x^2}-\frac{1}{2w_x^2+\frac{w_x^4}{4D\tau}}\right]\right\}}{D\left\{1+\frac{I_o}{I_s}\text{EXP}\left[-2\left(\frac{x^2}{w_x^2}+\frac{y^2}{w_y^2}\right)\right]\right\}^2} * \frac{\text{EXP}\left\{-4y^2\left[\frac{1}{w_y^2}-\frac{1}{2w_y^2+\frac{w_x^4}{4D\tau}}\right]\right\}}{\left[\left(\frac{1}{w_x^2}+\frac{1}{4D\tau}\right)\left(\frac{1}{w_y^2}+\frac{1}{4D\tau}\right)\right]^{1/2}} \qquad (70)$$

where the diffusion constant to be used is given by

$$D = \frac{D_{grd}D_{exc}}{f_1 D_{exc} + f_2 D_{grd}} \qquad (71)$$

which was obtained from solving (65) for D. Equation (70) was used as the theoretical form for the excited state diffusion constant measurements. The role this expression played in the analysis of excited state data will be explained in Chapter IV.

II-3. Determination of the Diffusion Constant From Kinetic Theory

Since we want to evaluate the diffusion constant experimentally, it would also be of benefit to know what the theoretical prediction for this constant is, for comparison purposes. A formula for calculating the diffusion constant can be derived from the kinetic theory describing gases. Currently the most complete (and widely used) theoretical treatment of the kinetics of a dilute gas is that of Chapman and Enskog.[14,15] In their theory, they assume the gas is near equilibrium and solve the Boltzmann equation by using perturbation theory. The resulting solutions yield the probability density functions for particles (atoms, molecules, etc.) which are just the probability that a particle has a given momentum at a given spatial location as a function of time. Using these solutions and the diffusion equation, one can obtain an expression for the diffusion constant.

II-3.1. Diffusion Constant For A Binary Mixture. The diffusion constant is a parameter that basically describes the average motion of a particle as a result of a large number of random collisional events. In order to calculate this parameter, the details of the collisional process must be considered. These details include, the relative kinetic energy of the two colliding species, impact parameters, the interaction potential between the two particles and the collisional frequency. The first three items essentially determine the deflection of the particles from their initial direction of motion and their respective energies after collision. Combining all these features, one would expect that the diffusion constant should depend on the pressure

or density (collisional frequency), the temperature (kinetic energy) and the interaction potential. The diffusion constant for a binary mixture of gases is given by[14]

$$D = 2.628 \times 10^{-3} \left(T^3(m_1+M_2)/2M_1M_2\right)^{1/2} \Big/ p\sigma_{12}^{\,2}\,\Omega_{12}^{(1,1)*} \qquad (72)$$

where

D is the diffusion constant (in cm^2/sec)

p is the pressure (in atmospheres)

T is the temperature (in Kelvin)

k is Boltzmann's constant (cys units)

M_1 and M_2 are the gram atom weights of species 1 and 2 (grams)

$\Omega_{1,2}^{(1,1)*}$ is the normalized collision integral (see below) and is a function of T_{12}^*

σ_{12} is a length characteristic of the interatomic potential, generally where $\phi(r) = 0$ (in Å)

ε_{12} is the well depth of the interaction potential (ergs)

T_{12}^* is the normalized temperature, kT/ε_{12}.

The collision integral is defined through the following set of relations[14]

$$\chi(g,b) = \pi - 2b \int_{R_m}^{\infty} \frac{dr/r^2}{\left[1 - \frac{b^2}{r^2} - \frac{2\phi(r)}{\mu g^2}\right]^{1/2}} \qquad (73a)$$

$$Q^{(1)}(g) = 2\pi \int_0^{\infty} (1-\cos\chi)\,b\,db \qquad (73b)$$

$$\Omega^{(1,1)} = (kT/2\pi\mu)^{1/2} \int_0^\infty e^{-\gamma^2} \gamma^5 Q^{(1)}(g)\, d\gamma \qquad (73c)$$

$$\gamma^2 \equiv \mu g^2/2kT \quad . \qquad (73d)$$

$\chi(g,b)$ is the angle of deflection in a collision, g is the relative velocity of the colliding atoms, b is the impact parameter for the collision, μ is the reduced mass, $\phi(r)$ is the interatomic potential, and γ^2 is the "reduced" relative kinetic energy. For a few standard forms for the potential $\phi(r)$, the collision integrals (73c) have been tabulated in the literature. In most of these tabulations, however, the quantity $\Omega^{(1,1)*}$ is given. This value is the ratio of the integral evaluated by (73c) to the corresponding integral for a hard sphere model. For this model

$$\phi(r) = \begin{cases} 0 & r > \sigma_{12} \\ \\ \infty & r < \sigma_{12} \end{cases} \qquad (74a)$$

where $\sigma_{12} = (\sigma_1 + \sigma_2)/2$ and σ_i is the diameter of the i^{th} species. Equations (73b) and (73c) reduce to[14]

$$Q^{(1)}_{HS} = \rho\sigma_{12}^2 \qquad (74b)$$

$$\Omega^{(1,1)}_{HS} = (kT/2\pi\mu)^{1/2}\, \pi\sigma_{12}^2 \quad . \qquad (74c)$$

Upon inspection of (67), we can see that the diffusion constant involves parameters related to the interaction potential in the form of σ_{12} and $\Omega^{(1,1)}(T_{12}^*)$. Three types of potential forms are considered

here, a Lennard-Jones potential, Morse potential and an exponentially repulsive potential. These three types are looked at because the He + Na($^2S_{1/2}$) interaction potential has been modeled using both a Lennard-Jones and an exponentially repulse potential and the He + Na($^2P_{3/2}$) interaction has been modeled using a Morse potential and a Lennard-Jones potential. The Lennard-Jones potential is given by

$$\phi(r) = 4\varepsilon\left((\sigma/r)^{12} - (\sigma/r)^{6}\right) \tag{75}$$

where ε is the well depth and σ is the value of r such that $\phi(\sigma) = 0$. The parameters ε and σ in (75) are also the parameters to be used in (72). The collision integrals corresponding to this potential can be found in Ref. (14). A Morse potential is of the form

$$\phi(r) = \varepsilon\left\{ \mathrm{EXP}\left[-2\left(\frac{B}{\beta}\right)(r-r_o)\right] - 2\mathrm{EXP}\left[-\left(\frac{B}{\beta}\right)(r-r_o)\right]\right\} \tag{76}$$

where ε is again the well depth and $\phi(r_o) = -\varepsilon$. If (76) is solved to find the value of r, r_{min}, such that $\sigma(r_{min}) = 0$, then we get

$$r_{min} = r_o - \frac{\beta \ell n^2}{B} \tag{77}$$

The values of ε and r_{min} are to be used in (72) (with $r_{min} = \sigma_{12}$). The values of the collision integrals for the Morse potential have been calculated by Smith and Munn.[17] Finally, the exponentially repulsive potential is given by

$$\phi(r) = Qe^{-r/\rho} \tag{78}$$

There is no well depth or zero crossing for this potential. Monchick[19] worked out the collision for this case and found

$$\sigma_{12}^{2}\,\Omega^{(1,1)*} = 4\alpha^{2}\rho^{2}J_{(1,1)} \tag{79}$$

where $\alpha = \ell n(Q/kT)$ and $J_{(1,1)}$ are the integrals he has tabulated. [In his nomenclature, $I_{(1,1)}$ is the symbol he used for the integrals and the potential was given by $Ae^{-r/\rho}$. The changes made here are so as to avoid confusion with previously used quantities denoted by the same symbols.] The results for D using these forms of the potential and for some values of the parameters ε_{12} and σ_{12} found in the literature will be presented in Chapter IV.

III. EXPERIMENTAL SET-UP AND PROCEDURES

In this chapter the various components of the experimental apparatus will be described, along with an outline of the procedure used during an experimental run. Particular emphasis will be given to the design of the cell, since this is perhaps the most critical element of the system.

III-1. General Experimental Set-Up

A block diagram of the experimental set-up is shown in Figure III-1. The equipment used in performing the experiment can be divided into six categories: the laser, beam steering optics, flow cell, light collection system, detector and the signal processing electronics. The same basic system was used for both the velocity measurements and diffusion constant measurements. The laser beam was directed to the flow cell with a system of lenses and mirrors. The fluorescence was monitored at right angles to the beam with a photomultiplier tube. The output of the photomultiplier was fed into an amplifier/discriminator. The signal was then processed by the digital autocorrelator. All these individual components will be described in detail below.

III-1.1. Laser System. The laser that we used in these experiments was a tunable, single frequency dye laser (Coherent Radiation, Model 599-21) pumped by an argon ion laser operating either at all

lines or at 5145 Å. The output of the dye laser was fed into a power stabilizing unit (Coherent Associates, Model 301 Noise Suppressor). The noise suppressor accomplished two things. First, it reduced broad band intensity fluctuations of the laser an order of magnitude. Secondly, the unit maintained a constant output level (to about 1%) despite input level excursions of up to about 20%. The main advantage of this device, for our experiments, was the latter point. We frequently had to tune the laser away from the sodium line (5890 Å) in order to determine the background level that was present. The Noise Suppressor eliminated the need to constantly check the power under these conditions.

The output of the Noise Suppressor was split by a glass plate (Corning Filter CSO-53), with most of the beam directed toward the flow cell. The two primary surface reflections from the glass plate were used for beam diagnostics. One of these beams was sent through a digital wavemeter, which measured the wavelength of the dye beam to an accuracy of approximately 1 GHz. This was very useful in tuning the laser to the sodium D_2 resonance. The other reflection was passed through a small sodium cell and into a spectrum analyzer. The sodium reference cell was heated to about 100°C and served as a visible indication that the laser was properly tuned. The single frequency operation of the dye laser was monitored with a Tropel (Model 201) spectrum analyzer with a free spectral range of 1.5 GHz. Single frequency operation of the laser was desired because the output of the laser became very noisy in multimode operation. Also if the modes lasing were further than about 2 GHz from the fundamental mode, these modes would be off the sodium resonance and hence contribute to the background scattering but not to the signal.

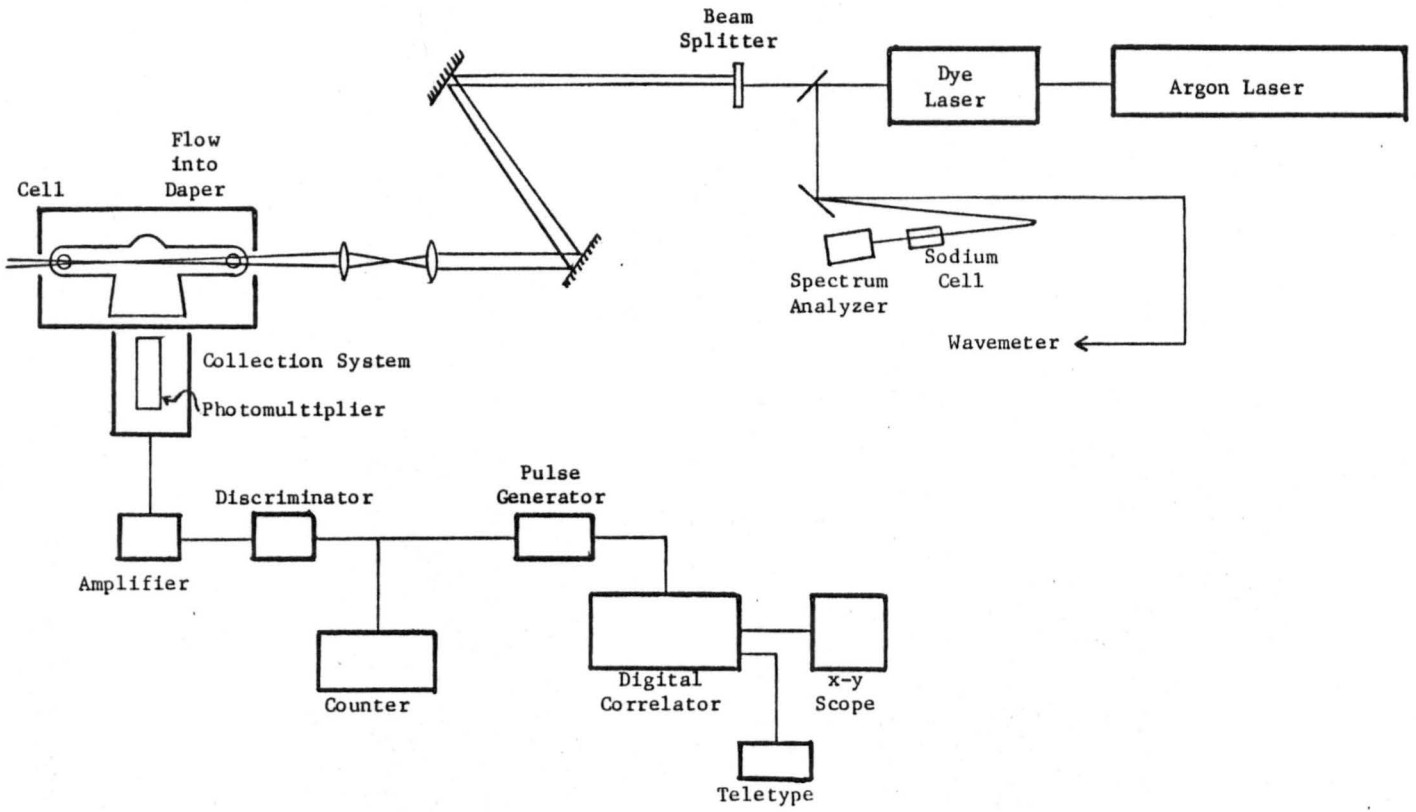

Fig. III-1. Block diagram of experimental set-up.

III-1.2. Laser Beam Steering Optics. The beam steering optics consisted of a system of mirrors and lenses needed to direct the beam from the table, which the laser system was on, to the table on which the experiment was located and into the flow cell. The steering mirrors were high quality (scratch/dig of 10/2), first surface mirrors (Newport Research), each with an enhanced aluminum coating. This coating is reasonably durable and has a reflectivity of 96% at 5890 Å. The lenses were used to provide the desired beam diameter throughout the cell. The parameters of interest were the laser beam waists in the observing volume and the size of the beam at the entrance and exit windows of the cell. The focal lengths of the lenses ranged from 10 cm to 60 cm. Care was taken to avoid having the beam hit a part of the lens that was marred in any way. These imperfections on the surfaces or in the interior of the lens would cause unwanted parasitic light to propagate along the main laser beam. This parasitic light could act as a source for eventual stray light detected by the photo tube.

As mentioned in the Introduction, two different beam geometries were used when measuring velocities, a two beam and a one beam system. The reason for this was that each type of geometry has its own advantages when setting the system up and when analyzing the resulting data. The single beam system was simpler to set up and the data was easier to interpret, however, the resulting velocity was more difficult to measure accurately (due to the low signal-to-noise ratio). The dual beam system was a little more difficult to set up, and the data for the single atom case allowing more possible interpretations, but it was easy to extract an accurate velocity from the correlation function. These data analyses for these two systems will be discussed in Chapter IV.

There were two different optical systems used to achieve the two-beam geometry. The first was to use a single element beam splitter, with one-half of the first surface fully coated and the opposite half of the second surface partially coated. The laser beam entered the beam splitter through the part of the front surface which was uncoated, but exited the back surface through the partially coated (approximately 50%) half. The beam splitter was tilted in such a way so that the internally reflected beam from the back surface struck the first surface on the fully coated half. The reflected beam from this surface then passed through the uncoated half of the back surface. The actual physical extent of the coated surfaces gave this beam splitter a minimum beam separation that was possible. Unfortunately, this separation, approximately 5 mm at the exit surface, had to be reduced to about 1 mm by the focussing lenses for the system. The procedure involved in achieving not only the desired beam separation but also the correct beam waist at the viewing volume entailed a substantial amount of time trying to find an adequate lens system. The second method used to generate two beams used four separate elements, two fully coated mirrors and two partially transmitting/reflecting (65%/30%) beam splitters. This type of arrangement allowed independent separation and focussing controls, the separation being controlled solely by the beam splitter arrangement while the focussing being controlled by the relative positions of the lenses. This system also provided the most flexibility in optimizing the positions of the two beams with respect to each other, the photomultiplier and the primary collection optics.

III-1.3. Flow Cell and Light Collection Optics. The cell used in our experiments is shown in Figure III-2. It was constructed in three

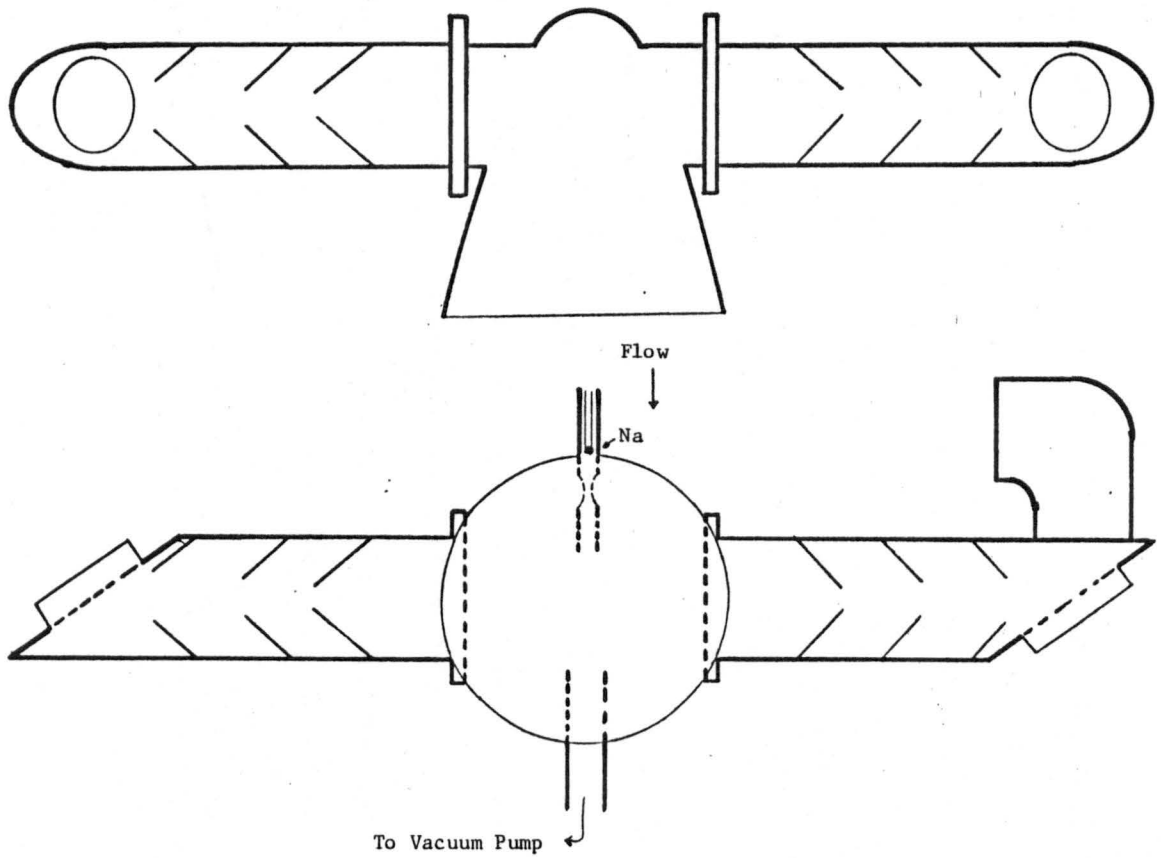

Fig. III-2. Flow Cell.

different sections. This aspect made it possible to change the central section, where the viewing volume was located, without having to redesign the entire cell. The entrance and exit sections, made out of an aluminum tube, were fitted with equally spaced diaphragms, also aluminum, the radius of each aperture being less as one gets closer to the central section. The angle between the cell wall and the diaphragm was approximately 35°; this allowed multiple scattering and therefore increased absorption of stray light rays which impinged on the diaphragm's surface. The innermost aperture on the input side was constructed so that the cone of light, defined by the aperture with the apex at the entrance window, would pass through the exit side of the central section cleanly. The aperture radii for the exit side were .5 cm, .75 cm and 1 cm; these sizes were not critical. The exit section also had a light trap mounted above the exit window to reduce the stray light caused by rays reflected from the window surfaces. After the beam exited the cell, it was partially absorbed by a filter (Corning CS7-69) which was canted 45° to the input direction, the reflection off this filter being terminated by a blackened copper pipe. No light traps were used for the front window because the reflections were naturally directed outside the cell.

The interior of the entrance and exit sections of the cell were blackened with the residue of an acetylene torch. First, the sections without the apertures were blackened. As each diaphragm was installed and fastened in place (with three screws), the section was re-blackened. It was found that the surfaces treated with the acetylene reflected less light than when these surfaces were treated with a colloidal graphite paint or an ultra-flat black latex paint. After these sections were

completely assembled and treated, the windows were epoxied in place. The windows were 1-1/2" in diameter, 3/8" thick and were made from laser quality fused silica. They were attached to the cell at about brewster's angle. Mounting the windows in this manner helps reduce the amount of scattering from the windows as much as possible.

There were two different central sections used during the course of this experiment. The first section that was used consisted of a pyrex cylinder approximately 5" in length. Small pyrex tubes, roughly 7 mm in diameter and 10 mm in diameter were joined to the cylinder in the middle, approximately 180° apart. The 7 mm tube was used as the input for the flowing gas and was vertically oriented. Most of the interior and exterior of this section was blackened to reduce stray light. The collection system used for this cell was a 1" radius of curvature mirror and two F/1 condensing lenses. The cell was not blackened along the collection axis (perpendicular to both the beam and the input tube). The overall optical collection of this system was 3%.

The other central section that was used contained a rhodium-coated ellipsoidal mirror. The ellipsoidal mirror provides high optical collection efficiency (between 50% and 70%) because for a light source at the primary focus, the effective solid angle seen by a detector at the secondary focus is quite large ($\sim$80% of 4 π steradians). A similar collection system was used by Greenlees[5] in his single atom detection experiment. The ellipsoid was purchased from Melles Griot (Part #REM006) and was modified by having four holes drilled through the ellipse at the primary focal plane. Two of these holes were 1" in diameter (located 180° around the focal plane from each other) and the other two holes were drilled perpendicular to the axis of these 1"

holes and were 3/8" in diameter. The major and minor axes for this ellipsoid were 167.7 mm and 89.0 mm. The predicted collection efficiency for this ellipsoid was 86%, the above modifications decreasing this number to 72%. The surface (rhodium) is approximately 80% reflective at 5890 Å, so the actual optical collection efficiency is predicted to be 57.6%. The experimental determination will be discussed in Section III-2.1-2.

The type of motion being studied, diffusion or flow velocity, determined which of two types of input tubes that were attached to ellipsoidal central section. The input tube was used for seeding sodium into the elliptical cavity and to create the flow itself. The procedure used for seeding will be discussed later. When measurements to determine the diffusion constant were made, the input tube was a piece of pyrex tubing, with a constant inside radius of 2 mm. This tube was connected to the buffer gas that was desired. A larger tube, directly opposite the input tube (these two tubes fit into the 3/8" holes drilled in the ellipsoid) was connected to a vacuum system. When the velocity dominate system was to be studied, the input tube was also a tube with an inside diameter of 2 mm, but there was an added narrowing approximately 1.5 cm above the end of the tube. This constriction was about 1 mm in diameter, so that the input tube formed a converging/diverging (De Laval) nozzle. The theory describing this type of nozzle can be found in references (27) and (28). For the above nozzle geometry a speed of approximately 35 m/sec (for the subsonic regime) is predicted (from the above references) for the center of the flow at the nozzle exit. Using this tube and an ambient pressure of 200 Torr of helium in the cell, velocities up to 80 m/sec were experimentally measured at the

primary focus of the ellipse. Possible reasons for this discrepancy will be dealt with in Chapter IV.

Two "sensors" were also incorporated into the cell, a pressure monitoring point and a thermocouple. The pressure measurement point was located on the input section of the cell. A hole was drilled into input section between middle diaphragm and innermost diaphragm. This site was chosen so that a measurement of the pressure in the cell was possible without any interference from the flow. The other sensor, a copper/constantan thermocouple, was installed for the diffusion measurements. Knowledge of the temperature variation as the pressure of the system or the heat applied to the sodium source were changed, allowed the data to be normalized to a constant temperature. [The diffusion constant, and hence the diffusion time, varies with temperature as seen from Eq. (II-72).] The thermocouple was attached to the vertex of the ellipsoidal collector, through a hole that had been used in the construction of the mirror. A mounting system was constructed, from a stainless steel bellows, which allowed the thermocouple to be extended into the viewing volume for a temperature measurement and then retracted for an experimental run.

The construction of the cell also allowed it to be evacuated. The three main sections were joined together by a flange/o-ring arrangement. The input and exhaust tubes were epoxied in place. The screws which fixed the diaphragms to the cell were also epoxied over to seal them. The main face plate for the ellipical cavity, a pyrex plate 90 mm in diameter, was epoxied to the ellipsoid. Since the vacuum requirements were not severe, these seals were adequate for our experiment. The entire cell was mounted on two translation stages in a light proof box.

III-1.4. The Photon Counting System. The fluorescence detector used in all our experiments was a RCA C31034A photomultiplier tube (PMT). It was mounted in a thermo-electrically cooled housing (Products for Research, Model TE-104) and was oriented such that the long dimension of the 1.0 cm by .4 cm photocathode was parallel to the laser beam. The PMT housing was translated with respect to the cell until the center of the PMT photocathode was at the secondary focus of the ellipsoidal mirror. The PMT was normally operated at -1500 V and was cooled to approximately -30°C, in order to reduce the dark current. At this temperature the measured dark count rate, usually about 40 to 50 counts/sec, were typically more than two orders of magnitude less than the count rate due to the stray light signal, thus, in effect, were negligible. When the sodium source was being heated, however, black body radiation produced a significant count rate at higher temperatures, as much as 40,000 counts/sec out of a total average rate of 60,000 counts/sec. The quantum efficiency measurements of this tube will be presented later.

The output of the PMT was directed to an Ortec 9302/9301 pre-amplifier-amplifier/discriminator unit. The discrimination of the signal was done by an Ortec 436, 100 MHz discriminator, whose output was large enough to trigger the pulse generator needed for the final stage of signal processing. At the conclusion of the experimental work, a PAR 1121 discriminator was also used. The quantum efficiency measured with either the Ortec 9302/9301 - Ortec 436 amplifier/discriminator set, or the PAR unit was the same. The PAR unit, though easier to adjust properly than the Ortec system (because of its built-in pulse height analyzer) did not have an output which could be

used to directly trigger the programmable pulse generator. The output of the Ortec 436 discriminator was also used on the input to a HP 5244L electronic counter, which then monitored the total count rate as seen by the PMT. This count rate was generally used to determine the sodium density in the viewing volume and also as a check on the total current being generated by PMT [which had a maximum rating of 100 ns, corresponding to approximately 4.4×10^5 counts/sec]. The pulse generator was used because its output could be adjusted to meet the input specifications of the digital correlator (pulse width = 25 ns, rise time $\leq$ 1 μs and voltage level of -1.5 to -3.0 volts).

III-1.5. Digital Correlator. The signal processing was done with a 48-channel digital autocorrelator (Malvern Scientific, Model K 7023). [See references (30) and (31) for a detailed discussion of its operating principles and limitations.] The primary mode of operation used in our experiments was the single clipped autocorrelation mode. The main advantages in generating the autocorrelation function with this type of device are two-fold. First, the signal is processed in real time, and second, the clipping feature allows some discrimination against unwanted "d.c." levels in the input signal.

Basically the digital correlator is a pulse counting/storage device. The correlator samples the input signal for a number, N_T, of equal time intervals, τ_s, called sample times. For each of these time intervals, a signal proportional to the input current, i(t), is sensed

$$g(t) \propto \tau_s \, i(t) = \tau_s \varepsilon \eta_o n(y,z) R(t) \qquad (1)$$

(where the last equality comes from Section II-2.1). The function g(t)

is the total number of pulses seen for a time τ_s. For the digital case, instead of an integral representative of the correlation function [Eq. (II-40)], one obtains an average of the sum of products $g(t)g(t+\tau)$ or for N_T samples

$$C(m\tau_s) = \frac{1}{N_T\tau_s} \sum_{\ell=1}^{N_T} \frac{g(\ell\tau_s)}{\tau_s} \frac{g(\ell\tau_s+m\tau_s)}{\tau_s} \tau_s \quad . \qquad (2)$$

where $C(m\tau_s)$ is the correlation coefficient in the m^{th} channel, and $g(\ell\tau_s)$ and $g(\ell\tau_s+m\tau_s)$ are integers representing the number of pulses counted in the ℓ^{th} sample time and $(\ell+m)^{th}$ sample time. (The function given by (2) for m = 1, 2, . . . is to be compared directly to the autocorrelation function generated, using R(t), in Chapter II.)

Equation (2) is slightly modified for a single clipped autocorrelation function. For such a function, $g(\ell\tau_s)$ is replaced by $g_k(\ell\tau_s)$ where

$$g_k(\ell\tau_s) = \begin{cases} 1 \text{ if } g(\ell\tau_s) > k \\ 0 \text{ if } g(\ell\tau_s) \leq k \end{cases} \qquad (3)$$

where k is a present integer. A discussion of the effects of the clipping feature can be found in reference (32). The general effect, though, is that the clipping level can be used as a "digital discriminator" to cut out unwanted parts of the input signal. If the clipping level is set equal to (or slightly greater than) the average number of counts per sample time, $\bar{g}$, then a reasonable amount of noise can be discriminated against. Due to the nature of processes being dealt with, however, there can still be a chance that more than k counts will occur, in a sample time, due to noise. The probability of this occurring is given by the poisson probability about an average of $\bar{g}$.

III-2. Experimental Procedures

The procedures discussed in the following sections describe what was actually done to collect the data and all auxiliary information needed to either set up to take the data or to analyze it. These procedures can be broken down into two distinct groups. First are those general procedures which are independent of the actual experimental run, and second are those needed in actually carrying out a particular experiment (measurement of flow velocities or diffusion constants). Items belonging to the first group include the determination of the quantum efficiency of the PMT, the optical collection efficiency of the ellipse, the total efficiency of the system and the measurements on the laser beam waist. The second category contains information about how the sodium source was set up, over-all optical alignment of the system and the methods used in conducting the actual experimental runs for determination of velocities or diffusion constants. A description of any computer models developed or computer analysis techniques will be included where applicable.

III-2.1. Procedures for Determining General Experimental Parameters

III-2.1-1. Quantum Efficiency of PMT. The absolute quantum efficiency of and the discrimination level appropriate to our C31034A photomultiplier tube was determined by standard methods. A laser beam, tuned to a 5890 Å, impinged directly on the photo cathode. The beam had a known, constant power of typically about one-tenth of a picowatt. The output of the PMT was fed into an Ortec 9301/9302 preamplifier/amplifier pair and the resulting signal put through an Ortex 436

discriminator. At a constant applied voltage to the tube (1500 V), the count rate was monitored as a function of discriminator level and a differential count rate determined. The results of two such determinations are shown in Figs. III-3(a) and (b). One can see that the second graph, 3(b), shows no characteristic photo-electron peak as is evident in the first graph. Figure III-3(a) was generated during the middle of 1979, just before starting to take the data presented in this thesis. Figure III-3(b) was the corresponding graph after the data taking phase was completed (June 1981). Apparently the characteristics of the PMT changed significantly during the intervening time. The measured quantum efficiency of the tube corresponding to the 1979 determination was 15% at -1500 V and 29% at -1800 V, with the discriminator set at 90 mV for both measurements. The efficiency of the tube as measured in 1981 was 2.8% at -1500 V and 3.3% at -1800 V. The impact of these facts will be discussed in Chapters IV and V.

III-2.1-2. Optical Collection Efficiency of Ellipsoidal Mirror. As stated earlier, the primary optical collector was the ellipsoid mirror used for the central section of the cell. The collection efficiency of this system was measured by a method similar to that used by Greenlees[5] et al. In our method a small steel ball, .945 mm in diameter, was suspended into the ellipsoid by a thin quartz fiber. (The fiber and ball were attached together by using a cyanoacrylate glue.) The laser was tuned to 5890 Å and the power incident on the cell and the power transmitted through the cell were measured to determine the loss due to the cell windows. The ball was then lowered into the ellipsoid and then positioned with a x-y-z translation stage to achieve the sharpest image at the secondary focus. This process entailed placing a card

Fig. III-3(a). Pulse height spectrum of RCA31034A, taken in the Summer 1979.

(b). Pulse height spectrum of RCA31034A, taken in the Summer 1981.

Fig. III-3

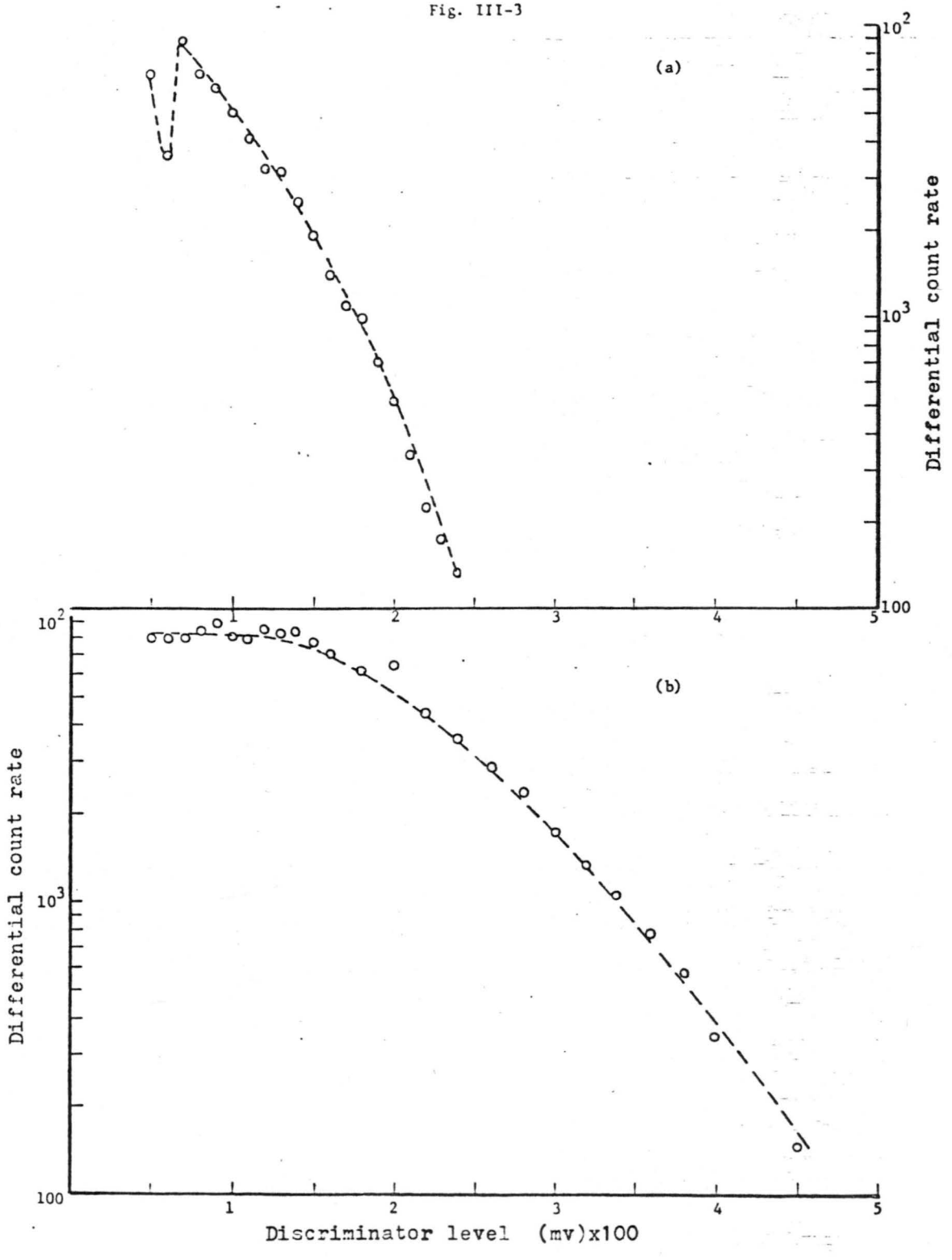
(a)
(b)
Differential count rate
Differential count rate
Discriminator level (mv)x100
10^2
10^3
100
1
2
3
4
5

in the vicinity of the secondary focus and moving it back and forth while adjusting the position of the ball until a combination was found that visually produced a very sharp image. The quality of the image was very dependent on the relative position of the ball and the primary focus. Therefore, the process was not excessively time consuming.

Once the correct position of the ball was found, the power at the secondary focus was measured. The power incident on the cell and the power transmitted through the cell were again measured. From these last two measurements correcting for the loss due to the windows, the amount of light scattered out of the beam by the steel ball cound be found. Assuming that the sphere acts as an isotropic scatterer (to be discussed below) then the efficiency should be

$$\text{eff} = \frac{P_D}{P_{SC}} \frac{1}{R} \qquad (4)$$

where P_D is the power detected at the secondary focus, P_{SC} is the power scattered out of the beam by the ball, and R is the average reflectivity of the ball. From our measurements, P_D = .24 mw, and P_{SC} = 1.05 mw; therefore, P_D/P_{SC} = .228. The reflectivity of the sphere was measured using a spectrophotometer, the value being .40 to ± .08 (the large error was due to the spectrophotometer itself). From (4), the calculated optical efficiency is then .56 ± .11, in excellent agreement with the previous prediction (Section III-1.3).

The above calculation was made assuming isotropic scattering. Actually the scattering of light off a conducting sphere is not isotropic. From electromagnetic theory, one can determine the differential cross sections for the scattering of polarized plane waves (our sphere

is small compared to the laser beam so the plane wave approximation is valid) off of a conducting sphere.[33-35] Due to the interactions of the light and the sphere, these cross sections are complicated. From reference (33), they are given by

$$\frac{d\sigma}{d\Omega}_{(E)} = \frac{a^2}{4}\left[4\cot^2\theta J_1^2(ka\sin\theta)+1+4\cot\theta J_1(ka\sin\theta)\right.$$

$$\left.\sin\left(2ka\sin\left(\frac{\theta}{2}\right)\right)\right] \qquad (5)$$

$$\frac{d\sigma}{d\Omega}_{(H)} = \frac{a^2}{4}\left[4\csc^2\theta J_1^2(ka\sin\theta)+1+4\csc\theta J_1(ka\sin\theta)\right.$$

$$\left.\sin\left(2ka\sin\left(\frac{\theta}{2}\right)\right)\right] \qquad (6)$$

where the subscript E refers to the case where the polarization vector is in the plane of incidence, H refers to the case where the polarization is perpendicular to the plane of incidence, a is the radius of the sphere, k is the wave number for the light, and J_1 is a Bessel function (of the first kind) of order 1. For the above equation, the incident light is traveling along the z axis, striking the sphere from the -z direction (θ is measured from the +z axis). We have plotted out Eq. (5) for our case with 2a = .945 mm and k = 1.06540^4/mm and found $15° \leq \theta \leq 165°$ and $195 \leq \theta \leq 345°$, Eqs. (5) and (6) predict a fairly constant differential cross section. However, for polar angles outside these regions, the cross sections oscillate rapidly and can attain relatively large values. The large cross sections for forward scattering (θ near 0°) are due primarily to diffraction effects,[35] however, and should not be considered when dealing with the reflective characteristics

of the sphere. On the other hand, the scattering in the backward direction (θ near 180°) needs to be considered. The exact effects of the large (and oscillating) differential cross sections in this direction are difficult to predict precisely but it would appear that this back scattered component is more than predicted for an isotropic scatterer. Since this would increase the percentage of light escaping through the input part of the ellipse (one of the 1" holes), the efficiency, as calculated above, would be somewhat low. The effect, however, is probably not high since the measured and calculated efficiencies are so close.

The collection efficiency of the ellipsoid will also change if the scattering center is not at the primary focus. With the steel sphere, these off primary-focus efficiency distributions were measured using the PMT at the secondary focus. As in the experimental runs, the long dimension of the photocathode was parallel to the laser beam. The ball was translated in three mutually perpendicular directions, along the beam, along the axis of the ellipsoid, and along the gas flow axis. The normalized results of these measurements were plotted as a function of distance from the focus and are shown in Figs. III-4, 5 and 6. The circled points in these graphs represent the data taken with the sphere. The solid line was generated by a computer model.

The computer model was set up to mimic the reflective properties of the ellipsoid. In this program, a constant number of rays per unit solid angle were generated at a specific point, i.e., an isotropic radiator. These rays were allowed to propagate until the surface was reached and then were reflected from the point of contact. The reflected rays were followed until they intersected the secondary focal plane.

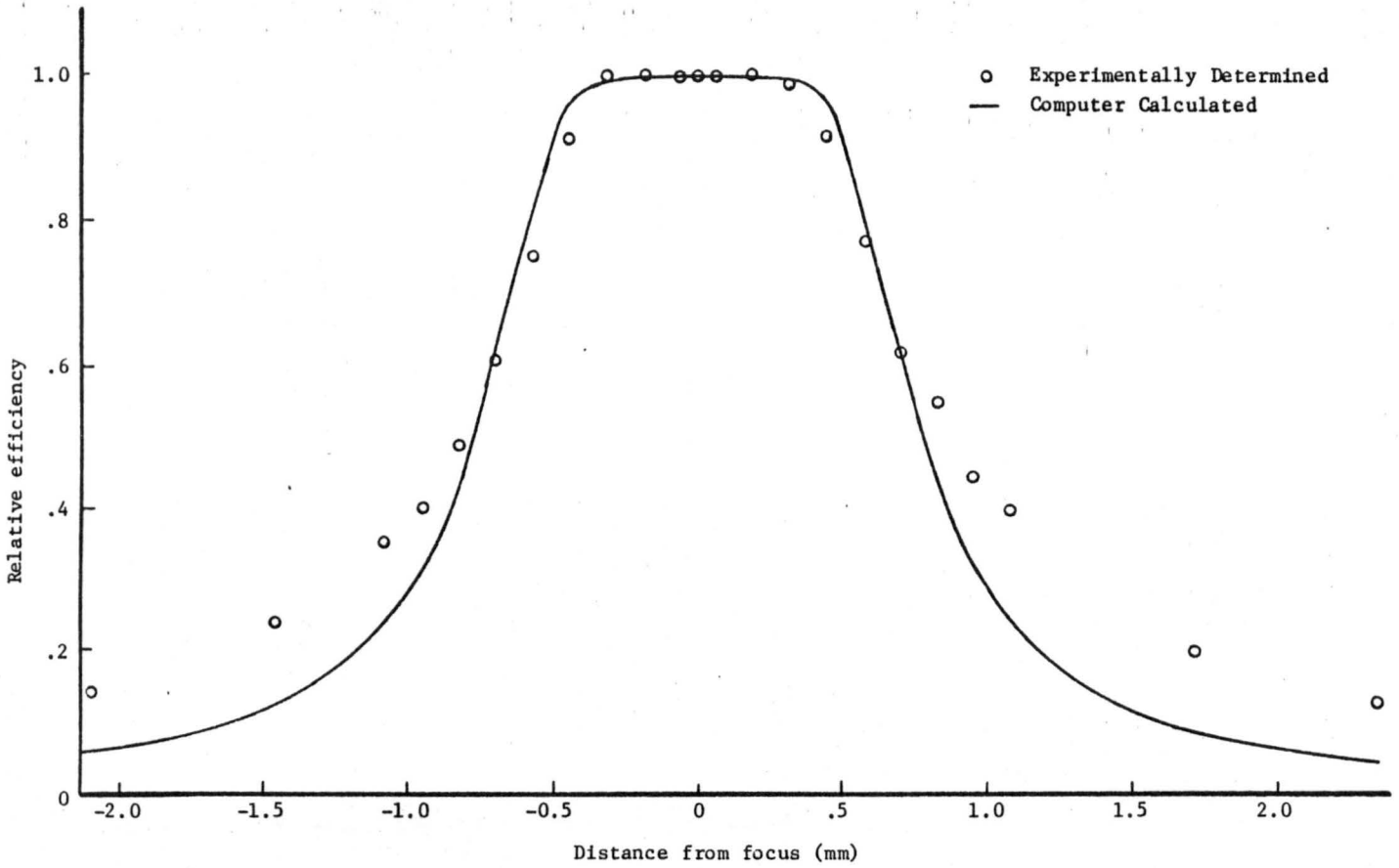

Fig. III-4. Focusing characteristics of our ellipsoidal reflector along the direction of the laser beam.

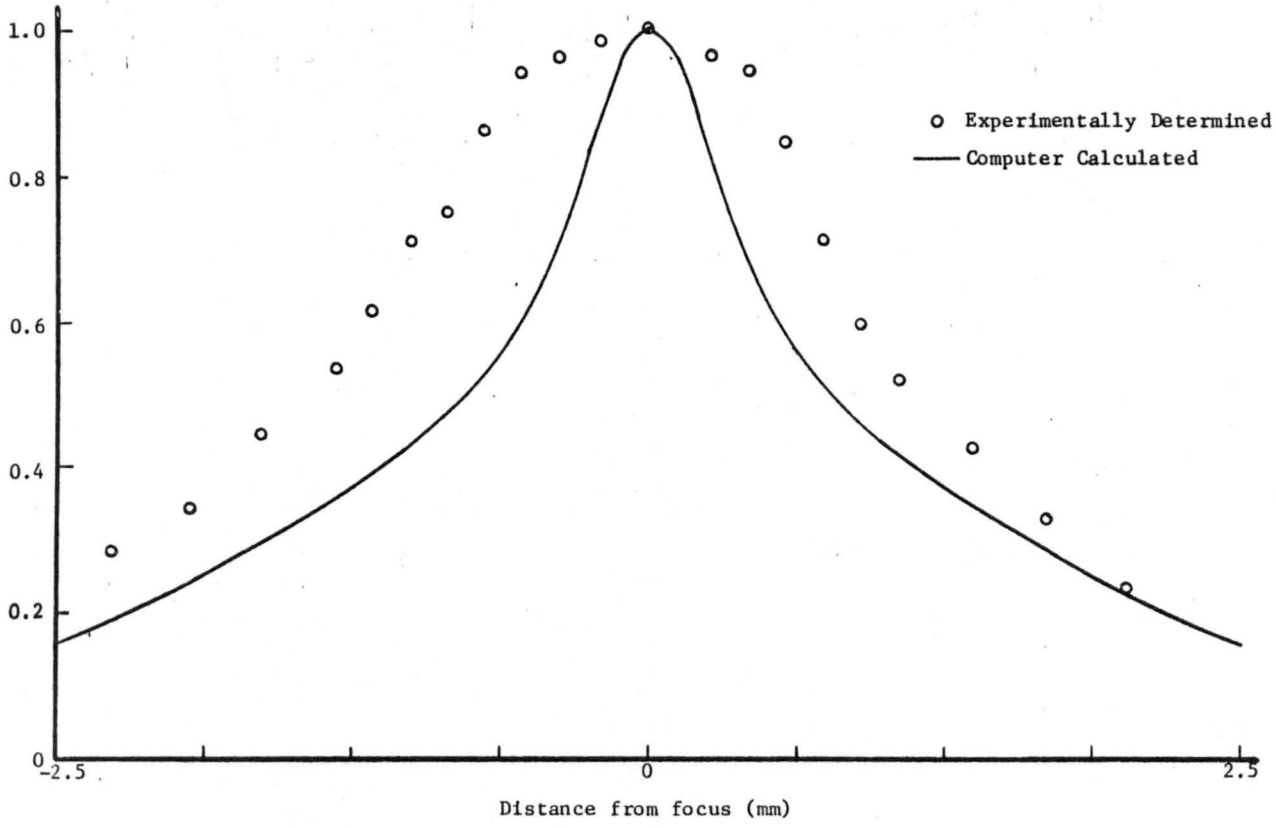

Fig. III-5. Focusing characteristics of our ellipsoidal reflector along the flow axis.

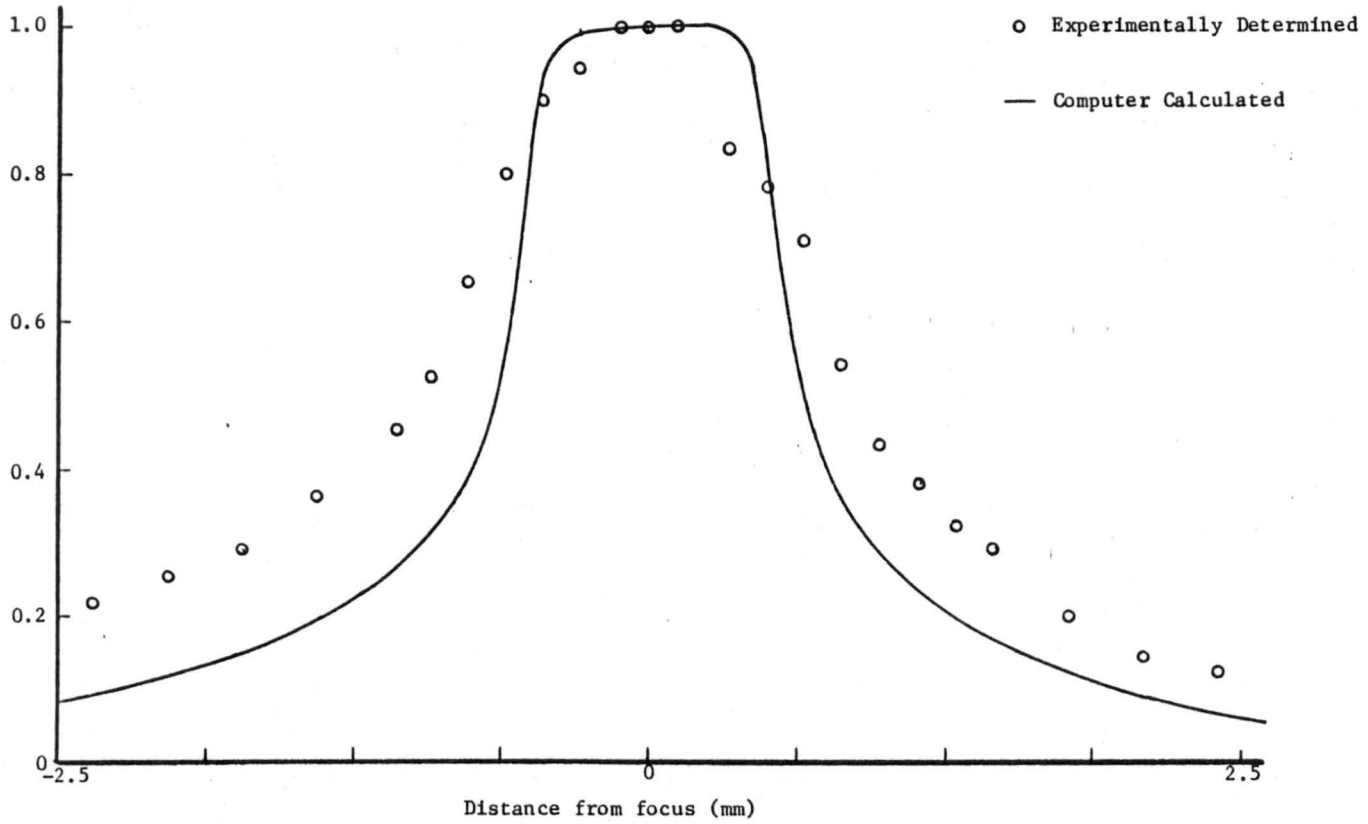

Fig. III-6. Focusing characteristics of our ellipsoidal reflector along the axis of the reflector.

An aperture was set up (the same size as the photocathode) in the secondary plane and those rays making it through the aperture were counted. The ratio of the number of rays making it through the aperture to the total number of rays generated is the collection efficiency. The point where the rays were generated was moved in the directions corresponding to the directions the steel ball was moved. It is these efficiencies (normalized to the value of 1 at the primary focus) that were plotted along with the experimental points in Figs. III-4, 5 and 6.

The broadening of the curves corresponding to the experimentally determined points, with respect to those generated by the computer, is immediately seen. This broadening is due to the fact that a steel ball of finite ("large") dimensions (d = .945 mm) was used. The differences between the individual curves can also be explained. The difference between Figs. 4 and 5 is primarily due to the shape and orientation of the photocathode, the long dimension parallel to the motion in Fig. 4. Since Fig. 6 represents motion along the axis of the ellipse, it should not be identical to Figs. 4 or 5, nor should the results be symmetric about the primary focus as Figs. 4 and 5 are. The absolute magnitude of the collection efficiency, corresponding to the scattering point being at the primary focus, was 71.5%. Since the elliptical surface is 80% reflective, the efficiency calculated by the computer is 57.1%, in excellent agreement with the previous two determinations.

III-2.1-3. Determination of Sodium Flux. In the derivation of the relations to determine the flux of sodium atoms from the detected count rate (Chapter II, Section II-1.3), the normalized position dependent optical collection efficiency, $n(y,z)$, was used. We are now at the point where this function can be numerically approximated, using

Figs. III-4, 5 and 6. First, remember that the z axis is along the laser beam, x along the flow direction (corresponding to Fig. III-5), making y along the axis of the ellipse (the origin of this system is at the primary focus). Notice also that the efficiency is a function of x [i.e., now $n(y,z) \rightarrow n(x,y,z)$], which was not included in the derivation (Eqs. II-29 to II-32). To correctly take all these features into account would unnecessarily complicate the relations mentioned above, so the efficiency will be replaced by an average value and taken out of the integrals. The procedure used to calculate the average is as follows. The integrals over dy and dz give an effective area through which the detectable flux is flowing. To find this area, the two curves (Figs. III-4 and III-6, computer generated curves) are numerically integrated. The value of this integral is then set equal to the area of a rectangle of height 1, and the corresponding length of the rectangle found (numerically equal to the value of the integral in this case). The calculated effective length Lz is then used in the evaluation of the integral. The effective length Ly is used if it is less than 2w, if not 2w is used as the effective length in this direction. From the integration, Lz = 2.0 mm and Ly = 1.54 mm. Over this rectangle of 1.54 mm x 2.00 mm then, $n(y,z) = 1$. To evaluate the exact contribution of the integrand over the y direction, as well as to find the effect of the changing efficiency in the x (flow) direction, one must use a particular value of w (the beam waist). Using this value of w, the curve in Fig. III-5 (x direction) is numerically integrated with limits ± w. The function F(y/w) is also integrated over ± w (or ± Ly/2, whichever is less). From the value of the integral over x, one obtains an average efficiency over the length 2w. When a beam waist of 400 μm was used, this average

value was .78. The value of the integral over y gives .61 mm. Therefore, combining all the contributions Eq. (II-30) becomes

$$\phi = \frac{T_r}{\varepsilon \eta_o F(o)} \quad \frac{1}{(.78)(1.21 \times 10^{-2}\ \text{cm}^2}$$

$$= 106 \frac{T_r}{\varepsilon \eta_o F(o)} \qquad (7)$$

where F(o) is the number of photons emitted by the atom going through the center of the beam, T_r the total detected fluorescence rate, ε is the quantum efficiency of the PMT, η_o is the peak optical collection efficiency and ϕ the flux of sodium atoms. From Eq. (II-32), the number of atoms passing through the observing column per second (k) is then

$$k = \frac{(1.6 \times 10^{-2}\ \text{cm}^2) T_r}{\varepsilon \eta_o F(o)} \quad \frac{1}{(.78)(1.21 \times 10^{-2}\ \text{cm}^2}$$

$$= 1.70 \frac{T_r}{\varepsilon \eta_o F(o)} \qquad (8)$$

where the factor $1.6 \times 10^{-2}\ \text{cm}^2$ is the A in Eq. (II-32). The ratio of $1.6 \times 10^{-2}\ \text{cm}^2 / 1.21 \times 10^{-2}\ \text{cm}^2$ accounts for the average take over the impact parameters for the atom. Using ε as 2.8% (from Section III-2.1-1) and η_o = 57%, then

$$k = 106.5 \frac{T_r}{F(o)} \qquad (9)$$

The number 106.5 just represents the inverse of the actual total system efficiency, which can also be calculated from Rayleigh scattering measurements as explained below.

III-2.1-4. Total Measured Efficiency of the System. The total efficiency of the system was also determined on a daily basis (when data was taken) from Rayleigh scattering off the background gas. The relative ease of making the measurements involved in this determination also allowed the optical alignment of the system to be adjusted slightly to get the best efficiency. The determination was accomplished by means of the following procedure.

Before the background gas was put into the cell, a count rate corresponding to a given power, P_o, was taken (normally the cell pressure was about 50mTorr). A flow of gas was then established and the cell pressure was allowed to increase to 200 Torr by partially valving off the pumping station. At this pressure, another count rate was taken (the sodium source had not been turned on yet). By comparing the two count rates, taking into consideration any laser power change, we can determine the increase in the measured count due to the background gas.

If I(o) is the incident intensity and I(z) is the intensity after traveling a distance, z, through the gas, then

$$I(z) = I(o)\ EXP(-\eta\sigma z) \qquad (10)$$

where η is the density of gas atoms and σ the Rayleigh scattering cross section. The total amount scattered out of the beam is just

$$I(o) - I(z) = I_o[1 - EXP(-\eta\sigma z)] \qquad (11)$$

Integrating expression (11) over the cross section of the viewing volume (determined either by the beam itself or the collection optics, whichever

is smaller) will give the total power scattered out of the laser beam in the distance z. The effective length seen by the PMT is 2 mm (calculated in the last section and labeled as Lz), the density is $6.439 \times 10^{18}/cm^3$ (at 200 Torr and 300°K) and the total Rayleigh cross section is 6.58×10^{-29} cm^2 [from reference (37), modified for scattering by 5890 Å light]. Using these values, the quantity $\eta\sigma z$ is 8.47×10^{-11}. The quantity $1 - EXP(-\eta\sigma L_z)$ can then be replaced by just $\eta\sigma L_z$, making the intensity scattered out of the beam

$$I_{scat} = I(o)\eta\sigma L_z \quad . \tag{11}$$

For a small beam (so that the ellipse sees the whole cross sectioned area of the beam) and 1 mW of power (2.966×10^{15} photons for light at 5890 Å), the total number of photons per second scattered out of the beam is

$$Ph(scat) = (2.966 \times 10^{15})(8.47 \times 10^{-11}) = 2.51 \times 10^5 \text{ photons/sec} \tag{12}$$

If we let ΔN be the measured count rate due to Rayleigh scattering, then the total system efficiency (T_{eff}) is

$$T_{eff} = [\varepsilon\eta_o(x,y,z)] = \frac{\Delta N}{2.51 \times 10^5} \tag{13}$$

Even if the beam is larger so that the viewing volume is determined by the ellipse and not the laser beam, (13) is still a measure of the efficiency of the system. The difference in count rates, ΔN, implicitly takes the integrals, done in the last section, into account. The total

efficiency as determined in this way, ranged from 4% down to approximately 1.4% during the course of the experiment. The lower values were obtained in the later stages of the experiment (roughly corresponding to the degradation of the PMT quantum efficiency as noted earlier).

III-2.1-5. Measurement of the Laser Beam Waist. The most important peripheral measurement needed during this entire experiment was that of the laser beam waist. This value was used in the diffusion analysis, single beam velocity analysis, determination of the laser power needed in any run, and, less critically, even in the determination of the amount of sodium present. The procedure used to measure the waist will be discussed in this section. Also the long term stability of the laser beam as it relates to the beam waist and the uncertainty in the value of the waist will be discussed.

The actual measurements on the laser beam were carried out by translating a power meter (masked by a $\sim$30 μm aperture) across the beam in two orthogonal directions. These directions were along the axis of the ellipsoid and the flow axis. To make these measurements, the cell was removed and a glass compensator plate was put into the beam to mimic the input window of the cell. [Actually since another 3/8" thick quartz window was not available, 5/16" of alumino-silicate (Corning 1723) glass was used.] The power meter was mounted on an x-y-z translator stage, with vernier micrometer [accuracy $\pm 5 \times 10^{-5}$ inches ($\pm$ 1.27 μm)]. The step size of the translation was adjusted, when possible, to get about 20 measurement points between the $1/e^2$ points of the beam. For experiments involving single beams, the beam was also measured at various distances from the viewing volume along the beam. Typically a full beam profile in both directions was taken at the "center" of the viewing area.

As the power meter was moved along the beam (in three or four steps of $2.5\ 10^{-2}$ inches) only measurements corresponding to the $1/e^2$ points of the beam were taken. For experiments that involved two beams (separated vertically), only vertical profiles were taken along with the beam separation at the viewing area. Since the beams were made very close to parallel, these measurements were considered adequate. For measurements along a particular axis, the power meter was translated in one direction to avoid any backlash problems in the micrometer movements.

The beam profiles were analyzed using the non-linear least squares fitting routines BMDO7Rand later BMDP3R(described in Appendix B). The fitting function used for each direction was of the form

$$h(x)=\left\{\frac{I_o w_y}{4}\,\mathrm{erf}\left(\sqrt{\frac{\pi}{2}}\,\frac{a}{2w_y}\right)\right\} w_x \left\{\mathrm{erf}\left[\frac{\sqrt{2}}{w_x}\left(x-x_o+\frac{\sqrt{\pi}a}{4}\right)\right] - \mathrm{erf}\left[\frac{\sqrt{2}}{w_x}\left(x-x_o-\frac{\sqrt{\pi}a}{4}\right)\right]\right\} \qquad (14)$$

where the first term in brackets is treated as a parameter, w_x is a parameter (the beam waist), x_o is a parameter (the position of the center of the beam), and a is the diameter of the aperature used to mask off the power meter. For the fitting function on the other direction, "y", w_x and w_y are replaced with w_y and w_x respectively, and x and x_o are replaced with y and y_o. The derivation of this function is given in Appendix A. The ordered pairs $[x,h^*(x)]$ or $[y,h^*(y)]$ were given to the fitting routine as well as estimates of the three parameters. A sample measured profile, along with the computer generated fit is presented in Fig.III-7. One can see that the computer fit is in very good agreement with the measured distribution. (h^* represents the measured value.)

Since the value of the beam waist is important for the analysis of the velocity and diffusion data, the uncertainties involved in this parameter need to be discussed. These uncertainties come from two different sources. First is the error estimate calculated by the computer, which is related to how "well" its own generated points agree with the experimental points. The magnitude of this uncertainty is quite small and is on the order of 2% (or less) of the estimated beam waist as shown in Table III-1). The second source of error comes from the laser itself and can be much larger than 2%. This source is the stability of the laser over a given time period and/or the changes in the beam waist measurements that occur on a day-to-day basis. In order to estimate the magnitude of this last error source, beam profiles were taken on successive days (with only routine adjustment of the laser at the beginning of the measurement period). Also the laser was allowed to stay on for an extended period of time and the beam profiles were measured several times during that period. The results of these measurements are also shown in Table III-1.

During the period over which the data in Table III-1 was taken, the laser was on continuously from 7:30 AM (4/5/80) to 4:30 PM (4/6/80). The laser was turned on at 7:30 PM (4/7/80) to collect the next profile measurements. During the first time period, the laser was adjusted before the 11:30 AM measurement and also needed adjustment just before the 10:30 AM (4/6/80) profile measurement. The waists corresponding to the last two measurements are not to be compared directly with the other waists. The difference between the 11:00 AM (4/9/80) measurement and the last measurement on 4/6/80, or the difference between the 8/31 and 8/30 measurements indicates the magnitude of the changes that are

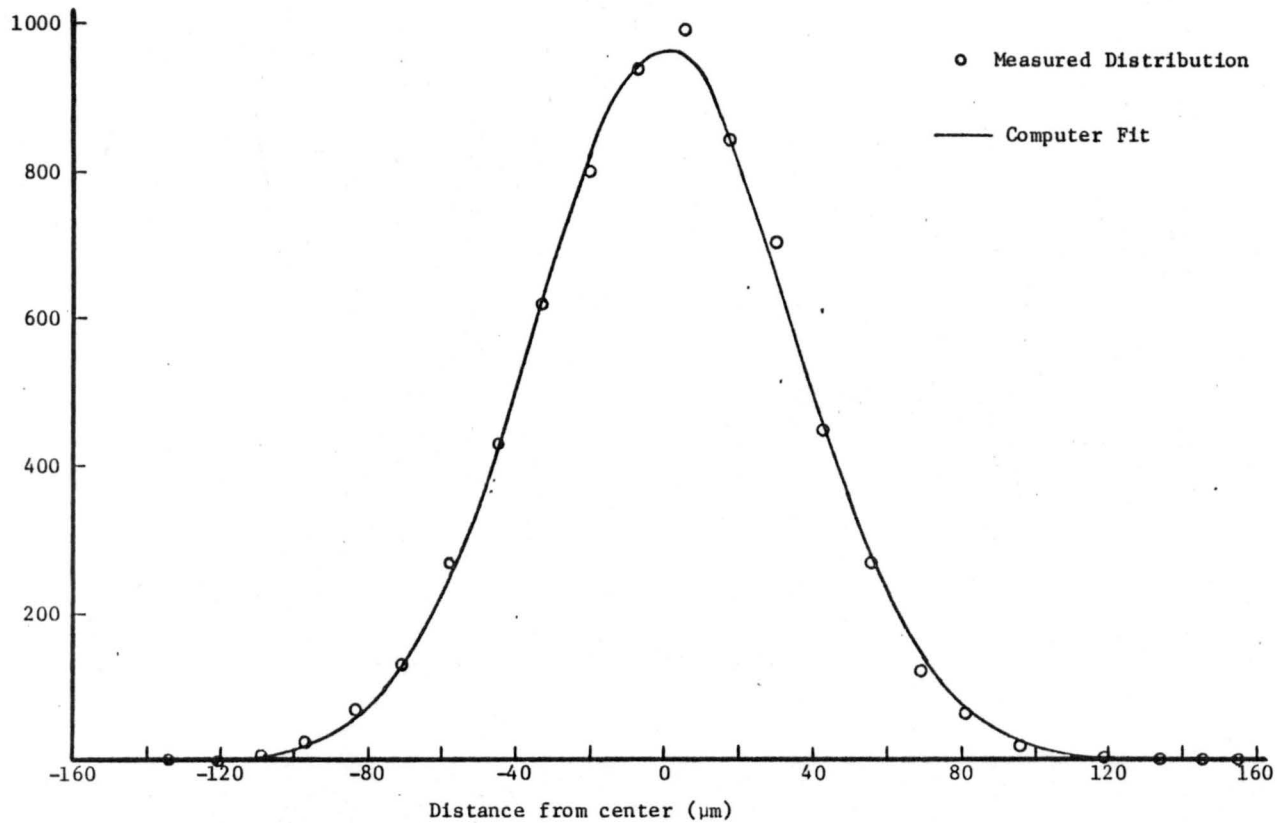

Fig. III-7. Laser Beam Profile

possible just from day-to-day variations (upwards to 15%). For all the determinations of the waist as listed in Table III-1, the "Horizontal" refers to the direction along the axis of the ellipse and "Vertical" is along the flow axis.

It was noticed, over the course of the experiment, that as a general rule the largest changes between successive measurements occurred when routine maintenance or alignment was performed on the dye laser between the measurements. Normally when such maintenance was performed, the waist was remeasured before any experiment was tried. Also for diffusion measurements, since the diffusion constant depends on the square of the waist [see Eq. (II-35)], a measurement of the profile immediately before and after the set of runs was taken when possible. The average of these two measurements was used unless they differed substantially (for example, 20% high or low). This averaging process would hopefully reduce the errors in comparing the individual sets of data to one another.

III-2.2. Specific Procedures Used in Performing the Experiments. The procedures explained in the next several sections deal with the specifics of getting the system configured to do an experiment and the execution of the experiment itself. These procedures include the preparation of the sodium source, optical alignment of the system, and the mechanics of doing a set of velocity experiments or diffusion experiments. Also a discussion of the procedures used to analyze the data will be given.

III-2.2-1. Optical Alignment of System. In order to insure the best possible signal from the atoms, care had to be taken when optically aligning the system. This alignment involved two separate procedures. The first was to set the PMT in its proper place with respect to the

Table III-1. Measurements on the stability of the laser beam waists.

Date	Time	Beam Waist			
		Horizontal		Vertical	
		Waist (μm)	% Deviation from Previous Measurement	Waist (μm)	% Deviation from Previous Measurement
4/5/80	11:30 AM	70.00 ± .70	-----	58.98 ± 1.23	-----
	4:00 PM	69.65 ± .33	- 0.5	59.73 ± 1.16	+ 1.3
	6:00	67.81 ± .56	- 2.6	57.46 ± .65	- 3.8
	8:00	68.02 ± .49	+ 0.5	56.53 ± .90	- 1.6
	10:00	69.02 ± .64	+ 1.5	53.24 ± .70	- 5.8
4/6/80	2:30 AM	68.92 ± .47	- 0.1	58.02 ± .56	+ 9.0
	4:30	68.48 ± .45	- 0.6	58.35 ± .99	+ 0.6
	6:30	68.23 ± .60	- 0.4	59.66 ± 1.08	+ 2.2
	8:30	66.59 ± .48	- 2.4	51.56 ± 1.60	-13.6
	10:30	66.16 ± 1.04	- 0.6	52.61 ± 1.22	+ 2.0
	12:30 PM	66.61 ± .51	+ 0.7	53.39 ± 1.10	+ 1.5
4/7/80	11:00 AM	63.16 ± .97	- 5.2	50.43 ± .83	- 5.5
8/30/79	---	75.36 ± 2.23	-----	66.35 ± 1.83	-----
8/31/79	---	86.25 ± 2.33	+14.4	60.73 ± 1.78	+ 8.5

ellipsoidal collector. After the initial alignment of the PMT in this fashion, the PMT housing was rarely moved, making it unnecessary to continually reposition the photomultiplier. The second procedure involved aligning the laser with the cell on a day-to-day basis.

The PMT was aligned when the efficiency of the ellipsoid was being determined using the steel sphere. When it was determined that the sphere was at the primary focus of the ellipse, the photomultiplier housing was positioned and low voltage was applied to the photocathode. The PMT housing was translated both horizontally and vertically until a position of maximum signal was found. The PMT housing was then fixed to the optical table. Micrometer settings from the cell's two translation stages were also noted. Since the cell was constantly being moved to measure the beam, this assured that the cell could always be moved to the proper position with respect to the PMT. After the ball was removed from the ellipsoid, the housing was moved slightly to pick up the signal from Rayleigh scattering off of nitrogen that was put into the cell.

While the above alignment was taking place, two diaphragms were also placed in the laser beam, one after the cell and the other before the cell, with approximately 1.6 m between them. Fixing the position of these two apertures allowed us to reposition the beam, when needed, in a reproducible manner. When a particular beam geometry (one or two beams) was chosen, and the desired waist had been produced, the laser and the cell were aligned using these apertures. Just prior to the commencement of the experiment, the position of the beam was usually adjusted slightly to minimize the noise due to detected scattered light.

III-2.2-2. The Sodium Source. In order to measure the flow velocity or diffusional motion of sodium atoms, a method had to be devised of getting the atoms into the viewing volume. This was accomplished by inserting a small piece of sodium metal into the input tube on the ellipsoid. The sodium was wrapped with a length of resistance wire to provide the necessary heating. Normally the sodium source was put into the cell after the beam had been configured, roughly aligned and measured. The sodium chip was prepared as follows.

A small piece of sodium metal was selectively cut from a larger block. The sodium was then wrapped (by "hand") in a normal atmosphere, with a length of 0.0035" diameter insulated manganin wire, the resistance of which is 23.8 ohms/ft. About 3/8" of the insulation was removed from both ends of the wire. Typically a total length of 8" of manganin wire was used, approximately 6" of which was actually wrapped tightly around the sodium. No precautions were taken to avoid having more than one layer of wire wrapping the sodium chip. After the wire was wrapped around the chip, the ends were soldered onto some small gauge (but larger than .0035") insulated copper wires which were connected to the outside of the cell through a vacuum feed-through arrangement. The soldered connections were coated with a small quantity of GE 7031 varnish to provide electrical insulation, so the soldered connections would not short together. Before the sodium (attached to the copper wire) was put in the input tube, the chip (and manganin) were immersed in a solution of xylene and acetone to remove the oxide layer.[37] The solution was made up of enough xylene to completely cover the sodium chip and then a few drops of acetone were added. The sodium was allowed to stay in the bath between 2 and 5 minutes (until the oxide appeared gone).

When the sodium was taken out of the xylene/acetone mixture, it was quickly put into the input tube of the cell (the cell had been back filled to 1 atmosphere of He) and the cell was evacuated. The resistance between the two copper wires was monitored to make sure that the solder joints remained electrically isolated from each other. The copper wires were then connected to a current limited power supply in order to heat the sodium to the needed temperature. (The current limited power supply not only supplied the current to heat the sodium up, but also served as an "active" check on the resistance of the manganin wire.)

III-2.2-3. Collection of Flow Velocity Data. Once the entire system had been set up, the particular experiment could start. In this section, the mechanics of doing a set of velocity measurements will be described. This procedure is basically the same for both one beam and two beam laser geometries. Also described is a program that mimics the correlator, which was used as a tool to see if, under the experimental conditions (noise level, system efficiency, beam waist and transit time of the atom across the beam) a correlation function for an atom could be expected to be seen.

To configure the system for flow velocity measurements, normally an expected velocity, a noise level and a value of the diffusion constant were assumed. With those three numbers, a waist (and beam separation, if needed) could be determined. The values of the waist chosen would be such that $2w/v < w^2/4D$ (transit due to velocity is less than the characteristic diffusion time). See Fig. III-8 for a comparison of transit times and diffusion times as a function of laser beam waist. Another condition that needed satisfying was

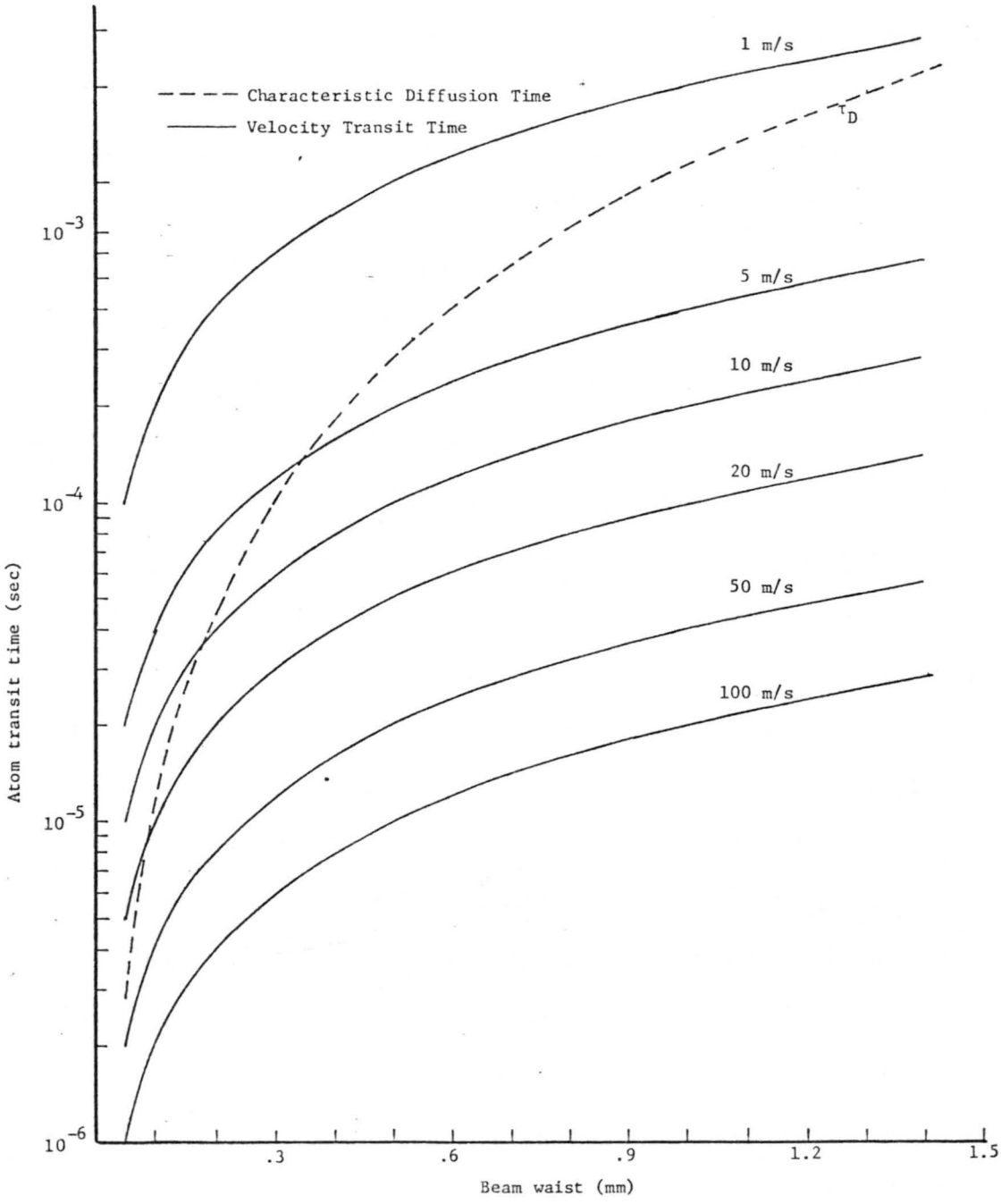

Fig. III-8. Atom transit time vs. beam waist.

$$[F(o)/(2w/v)]\tau_s > \bar{n}\tau_s \qquad (15)$$

where F(o) is the number of fluorescence photons emitted by the atom going through the center of the beam, τ_s is the sample time for the correlator (normally set so that the atom would cross the beam in 5-10 channels) and $\bar{n}$ is the average noise count rate. The bracketed term represents the "average" number of fluorescence counts per unit time during the atom's crossing. Therefore relation (15) essentially expresses the desire for the average signal counts in a sample time to be greater than the average noise counts in the sample.

In order to aid in the set-up of the system, a computer program was developed to model the fluorescence signal from an atom, the noise level and the expected single-clipped autocorrelative function from the counts of signal plus noise. The signal was assumed distributed over a given number of correlator sample times (as a gaussian) and a noise count for each sample was calculated assuming a poisson distribution about the measured average value. Using a random number generator, the noise was distributed randomly in 100 sample times. The calculated signal distribution was added to this distribution and the single clipped autocorrelation function of this input was generated for various clipping levels. These correlation functions were plotted for convenience by a line plotter. If no correlations could be seen, different parameters would be changed to see for what condition a distinct correlation function could be expected to be observed. The parameters that were changed could include the number of expected fluorescence photons emitted by the atom, how many channels the signal would be spread over and the

noise level. When a situation was found that produced a recognizable correlation function, the experimental set-up would be modified to match those conditions as best as possible.

After the system was completely set up, the data (correlation functions) were acquired as follows. A helium flow rate was imposed on the cell and the ambient pressure in the cell was allowed to increase to about 200 Torr. (This pressure was measured using a mercury manometer. In the later stages of the experiment, an oil manometer was also installed to measure the pressure drop across the nozzle.) The laser (tuned to 5890 Å) was directed through the cell and the count rate detected by the PMT was monitored. The current through the sodium heater wire was increased until a measurable fluorescence signal from the sodium was seen. The correlator was set up to "look" for 100 sample times. From the observed sodium fluorescence count rate and from Eq. (9), the average number of atoms passing through the viewing volume was determined. Multiplying this number by 100 τ_s gives the number atoms in the viewing volume during a measurement time. The amount of sodium was adjusted so that, on the average, there was less than one atom in the viewing volume during a measurement time.

When the proper level of sodium was reached, autocorrelation functions characteristic of a single atom flowing through the beam were looked for. First the laser would be blocked and the correlator turned on twice (each time for 100 sample times). The purpose of this action was to clear any residual signal left in digital storage in the correlation. The laser was then unblocked and a "data" run was taken. The correlation function that was generated was examined on an oscilloscope. If only random fluctuations were seen, then the process was repeated

(two tries with the laser blocked, and one with the laser unblocked). Since the density of sodium was usually quite low, most correlation functions did not show any discernible form. The functions which did show the form expected from an atom crossing the beam were photographed and the information in the correlator printed out on a teletype for later analysis. Correlation functions were accumulated both on and off the sodium resonance. This was done to see if any small particles were in the system (since they would scatter light both on or off resonance) whose signal could be comparable to the sodium fluorescence burst. If enough attempts were made (both on and off resonance), then one could use simple statistical arguments to determine the percentage of the correlations found on resonance which were due to single atoms.

In addition to the attempts to measure single atom autocorrelation functions, long-term correlation functions were also generated. The accumulation times for these runs were from 100 seconds to approximately .5 seconds. These runs were made in order to determine the length of time needed for a correlation function to build up and still be able to measure the velocity reliably. Generally these correlation functions were quite clear and the measurement of the width (single beam) or the separation of the two peaks (two beam) could be made accurately.

The single beam velocity correlations were analyzed assuming that the τ (the correlation parameter) dependence was of the form given by Eq. (II-54), i.e., gaussian with a width in τ given by (55). By measuring τ_v, one can calculate the velocity using [Eq. (II-56)]

$$v = \frac{\sqrt{2}w_x}{\tau_v} \quad . \qquad \text{(II-56)}$$

The errors involved in this determination can arise from three different sources. The first two come from the errors inherent in the assumed value of w_x (as discussed earlier) and the error in estimating the value of τ_v. A reasonable error limit on this quantity is 1-2 channels, since the correlation functions for single atoms are generally of poor quality (see next chapter). For most cases, this uncertainty corresponds to a 20% error limit. Combining this limit with the error limit in w_x (~10%), one gets a total error of 30% on the velocities measured in this way. For the correlation functions generated by averaging over many samples (10^4 or 10^5 instead of 100), the error in τ_v is probably less than 5%, or a total error of 15%.

The third source of error comes from the assumption that the correlation function is a simple gaussian [this assumption was used in the derivation of (II-56)]. As the intensity ratio, I_o/I_s, approaches 0, this assumption becomes more valid. As mentioned in Section II-2.2, the integral for the autocorrelation was numerically evaluated for several different values of I_o/I_s and the widths of these functions were measured (the width being defined as the distance, in time, to the function's $1/e^2$ point). Assuming that the generated function was a simple gaussian, that is

$$C_1(\tau) \propto \mathrm{EXP}(-v^2\tau^2/w_x^2) \qquad (16)$$

the velocity corresponding to the computer generated autocorrelation function was calculated. This calculated velocity was compared to the actual velocity used in generation the correlation function. The plot of the result is given in Fig. III-9. The abscissa is in I_o/I_s units

and the ordinate is v_a/v_m where v_a is the actual velocity, and v_m is the velocity calculated from the width of the observed correlation function. One can see that for an optimum value of $I_o/I_s = 1.91$, the actual velocity is 1.21 times the calculated velocity. Since this source of error can be corrected for the error limits on the velocity would remain as given above.

When the two laser beam geometry was employed, the determination of the velocity was less complicated. All that had to be done was to measure the number of channels between the two characteristic peaks and multiply by the time per sample. For long term correlations, the separation between the two peaks in the observed correlation could be found to within ± .5 channels, corresponding to about a 5% error or less. (The separation of the two peaks in the correlation function was usually 10-20 channels.) Since the spatial separation of the two beams was on the order of 1 mm, which could be measured to ± .002 mm (0.2% error), this source did not contribute appreciably to the error. Therefore, the error for this case is estimated to be $\leq$ 5%.

III-2.2-4. Collection of Diffusion Data. The acquisition of data related to the diffusion constant was somewhat less complicated, though more time-consuming than the procedure involved in taking velocity measurements. In this section the procedures followed to collect the data will be explained. Also included will be a discussion of the fitting functions used in the computer analysis of the observed correlation functions.

For the diffusion constant measurements (actually, the measured quantity was the characteristic diffusion time), the laser beam was set up with a smaller waist than was used in the velocity runs. Normally,

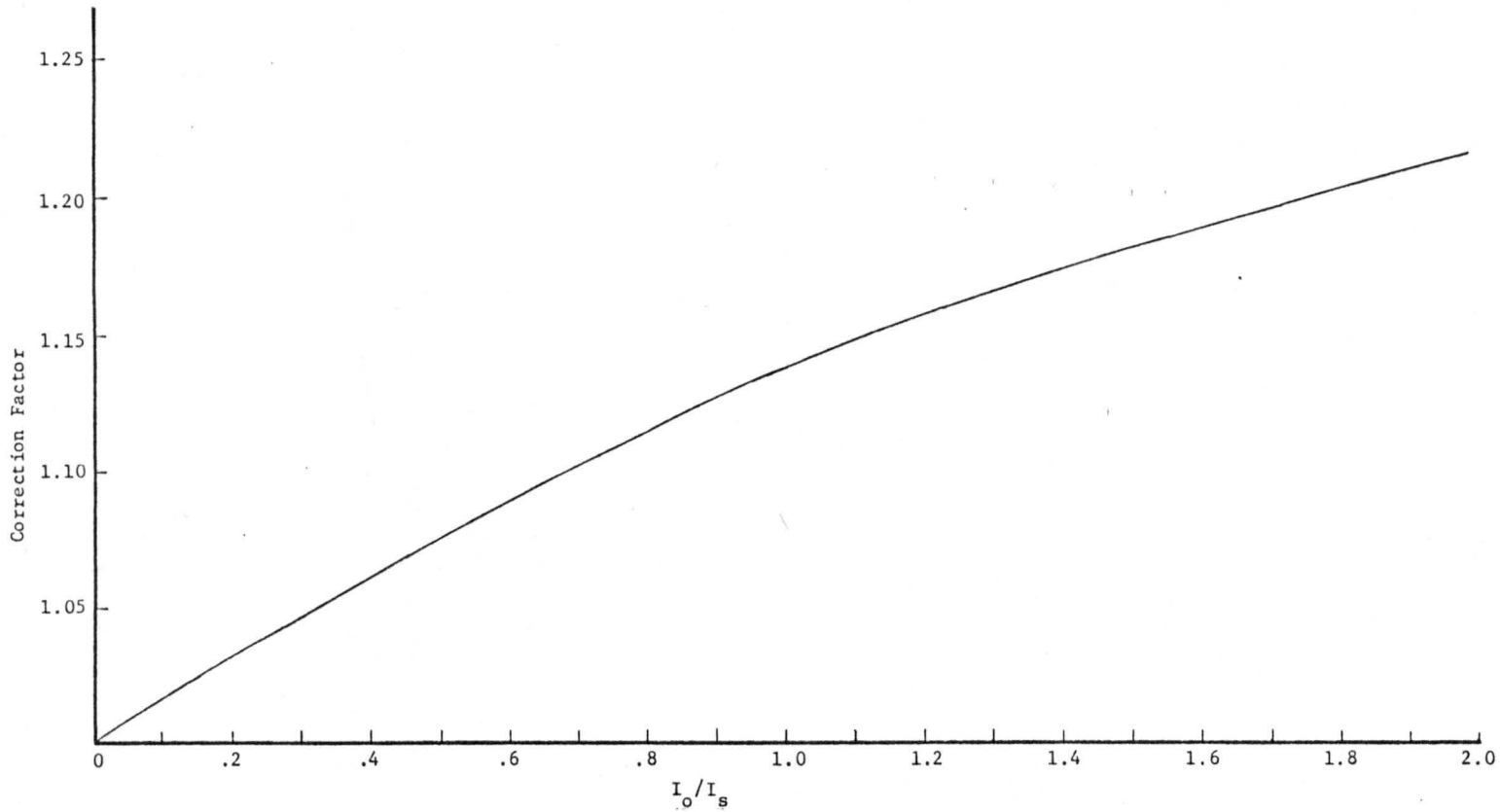

Fig. III-9. Correction Factor for Measured Single Beam Velocity vs. I_o/I_s

a beam waist of between 80 and 200 μm was used. This was usually sufficient to put the system into the diffusion dominated regime. Also the laser beam was more extensively measured for the diffusion measurements because of the w^2 factor relating the diffusion time and the diffusion constant. For the ground state diffusion runs, low intensities ($I_o/I_s \leq .1$) were used, therefore the excited state contributions to the measured characteristic diffusion time was low (about 6% or less). Also the observed correlation should be given by Eq. (II-63) for these conditions. For excited state data intensities up to $I_o/I_s=2$ were used (this limit was generally determined by the maximum rated current limit of our PMT). All the diffusion constant data was taken using a one beam geometry.

Once the experimental system was configured appropriately, the laser beam aligned, and the sodium source loaded into the cell, the actual experiment could be started. A small flow of an inert gas (helium, argon or neon) was imposed on the system. The vacuum station was partially valved off in order to let the cell pressure rise to the desired value. A voltage was put across the heater wire leads and increased until a fluorescence signal was seen (either by monitoring the rate meter or by looking at the correlation function). Before sodium was found, normally particles would be generated and flow through the beam. Correlation functions characteristic of a velocity dominant system (with respect to the particles) could be seen from these particles and their velocity measured (using this value for the velocity, we could confirm that we were in the diffusion dominant situation). Once a signal due to the sodium was found, the long term correlation functions could be acquired. Typically the time spent acquiring a correlation

function ranged from 1 minute to about 25 minutes. (This time depended on the sodium density and the background pressure.)

At each value of pressure (or intensity, if we were collecting excited state diffusion data), several, usually five, correlation functions were taken using somewhat different values of the correlator sample time. This allowed comparisons to be made in order to determine whether any systematic errors arose due to the particular choice of the sample time. The sample time was usually chosen so that the characteristic diffusion time would span 8-15 channels on our correlator. After a set of runs were completed, the laser was blocked and the thermocouple was extended into the viewing volume. The temperature was recorded and the thermocouple was retracted. The pressure (or intensity) was changed and another such set of correlation functions were taken. The pressure range used for the ground state measurements was 100 Torr to 400 Torr. The excited state measurements were taken at 200 Torr and the intensity was varied from approximately I_o/I_s = .02 to 2. A hard copy of the correlator channel contents was produced for every run.

In order to analyze the correlation functions, a least squares fit was done to each function. From this fit, the characteristic diffusion time was extracted. The fitting routine used (from the Biomedical Program Library) was initially BMD07R and more recently BMDP3R. The general operation of these routines is given in Appendix B. Two fitting functions were used, with these routines, as the expected form for the correlation functions. The first was

$$g(\tau) = A + \frac{B}{\sqrt{(1+\tau/\tau_D)(1+G\tau/\tau_D)}} \qquad (17)$$

where A is a background level, B is an amplitude factor [equal to $NR_s^2 w_z \pi/4$ from Eq. (II-63)], τ_D is the characteristic diffusion time for the "long" dimension of the laser beam intensity profile and G is the square of the ratio of the long dimension to the short dimension of our elliptical laser beam. Equation (17) is basically the same as Eq. (II-63) with a background constant added. The parameters A, B and τ_D are those used by the computer to generate the least squares fit. The values of these parameters, corresponding to the "best" fit, are determined by the computer.

Equation (17) does not allow any dependence on the flow velocity (which was assumed insignificant). In order to check this assumption, another fitting function was used of the form of Eq. (II-54) and is given by

$$g(\tau) = A + \frac{B}{\sqrt{(1+\tau/\tau_D)(1+G\tau/\tau_D)}} \text{EXP}\left[-\frac{v^2\tau^2}{w_x^2}/(1+G\tau/\tau_D)\right] \qquad (18)$$

where there are four parameters to be used: A, B, τ_D and v where A, B, G and τ_D have the same meaning as before and v is the velocity. An example of a diffusion autocorrelation function along with the computer fit (18) is presented in Fig. III-10. One can see that the fit is quite good for this particular data run. The above fitting function, as well as (17), were used for both the ground state and excited state analyses. (The extent of any problem this may have caused in the excited state analysis for the high intensity runs is uncertain.)

The value of τ_D that was extracted from the fitting from these two fitting routines (17) and (18), were used to calculate the diffusion constant using the defining relation for τ_D [Eq. (II-35b)]. Using the

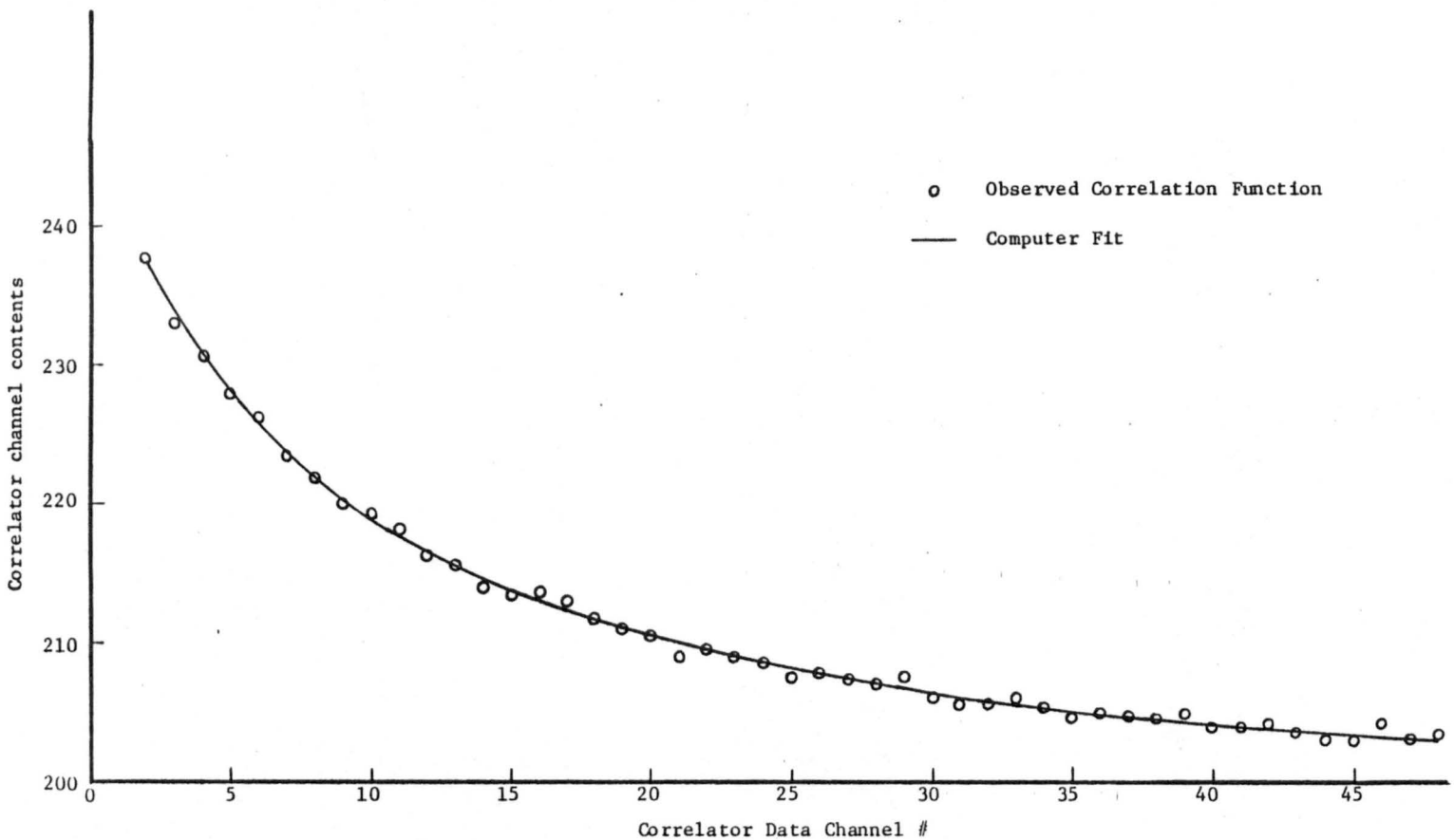

Fig. III-10. Observed correlation function and computer fit.

temperatures that were measured after each set of diffusion runs, these values of τ_D were corrected to 315°K assuming a $T^{-3/2}$ variation. [The value of 315°K was chosen for normalization because the deviations of the measured temperatures from this value were not very large (at most about 10°K), so the corresponding correction is small (about 5% for 10°K difference). This has the advantage of reducing any errors introduced by the $T^{-3/2}$ dependence assumption, since the collision integrals, in Eq. (II-72) are also somewhat temperature dependent.]

As a further step in the data reduction for the ground state diffusion measurements, the values obtained from τ_D were multiplied by the pressure under which the associated diffusion time was measured. This product, Dp, should be independent of the pressure. For a constant temperature, a plot of Dp versus p should yield a straight line parallel to the p axis. The results obtained for τ_D (from the fitting functions) and the corresponding values of Dp will be presented in Chapter IV.

For the excited state measurements, the values of τ_D (un-normalized) were plotted as a function of I_o/I_s. Equation (II-70) was then numerically evaluated for different ratios of D_{exc}/D_{grd}. The value for the ground state diffusion constant (D_{grd}) was chosen such that the value of τ_D extracted by fitting the above theoretical function to (17) matched the value of τ_D for the low intensity (I_o/I_s = .05) experimental runs. The family of curves generated by changing the rates, D_{exc}/D_{grd}, were plotted with the experimental curve. The value of D_{exc}/D_{grd} that gave the closest fit to the data was then determined. These results will be given in Chapter IV.

IV. EXPERIMENTAL RESULTS AND DISCUSSION

Using Fluorescence Correlation Spectroscopy, our group has been studying the motions of sodium atoms for several years. Autocorrelation functions generated from the fluorescence of sodium atoms moving through laser beams and the information they contain related to flow velocities and diffusion constants will be presented in this chapter. This data includes studies of the diffusional motion of ground-state sodium atoms in argon, helium and neon; information about the diffusion constant for the helium-sodium system with the sodium atoms in the excited state; and correlation functions characteristic of one-dimensionally flowing sodium atoms.

IV-1. Flow Velocity Studies

The studies related to measuring the velocity of sodium atoms flowing in one dimension will be considered first. As mentioned previously, we had two different systems for measuring flow velocities, a one and a two laser beam configuration. Data from the one beam experiments includes single atom autocorrelation functions and long term correlations which averaged over many atoms. The two beam correlation functions presented are only from averaging over many atoms.

IV-1.1. Results from Velocity Experiments Using a Single Laser Beam. Figures IV-1, IV-2, IV-3 and IV-4(a) are autocorrelation functions

representing single sodium atoms transiting the laser beam. Although the signal is somewhat noisy , a distinct structure similar to the form predicted in Chapter II (see Fig. II-6) is clearly seen. The velocities calculated from Figs. IV-1 through 5 [except 4(b)] range from 7.4 to 27m/sec. For all these cases, as per the procedure outlined in Chapter III, many attempts (usually > 300) were made to find "distinct" correlation functions with the laser tuned off resonance. Generally correlation functions of the type shown in Fig. IV-4(b) were obtained and no distinct correlations were found (except in Fig. IV-5(a), as will be discussed later). This kind of information implies that the correlation functions observed on resonance were due to sodium atoms.

Table IV-1 gives a summary of the relevant data corresponding to Figs. IV-1 through 5. The velocities given in this table have been corrected for the intensity of the laser according to Fig. III-9. The second and third columns of this table give a comparison of the predicted number of spontaneous photons emitted by an atom [from Eq.(II-21)] to the number of photons calculated from the observed autocorrelation function. This last quantity is determined by extrapolating the correlation function back to 0, and sutracting from the result, the background found from the later channels.[12]) Looking at the results from the first six correlation functions, we see that the number of emitted photons predicted for a single atom exceeds the number measured from the correlation function itself. This is to be expected for a single atom, since Eq.(II-21) gives the prediction for an atom moving through the <u>center</u> of the beam and few atoms would be expected to do that. For Fig. 4(a), the number of "photons" measured is over twice the predicted value. This could be explained by assuming that Fig. 4(a) represents

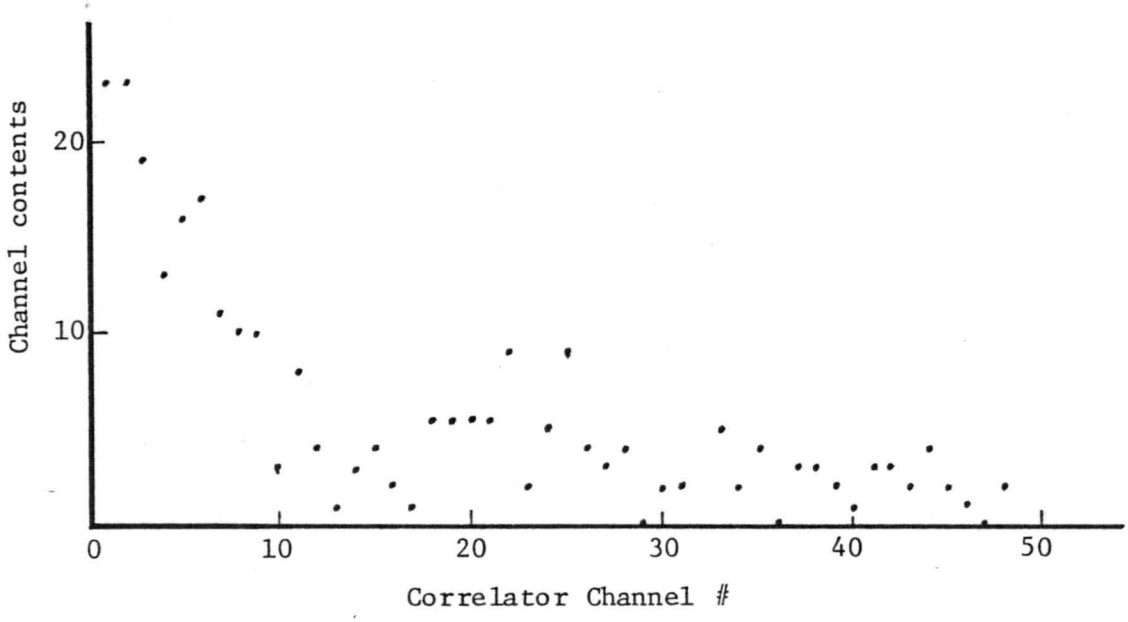

Fig. IV-1(a). Single atom correlation function with 5 μs/channel and a beam waist of 273 μm in flow direction.

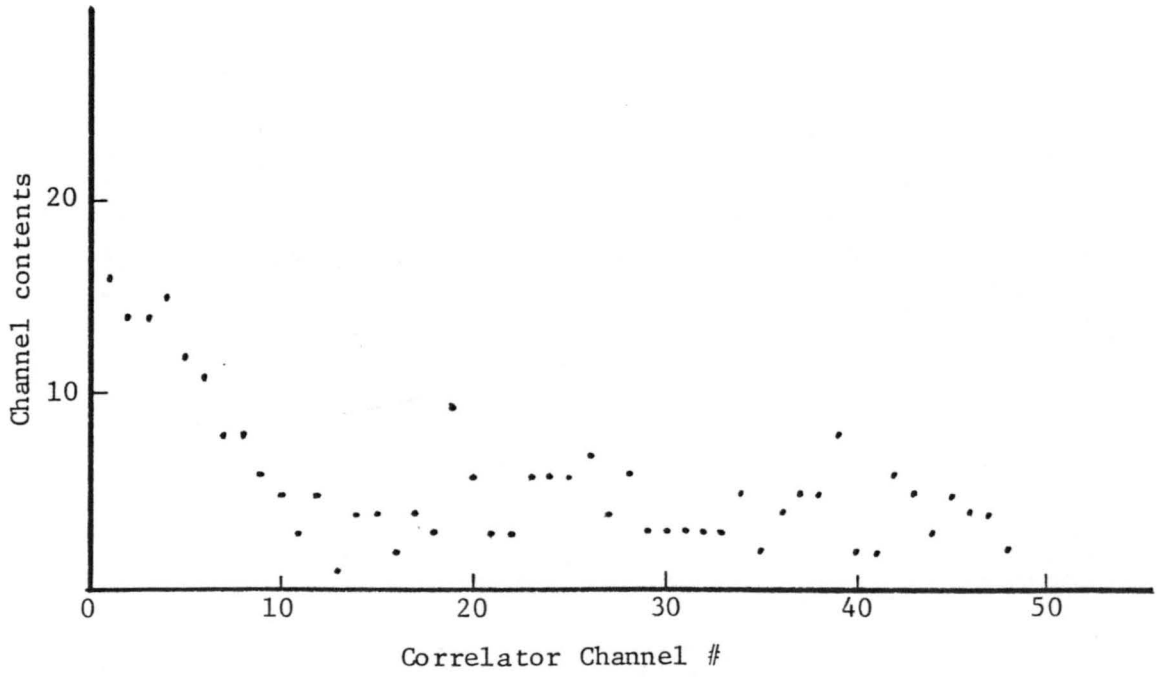

Fig. IV-1(b). Single atom correlation function with 5 μs/channel and a beam waist of 273 μm in flow direction.

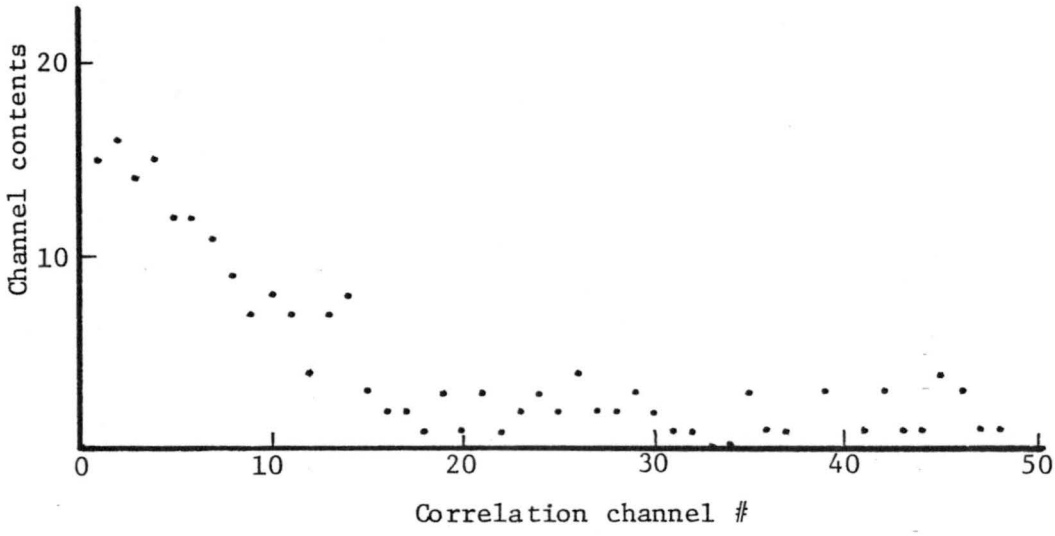

Fig. IV-2(a). Single atom correlation function with 5 μs/sample and a beam waist of 273 μm in flow direction.

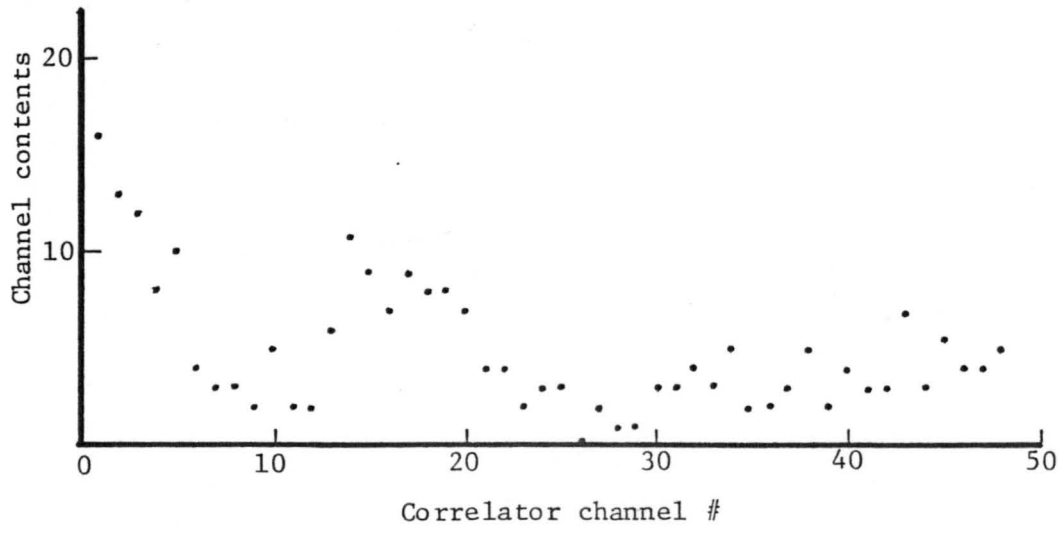

Fig. IV-2(b). Two atom autocorrelation function with 3.3 μs/sample and a beam waist of 273 μm in flow direction.

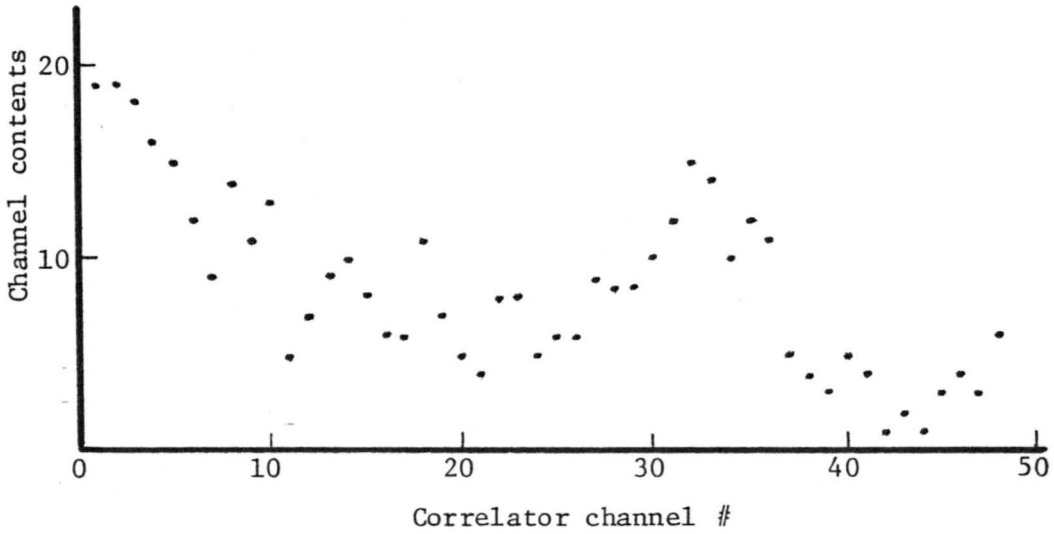

Fig. IV-3(a). Two atom autocorrelation function with 4.5 μs/sample and a beam waist of 273 μm in flow direction.

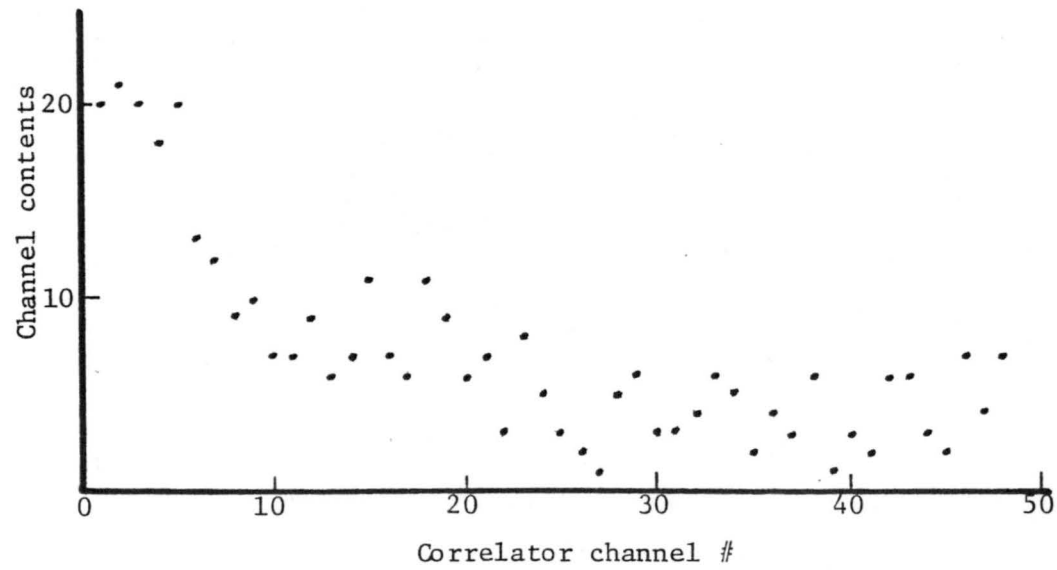

Fig. IV-3(b). Single atom autocorrelation function with 4.5 μs/sample and a beam waist of 273 μm in flow direction.

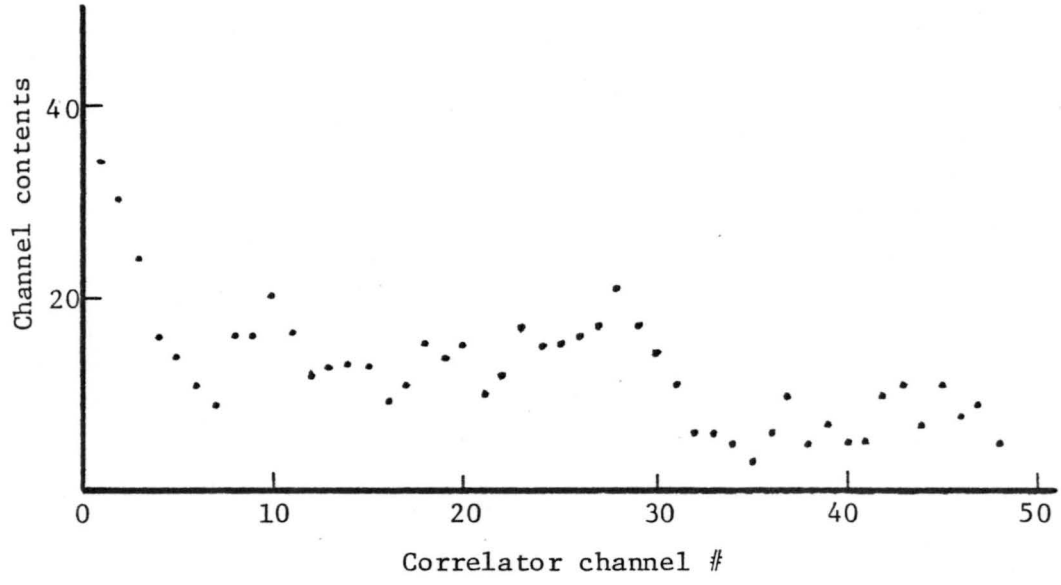

Fig. IV-4(a). Two atom autocorrelation function; 4.5 μs/sample and a beam waist of 273 μm in the flow direction.

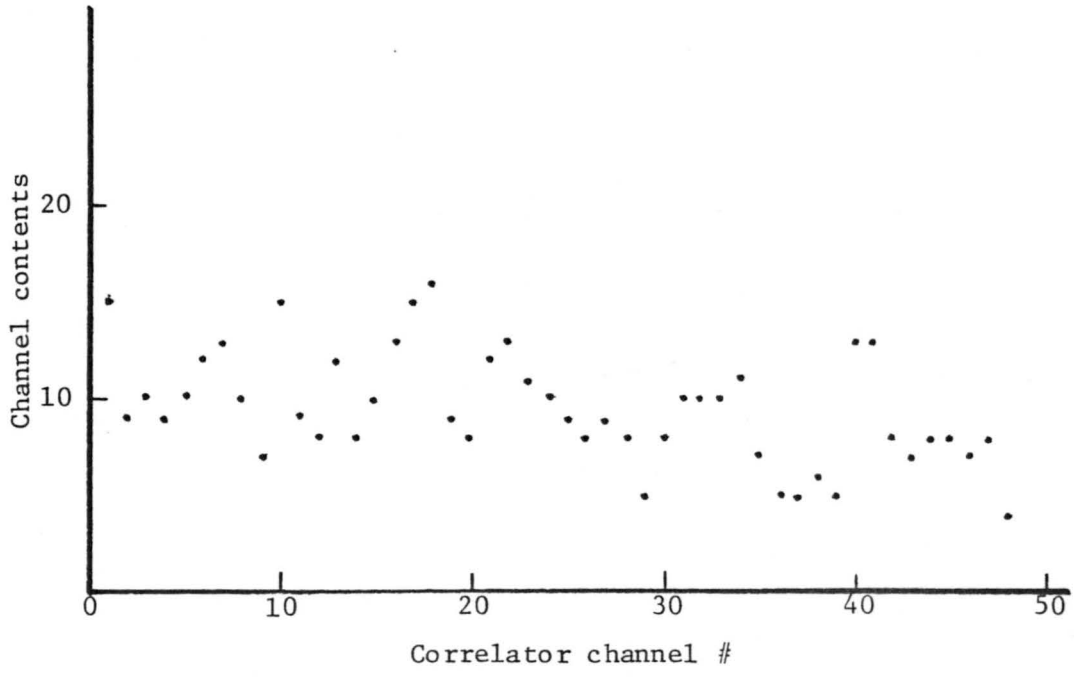

Fig. IV-4(b). Autocorrelation function due to noise.

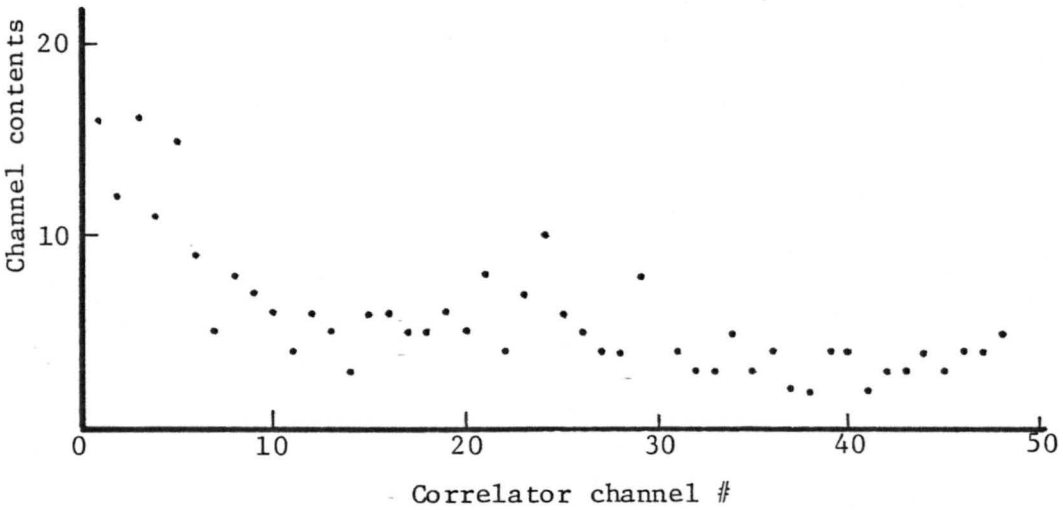

Fig. IV-5(a). Autocorrelation function due to particle with 4.5 μs/sample and a beam waist of 273 μm in the flow direction.

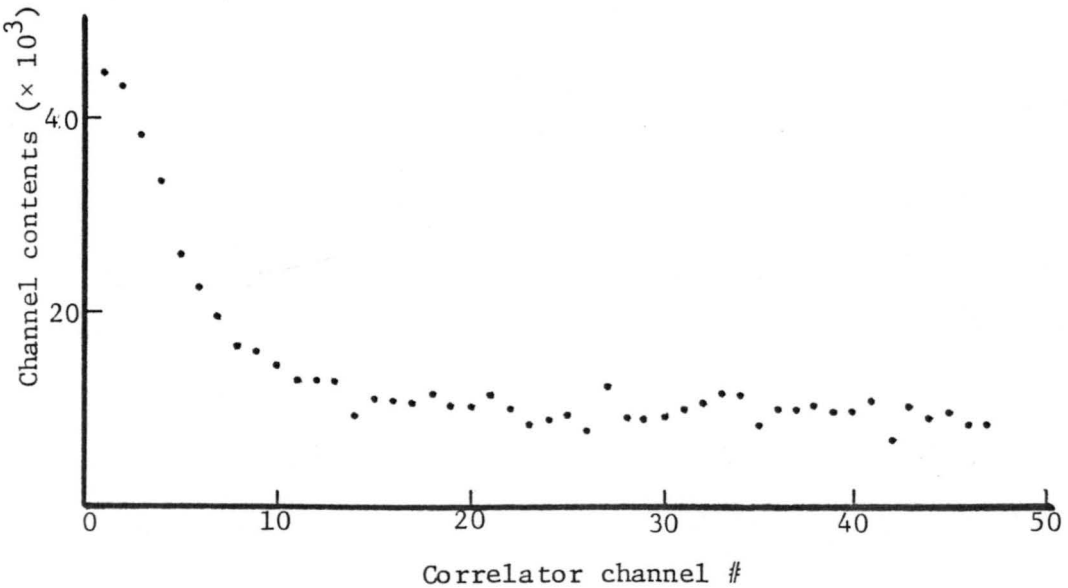

Fig. IV-5(b). Autocorrelation function due to averaging over many sodium atoms, 4.5 μs/sample and a beam waist of 273 μm.

two atoms (whose arrival times are separated by over 48 sample times, corresponding to 216 μs for this case) going through the viewing volume during the measurement time. If the second atom is within 48 sample times of the first, its signal will cause a second peak to occur, as in Fig. IV-2(b) and 3(a).

Even though the average number of atoms passing through the beam during the measurement is 0.51, there is still a probability that two atoms can be seen. This fact is clearly shown by Figs. 2(b) and 3(a). (The two numbers given for the various quantities in Table IV-1 represent the particular values determined by first using the $\tau \simeq 0$ correlation and then using the second peak.) Although the probability of seeing two atoms is small, $\sim$1% for Fig. 2(b), 2% to 4% for 3(a), and 10% for 4(a), it is obviously still possible. These correlation functions also point out the advantage of using a single laser beam, i.e., generally it is easy to tell if the correlation is due to one atom or more than one atom (for the two laser beam case, it is difficult to determine this for single atom levels). The fact that there were two atoms in these correlation functions, however, does not detract from the fact that velocities due to single atoms have been measured.

The first three autocorrelation functions [1(a), 1(b) and 2(a) were all taken under the same flow conditions (on the same day). One would, therefore, expect them to yield the same velocity. The average velocity calculated from these three correlation functions is 8.4 m/sec with the range being from 7.4 to 9.8 m/sec (about a 15% variation). The reason for this variation is most likely due to the inability to accurately determine the width of the observed correlation function (the distance to its $1/e^2$ point). This fact is shown more clearly by the set of

of figures which includes 3(a), 3(b), 4(a) and 5(b). These four were also taken under identical flow conditions (not the same as the first set, given above). Figures 3(a) through 4(a) are from single atoms and, due to the noise, their widths are hard to measure accurately. The range of velocities determined is from 8.2 to 18.6 m/sec. However, the width of Fig. 5(b) (which was obtained after averaging over many atoms) is easy to determine quite accurately and the resulting apparent (to be discussed below) velocity is 11.9 m/sec. There are several interpretations of this result. First we can say that, indeed, 11.9 m/s is an <u>average</u> velocity and 3(a), 3(b) and 4(a) are measuring accurately, velocities of single atoms. Another possibility is that since the correlation functions for the atoms are so noisy, it is not possible to get an accurate velocity determination from any one of them. A third possibility is that diffusion is significant and thus is effecting the correlation functions. The first interpretation assumes that a wide range of measured velocities is possible for a given flow condition. The viewing volume is located 2 cm from the nozzle exit plane, and the viewing volume itself has a smaller cross sectional area (2 mm^2) than the nozzle opening (12.5 mm^2). Therefore, we would not expect the range of velocities seen by the PMT to be large. For the flow conditions and the beam waist $\tau_r/\tau_D = .66$ which implies that flow is dominant (but not by much) and therefore could be effecting the correlation functions somewhat. Since the single atom correlations are noisy, we would expect that perhaps both the second and third possibilities given above are needed to explain the result. The value of the velocity given in the table has been corrected to account for the effect of diffusion.

Table IV-1. Summary of the results from single beam velocity measurements.

Figure #	Measured Velocity (m/sec)	# Photons Emitted (Measured)	# Photons Emitted (Predicted)	Average # Atoms Passing Through Viewing Vol During Measurement	Comments
IV-1(a)	8.1	21	31	---	Single beam, single atom on resonance and off resonance count rates indistinguishable
IV-1(b)	9.8	12	27	.29	Single beam, single atom
IV-2(a)	7.4	14	37	.49	Single beam, single atom
IV-2(b)	25.1/ 27.5	7 (per atom)	10/ 9	.15/ .16	Single beam, two atoms
IV-3(a)	8.5/ 17.1	6 (per atom)	22/ 11	.20/ .40	Single beam, two atoms
IV-3(b)	8.2	15	23	.19	Single beam, single atom
IV-4(a)	18.6	22	10	.51	Single beam, two atoms
IV-4(b)	---	--	--	---	Single beam, noise
IV-5(a)	9.0	"13"	"23"	---	Single beam, particle
IV-5(b)	10.3	--	19	1.93×10^4	Single beam, long term average

Figure IV-5(a) deserves somewhat special consideration. From Table IV-1, one can see that the velocity calculated is 9.0 m/sec (reasonable for the flow conditions that were present) and that the measured number of photons "emitted" is less than the predicted number, in accordance with arguments previously given. However, this correlation function was generated when the laser was tuned 15 GHz from the D_2 resonance, i.e., this correlation function is due to a particle. This fact brings out the importance of making the attempts at getting correlation functions off resonance as a check on whether the correlation functions and resonance are due to atoms and not particles. This figure does, however, represent the most "distinct" autocorrelation for a 100 sample measurement that was acquired off resonance. For Figs. IV-1 through IV-4(a), such tests were made and the results were that no correlations were found in the attempts made off resonance. Figure IV-4(b) represents what a normal correlation function looked like off resonance. Corresponding to Fig. IV-5(b), a correlation function was also allowed to build up off resonance as a check. The result was a straight line, indicating that there were no particles in the system.

One of the most serious problems which limited the accuracy attainable in these velocity measurements from single atoms was the high background that existed. Even though many measures were taken to reduce the background contribution, it was still a limiting factor in this experiment. Realistically, we should be able to reduce the background due to stray light scattering to much less than Rayleigh contribution. Much clearer signals could have been seen from single atoms, had we been able to reach this criteria. Another limiting

factor that hampered single atom velocity measurements was the low quantum efficiency of the photomultiplier tube that was used (RCA 31034A). We discovered that in the last two years the PMT had degraded considerably and the quantum efficiency had dropped a factor of four to five from its originally measured efficiency. As a result of this, the overall detection efficiency was only 1.5%, whereas with the ellipsoidal collector we had hoped to achieve a 10% overall efficiency. The degradation of our PMT quantum efficiency had unfortunately negated the gain the ellipsoidal collector obtained.

Since the single atom correlation functions were so noisy, to determine their widths more accurately, or at least without visual guesswork, it would be better to fit the function by regression methods. Perhaps the same fitting routine as used for the laser beam waist analysis or the diffusion analysis could be used. The difficulty that occurs, in this case, is that the fitting form [from Fig. II-6, for $C(\tau)$] is a very complicated integral. For the fitting routine that was used (BMDP3R), there are problems in setting up the required fitting function when that function is an integral that has to be numerically evaluated. Therefore, this approach was not tried.

IV-1.2. Results from Velocity Experiments Using Two Laser Beams. Representative correlation functions obtained from averaging over many atoms crossing the two laser beams are shown in Figs. IV-6, 7 and 9(b). As can be seen, these signals are much "cleaner" than the single atom correlation functions shown in the previous section. The distance between the peaks can be measured to within .5 channels (about a 5% error) visually. The first four correlation functions represent a flow of approximately 88 m/sec. The number of detected photons emitted by

single atom moving at that velocity [with a beam waist (width) of 330 μm, as was the case here, an intensity of 0.63 I_s, and an efficiency of .014] is approximately 1. Thus it can be seen why averaging was necessary.

A summary of the relevant information concerning Figs. 6 through 9 is given in Table IV-2. The information present includes the calculated velocity, the observing time and the estimated number of atoms crossing the viewing volume during the viewing time. From the table one can see that the sequence Fig. 6(a) to 7(b) represents the autocorrelation functions as a function of accumulation time. Figure 6(a) was allowed to accumulate for 110.4 seconds, while Fig. 7(b) took only .5 seconds to be acquired. Although the signal is somewhat noisy in this last figure, one can still determine the velocity to about 5%. Therefore, we have demonstrated that in a time of half a second, we can measure the flow velocity with reasonable accuracy. The measured speed 88 m/s, represents the flow speed truthfully because atoms are part of the flow. The measurable speeds in our experiments have already reached Mach 0.25 and higher speeds appear to be measurable.

One further observation that can be made concerning these correlation functions is that the height of the second peak is not one-half the height of the first peak. Such would be the predicted result (Section II-2.3) if all the atoms were going through both beams in the same manner. The relative height of the second peak with respect to the first is approximately .25. This would indicate that on the <u>average</u>, atoms going through the second beam are emitting .27 of the photons being emitted by that atom going through the first beam. (This result can be interpreted as not all the atoms are going through both beams.

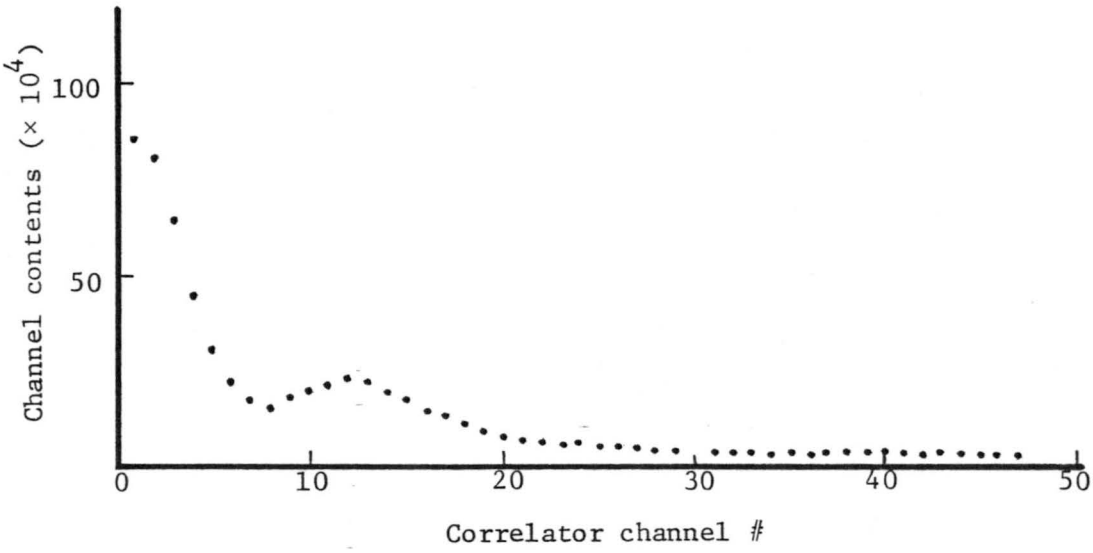

Fig. IV-6(a). Two beam autocorrelation function averaging over many atoms with a beam separation of 1.059 mm and 6 μs/sample. Observation time, 110.4 seconds.

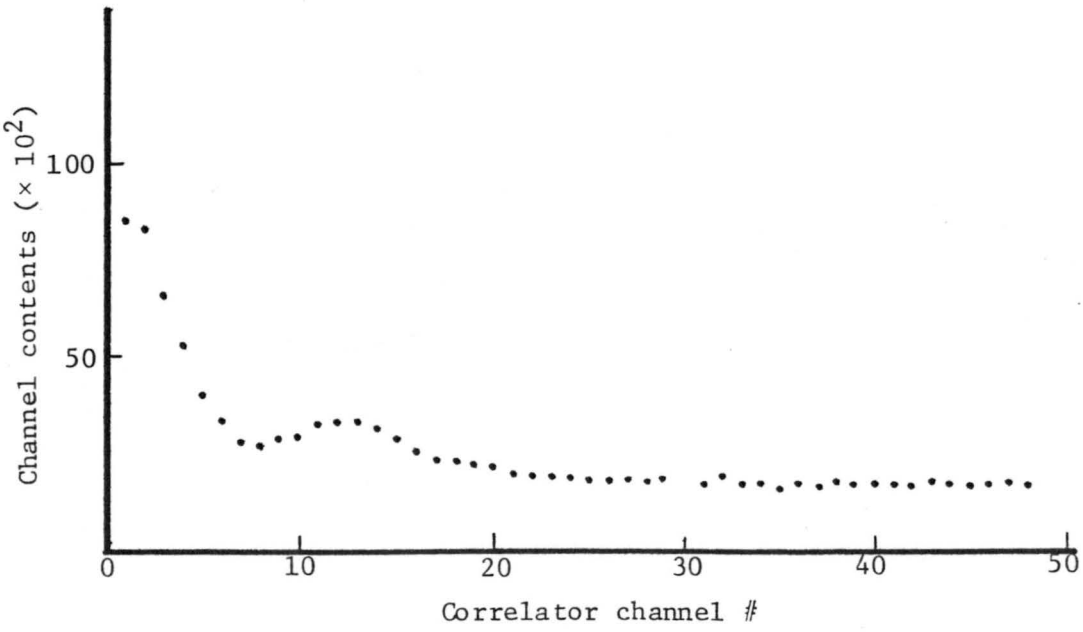

Fig. IV-6(b). Two beam autocorrelation function averaging over many atoms with a beam separation of 1.059 mm and 6 μs/sample. Observation time, 10.8 seconds.

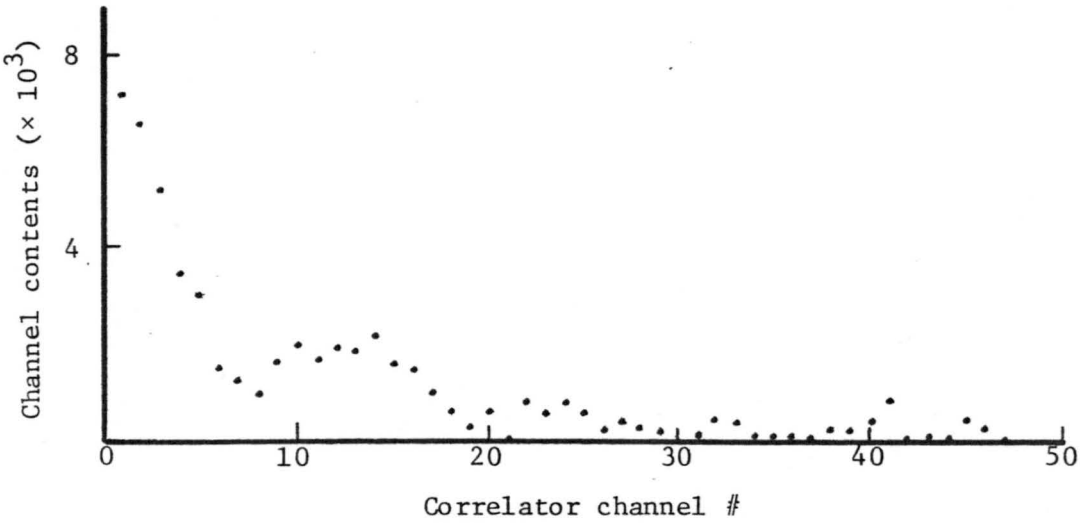

Fig. IV-7(a). Two beam autocorrelation function averaging over many atoms with a beam separation of 1.059 mm and 6 μs/sample. Observation time, 1.0 seconds.

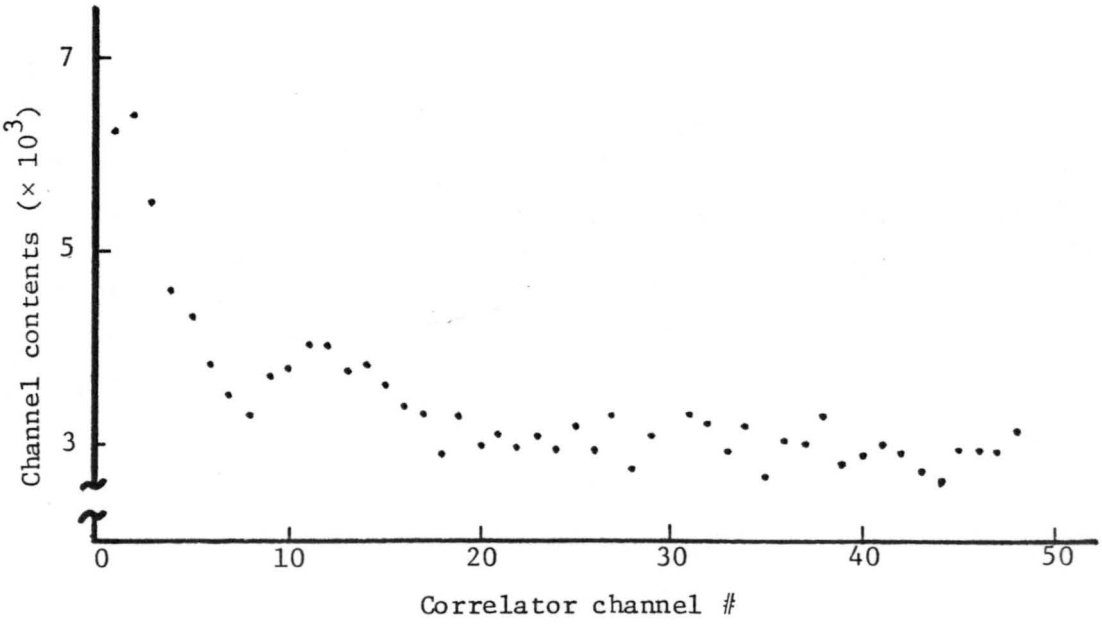

Fig. IV-7(b). Two beam autocorrelation function averaging over many atoms with a beam separation of 1.059 mm and 6 μs/sample. Observation time, .5 seconds.

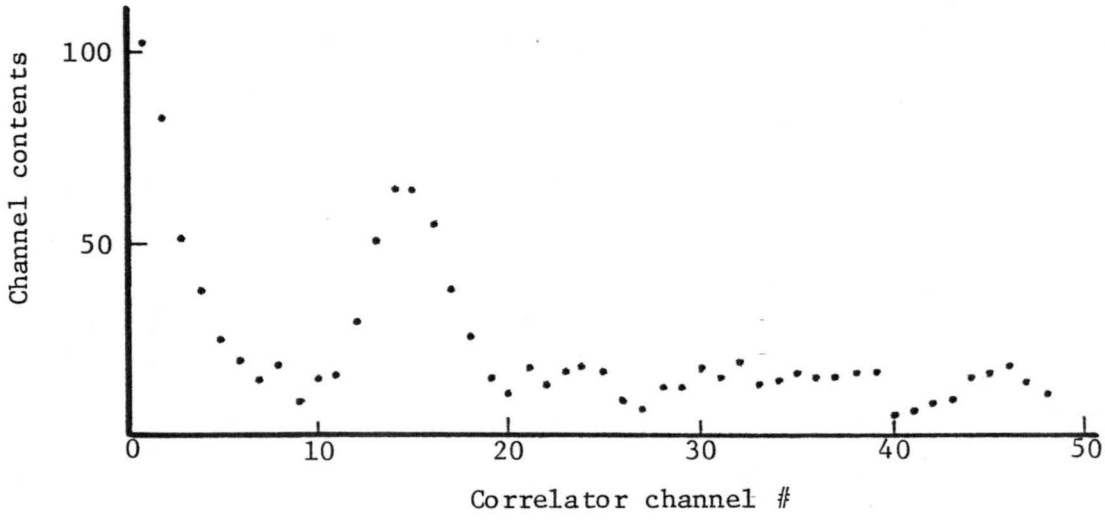

Fig. IV-8(a). Two beam autocorrelation function for a single particle with a beam separation of 1.059 mm and with 6 μs/sample.

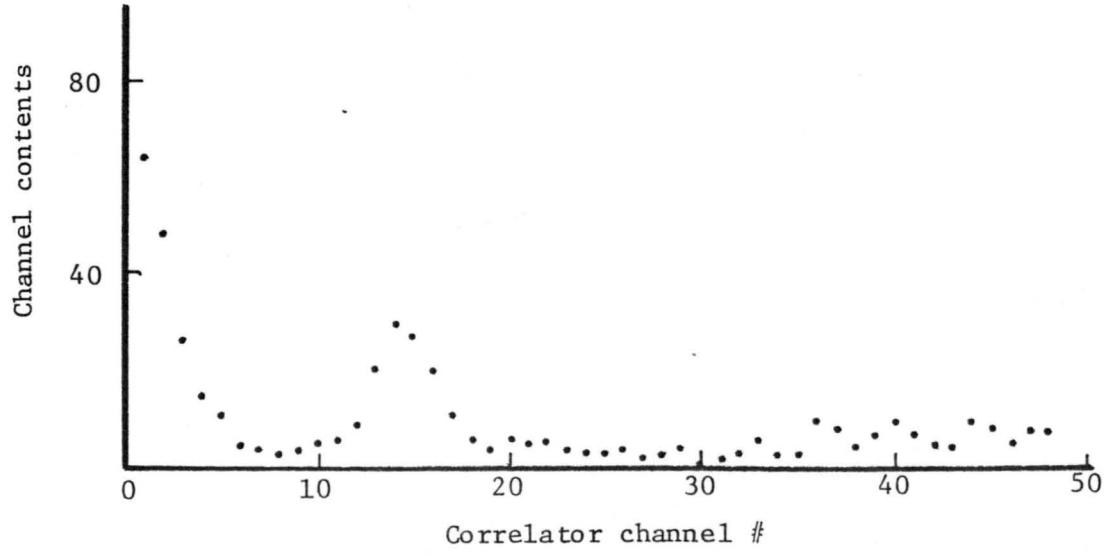

Fig. IV-8(b). Two beam autocorrelation function for a single particle with a beam separation of 1.059 mm and with 6 μs/sample.

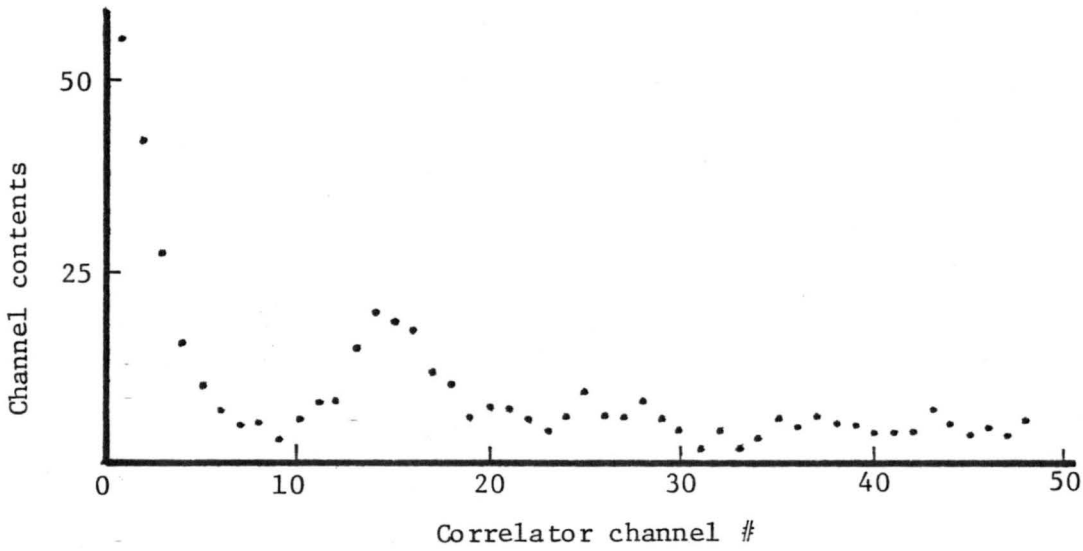

Fig. IV-9(a). Two beam autocorrelation function for a single particle with a beam separation of 1.059 mm and with 6 μs/sample.

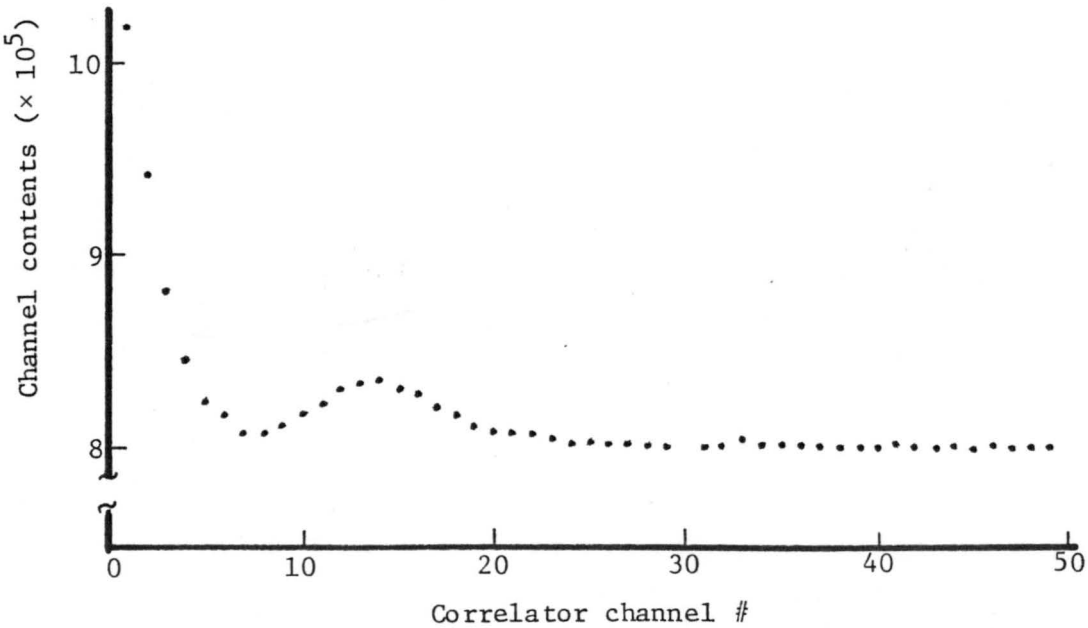

Fig. IV-9(b). Two beam autocorrelation function averaging over many sodium atoms with a beam separation of 1.059 mm and with 6 μs/sample.

Table IV-2. Summary of the results from dual beam velocity measurements.

Figure #	Calculated Velocity (m/sec)	Sodium Density (atoms/cc)	Total Observation Time (sec)	Fluorescence Signal Rate (per sec)	# Atoms Looked At	Notes
IV-6(a)	88.0	790	110.4	220,000	5.59×10^6	
IV-6(b)	88.0	790	10.8	220,000	5.46×10^5	
IV-7(a)	84.5	790	1.0	220,000	5.06×10^4	
IV-7(b)	88.0	790	.5	220,000	2.53×10^4	
IV-8(a)	11.4	---	---	---	---	Particle
IV-8(b)	11.6	---	---	---	---	Particle
IV-9(a)	11.4	---	---	---	---	Particle
IV-9(b)	13.0	---	94.8	22,000	---	

From diffusive considerations alone, the relative height of the second peak should be approximately 0.35.)

The velocity indicated above (88 m/sec) was the maximum obtainable with the imposed pressure restrictions (200 Torr background pressure in the cell) and the vacuum pump that was used. Earlier, it had been predicted that a velocity of 35 m/sec was possible with the nozzle we used, even if the nozzle was overpressured.[28,39] There are several suspected reasons for this discrepancy. First, a velocity of 35 m/sec is predicted at the exit plane of the nozzle and our viewing volume is 2 cm away from this plane. In the theory describing the flow from this type of nozzle[27,28] (a converging/diverging or DeLaval nozzle), little attempt was made to describe the flow velocity as a function of distance from the nozzle mouth (for distances relatively close, for example, up to five nozzle diameters away). It is in this range that perhaps overpressuring the nozzle would have an effect. The second consideration is that a vacuum pump was also attached to the cell (directly opposite the input tube). The entrance to a tube whose other end is connected to a vacuum pump is known as a Borda Mouth.[39] This will also affect the gas flow in the center of the cell. The combined effect of the overpressured nozzle and the Borda Mouth are uncertain, so at best the 35 m/sec can only serve as an order of magnitude guess for the flow at the viewing volume.

The information contained in the last two figures of this set, Figs. IV-8 and 9, is of a different sort than is contained in Figs. IV-6 and 7. (Figures IV-8 and 9 were also generated under different flow conditions than existed for Figs. IV-6 and 7.) Figures 8 and 9(a) represent single particles transiting the two laser beams. The

velocities of these particles are calculated to be 11.4, 11.6 and 11.4 m/sec. The average velocity for all the particles measured for this particular day was 11.04 m/sec with a standard deviation of 1.85 m/sec. Figure 9(b) is the correlation function due to averaging over many atoms [under the same flow conditions as Figs. 8(a), 8(b) and 9(a)]. Several such correlations were taken with the average of 13.5 m/sec and a standard deviation of .55 m/sec. It appears, then, even at these relatively low velocities, that the particles are starting to lag behind the actual flow, thus making the ability to use atoms as traces important.

IV-2. Diffusional Motion Studies

The second phase of this experiment involved the measurement of the motion of atoms when dynamics of the motion were described by the diffusion process. The autocorrelation functions that were produced during these experiments yielded the diffusion times and hence the diffusion constants for the particular system being studied. The results presented here include the characteristic diffusion times and the diffusion constants for the $Na(^2S_{1/2})$ + He, $Na(^2S_{1/2})$ + Ne, $Na(^2S_{1/2})$ + Ar and $Na(^2P_{3/2})$ + He systems.

IV-2.1. Results From the Experiments Involving $Na(^2S_{1/2})$ and Helium, Neon and Argon. The results obtained by fitting the observed diffusion correlation functions with Eq. (17) [or Eq. (18) when necessary] are presented in Tables IV-3, 4 and 5, and Figs. IV-10 through IV-18. The data that is tabulated includes the pressure (p) of the background gas, the normalized (to 315°K) characteristic diffusion times (τ_D), the long

TABLE IV-3

Summary of Diffusion Data for the Na($^2S_{1/2}$) + He System

Run #	Pressure (Torr)	τ_D(315°K) (μs)	w_L (cm)	Diffusion constant (cm^2/sec)	Dp (Torr - cm^2/sec)
90103B	100	4.875 ± .176	8.89×10^{-3}	4.051 ± .146	405.1 ± 14.6
90104A		5.163 ± .181		3.825 ± .134	382.5 ± 13.4
90104B		4.771 ± .197		4.192 ± .175	419.2 ± 17.5
90105A		4.955 ± .383		3.986 ± .308	398.6 ± 30.8
90106A	150	6.814 ± .361		2.899 ± .163	434.8 ± 24.4
90106B		7.030 ± .247		2.809 ± .099	421.4 ± 14.8
90107A		7.598 ± .469		2.599 ± .161	389.9 ± 24.1
90107B		7.075 ± .213		2.791 ± .084	418.7 ± 12.6
90108A	195	8.290 ± .242		2.383 ± .071	464.6 ± 13.8
90108B		9.262 ± .392		2.132 ± .090	415.8 ± 17.6
90109A		9.231 ± .406		2.139 ± .094	417.2 ± 18.3
90109B		9.553 ± .765		2.067 ± .165	403.1 ± 32.3
90110B	250	11.952 ± .775		1.652 ± .107	413.1 ± 26.8
90111A		11.285 ± .340		1.750 ± .053	437.5 ± 13.2
90111B		9.602 ± .353		2.057 ± .076	514.2 ± 18.9
90112A		11.309 ± .392		1.746 ± .060	436.6 ± 15.1
90113A	288	13.646 ± .601		1.447 ± .064	416.8 ± 18.3
90113B		12.721 ± .491		1.552 ± .060	447.1 ± 17.3
90114A		12.264 ± .867		1.610 ± .114	463.8 ± 32.8
90114B		11.237 ± .547		1.758 ± .085	506.2 ± 24.6
90116		14.589 ±1.201		1.354 ± .111	389.9 ± 32.1
90117A	400	15.643 ±1.995		1.263 ± .161	505.0 ± 64.4
90117B		18.978 ±5.093		1.041 ± .279	416.3 ±111.7
90320A		20.213 ±2.74		.939 ± .127	375.5 ± 50.9
90320B		21.302 ±3.408		.891 ± .143	356.3 ± 57.0
90321A		17.206 ±3.382		1.103 ± .217	441.1 ± 86.7
90321B		17.455 ± .857		1.087 ± .053	434.8 ± 21.3
90322		13.374 ± .2.220		1.033 ± .124	413.1 ± 49.9
112801A	103	2.727 ± .267	7.14×10^{-3}	4.672 ± .457	481.2 ± 47.1
112801B		3.049 ± .x68		4.175 ± .367	430.0 ± 37.8
112802B		3.195 ± .254		3.987 ± .316	410.7 ± 32.6
112803A		3.520 ± .305		3.620 ± .362	372.9 ± 37.3
112804A	192	7.020 ± .680		1.815 ± .176	348.4 ± 33.7
112804B		7.027 ± .570		1.813 ± .147	348.1 ± 28.2
112805B		8.330 ± .405		1.529 ± .074	293.6 ± 14.3
112806A		8.135 ± .610		1.566 ± .117	300.7 ± 22.5
112807A	243.5	7.702 ± .525		1.654 ± .113	402.8 ± 27.5
112807B		8.764 ± .813		1.454 ± .135	354.0 ± 32.8
112808A		8.171 ± .771		1.559 ± .147	379.7 ± 35.8
112808B		8.234 ± .210		1.547 ± .039	376.6 ± 9.6
112809A	300	10.132 ± .675		1.257 ± .078	377.2 ± 23.3
112809B		10.260 ± .705		1.242 ± .085	372.5 ± 25.6

TABLE IV-3 (cont.)

112810A	300	9.405± .681	7.14×10^{-3}	1.355 ± .098	406.4 ± 29.4
112810B		10.634± .871		1.198 ± .098	359.4 ± 29.4
112812A	342	14.127± 3.505		.902 ± .223	308.4 ± 76.4
112812B		11.579± .911		1.100 ± .086	376.3 ± 29.6
112813A		12.684± 1.300		1.004 ± .103	343.5 ± 35.2
112813B		10.315± 1.388		1.235 ± .166	422.4 ± 56.8
216104	102.0	36.240± 1.714	2.36×10^{-2}	3.849 ± .182	392.6 ± 18.6
216105		36.431± 2.023		3.828 ± .213	390.5 ± 21.7
216106		33.481± 1.282		4.165 ± .160	424.9 ± 16.3
21596		36.034± 1.278		3.871 ± .137	394.8 ± 14.0
216108		35.083± 1.143		3.975 ± .129	405.5 ± 13.2
216109	150.7	49.623± 1.334		2.811 ± .076	423.7 ± 11.4
216110		52.764± 5.537		2.644 ± .277	398.5 ± 41.8
216111		71.303±13.032		1.957 ± .366	294.9 ± 55.1
216112		56.625± -		2.464 ± -	371.3 ± -
216113		55.601± 5.036		2.510 ± .228	378.2 ± 34.3
216114	211.5	70.343±12.826		1.983 ± .362	419.4 ± 76.5
216115		63.261± 8.332		2.205 ± .290	466.3 ± 61.4
216116		74.050±10.362		1.884 ± .263	398.4 ± 55.7
216117		69.311± 9.948		2.012 ± .289	425.6 ± 61.1
216118		58.343± 3.968		2.391 ± .163	505.6 ± 34.4
216119	257.0	74.104±11.273		1.882 ± .286	483.7 ± 93.6
216120		64.564± 7.241		2.160 ± .242	555.2 ± 62.3
216121		85.458± 8.909		1.632 ± .170	419.3 ± 43.7
216122		67.806±10.204		2.057 ± .309	528.6 ± 79.5
216123		71.433±10.558		1.953 ± .289	501.8 ± 74.2
216130	300.5	122.81 ±33.54		1.136 ± .310	341.3 ± 93.2
216131		80.319±18.255		1.736 ± .395	521.8 ±118.6
216132		61.675±13.186		2.261 ± .483	679.6 ±145.3
216133		154.17 ±52.94		.905 ± .311	271.9 ± 93.4
216134		201.67 ±71.37		.692 ± .244	207.8 ± 73.5
216135	344.5	92.369±25.979		1.510 ± .425	520.2 ±146.3
216136		85.448±31.230		1.632 ± .597	562.3 ±205.5
216137		77.705±23.892		1.795 ± .552	618.4 ±190.1
216138		120.20 ±52.70		1.160 ± .508	399.7 ±175.2
216139		77.595±19.830		1.797 ± .459	619.2 ±158.2
217101	101.0	34.616± .650	2.46×10^{-2}	4.450 ± .084	449.4 ± 8.5
217102		36.804± 1.814		4.185 ± .206	422.7 ± 20.8
217103		34.716± 2.366		4.437 ± .302	448.1 ± 30.5
217104		35.229± 2.746		4.372 ± .341	441.6 ± 34.4
217105		33.240± 1.111		4.634 ± .154	468.0 ± 15.6
217109	304.0	97.477±12.039		1.546 ± .191	470.1 ± 58.1
217110		73.421± 7.559		2.053 ± .211	624.1 ± 64.2
217111		112.47 ±20.28		1.340 ± .240	407.4 ± 73.2
217112		59.317± 7.758		2.551 ± .334	775.4 ±101.4
217113		78.686± 8.919		1.923 ± .218	584.5 ± 66.3
217114	202.0	57.157± 4.316		2.647 ± .205	534.7 ± 40.3
217115		61.444± 4.833		2.474 ± .395	499.8 ± 39.5

TABLE IV-3 (cont.)

217116		60.194 ± 6.547		2.513 ± .273	507.7 ± 55.2
217117		62.761 ± 6.385		2.410 ± .245	486.9 ± 49.5
217118		72.367 ±12.315		2.091 ± .356	422.3 ± 71.9
509104	103.0	10.476 ± -	1.37×10^{-2}	4.479 ± -	461.3 ± -
509106		12.011 ± .932		3.907 ± .303	402.4 ± 31.2
509107		11.066 ± .636		4.240 ± .244	436.7 ± 25.1
509108		10.310 ± .529		4.418 ± .227	455.1 ± 23.4
509116	192.0	21.390 ± .430		2.194 ± .044	432.2 ± 8.7
509117		21.068 ± .658		2.227 ± .070	438.8 ± 13.7
509118		22.006 ± .708		2.132 ± .069	420.1 ± 13.5
509119		21.246 ± .647		2.209 ± .008	435.1 ± 13.3
509120		21.726 ± .272		2.160 ± .027	425.5 ± 5.3
510101	103.3	11.674 ± .949		4.200 ± .342	433.9 ± 35.3
510102		10.333 ± .769		4.745 ± .353	490.2 ± 36.5
510103		12.487 ± .582		3.926 ± .183	405.6 ± 18.1
510104		11.204 ± .825		4.377 ± .322	452.1 ± 33.3
510105		10.700 ± .699		4.582 ± .299	473.3 ± 30.1
510118	200.5	22.839 ± 1.717		2.079 ± .156	416.9 ± 31.3
510119		20.519 ± 2.151		2.287 ± .240	458.5 ± 48.1
510120		20.876 ± 1.897		2.248 ± .204	450.7 ± 41.0
510121		17.139 ± .873		2.737 ± .139	548.9 ± 27.9
510122		19.452 ± 1.20			483.7 ± 29.9
510123	145.5	16.572 ± -		2.910 ± -	423.4 ± -
510124		15.120 ± 1.28		3.190 ± .246	464.1 ± 35.8
510125		18.289 ± -		2.637 ± -	383.7 ± -
510126		15.524 ± .846		3.107 ± .147	452.0 ± 20.9
510127		16.785 ± 1.180		2.873 ± .202	418.0 ± 29.4
510128	244.5	22.311 ± 2.01		2.114 ± .190	516.8 ± 46.4
510129		23.882 ± 1.95		1.983 ± .163	484.8 ± 39.8
510130		22.960 ± .666		2.062 ± .060	504.2 ± 14.6
510131		22.700 ± .783		2.077 ± .072	507.9 ± 17.5
510132		23.324 ± .845		2.022 ± .073	494.4 ± 17.9
510133	303.5	26.28 ± 1.660		1.782 ± .113	540.8 ± 34.2
510134		23.416 ± 1.092		2.000 ± .093	607.0 ± 28.3
510135		24.485 ± 5.310		1.913 ± .415	580.5 ±125.9
510136		24.228 ± 3.790		1.933 ± .302	586.6 ± 91.8
510137		30.844 ± 5.222		1.518 ± .257	460.8 ± 78.0

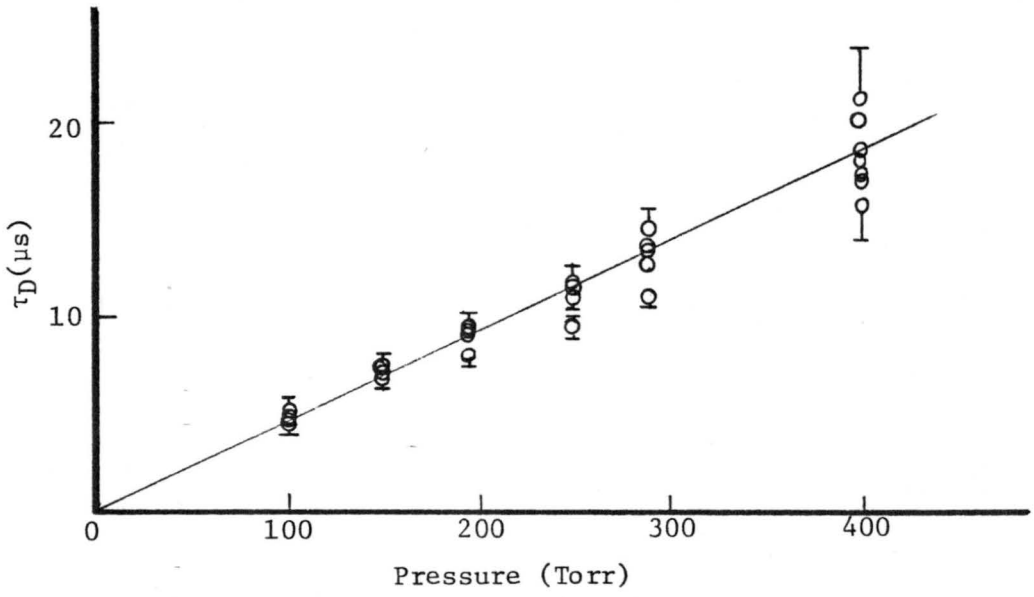

Fig. IV-10(a). Graph of τ_D vs. p for Na+He, taken 9/1/79.

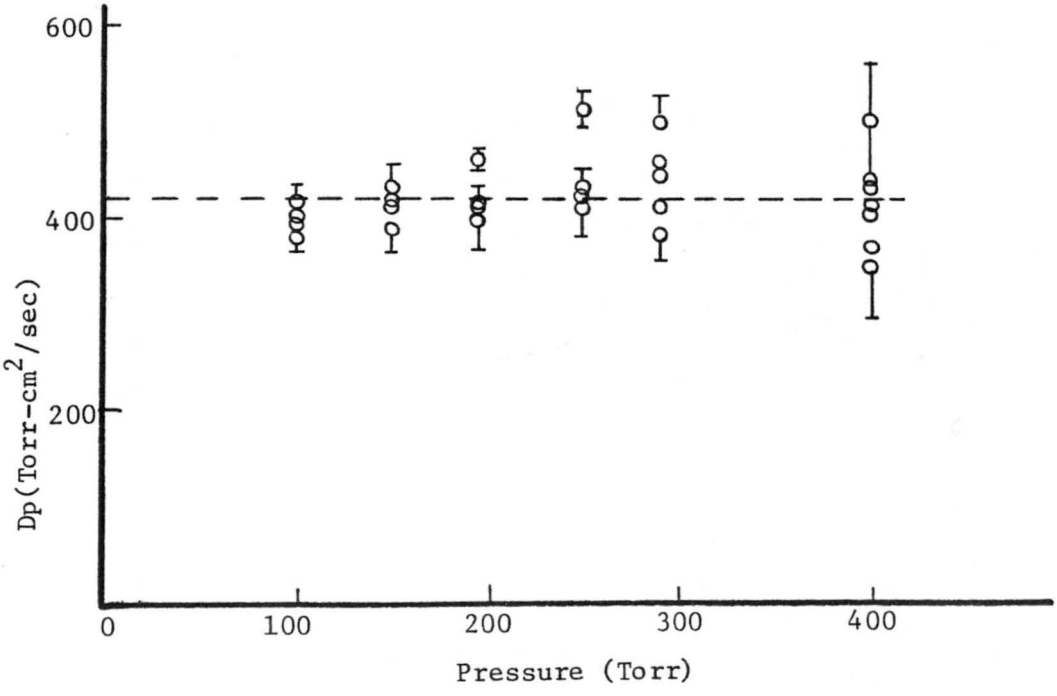

Fig. IV-10(b). Graph of Dp vs. p for Na+He, taken 9/1/79.

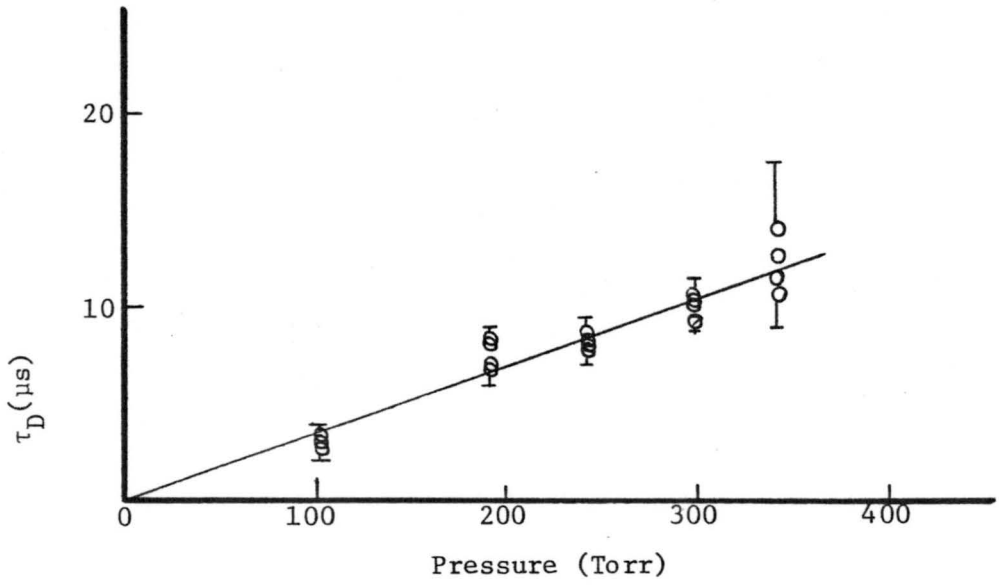

Fig. IV-11(a). Graph of τ_D vs. p for Na+He, taken 11/28/79.

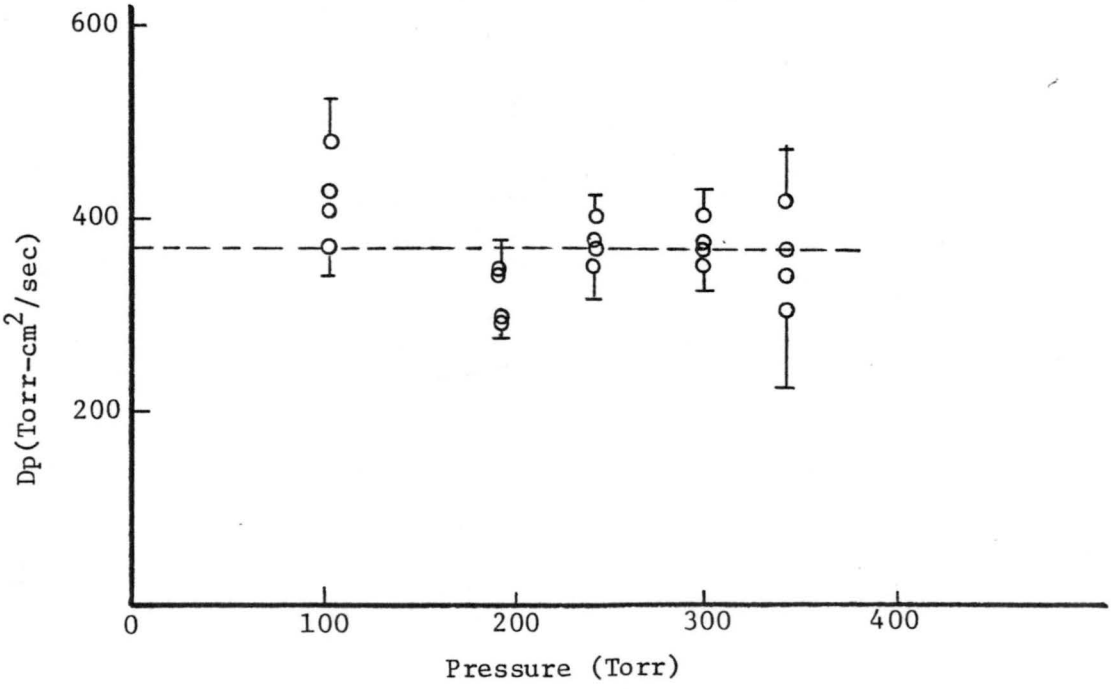

Fig. IV-11(b). Graph of Dp vs. p for Na+He, taken 11/28/79.

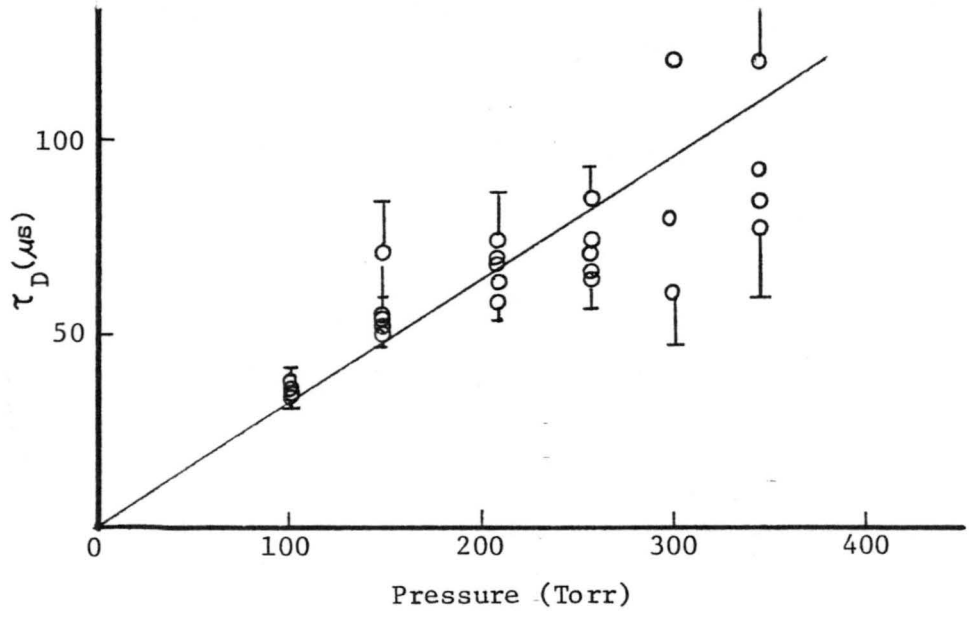

Fig. IV-12(a). Graph of τ_D vs. p for Na+He, taken 2/16/81.

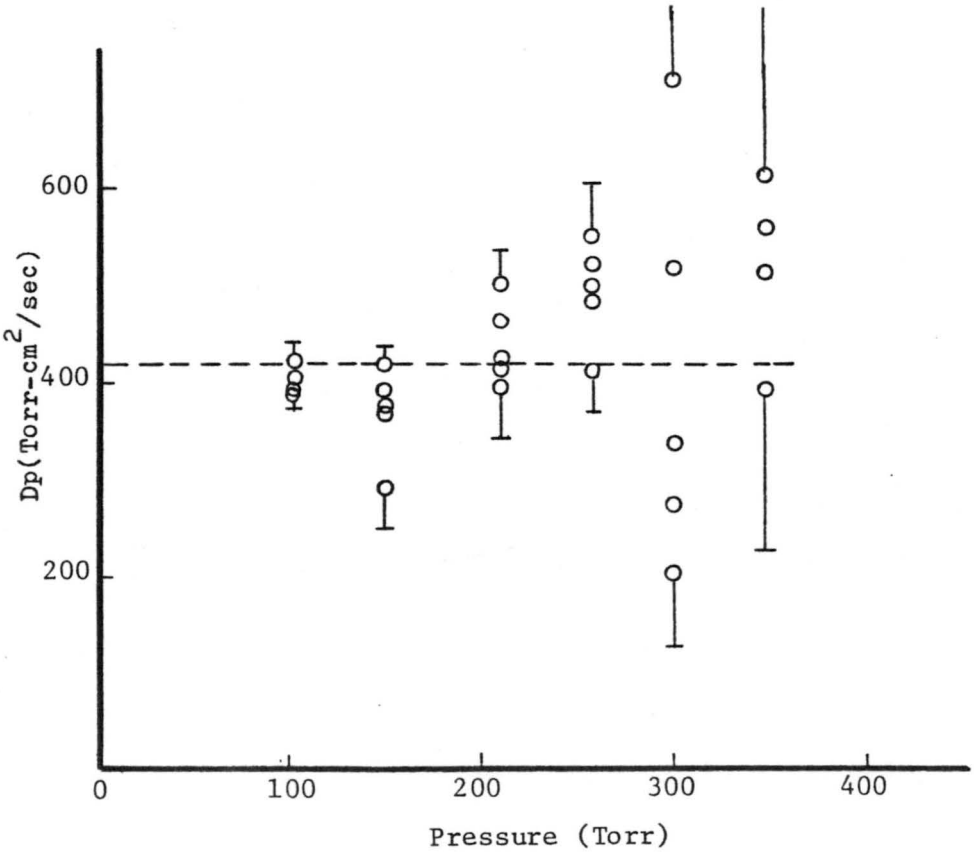

Fig. IV-12(b). Graph of Dp vs. p for Na+He, taken 2/16/81.

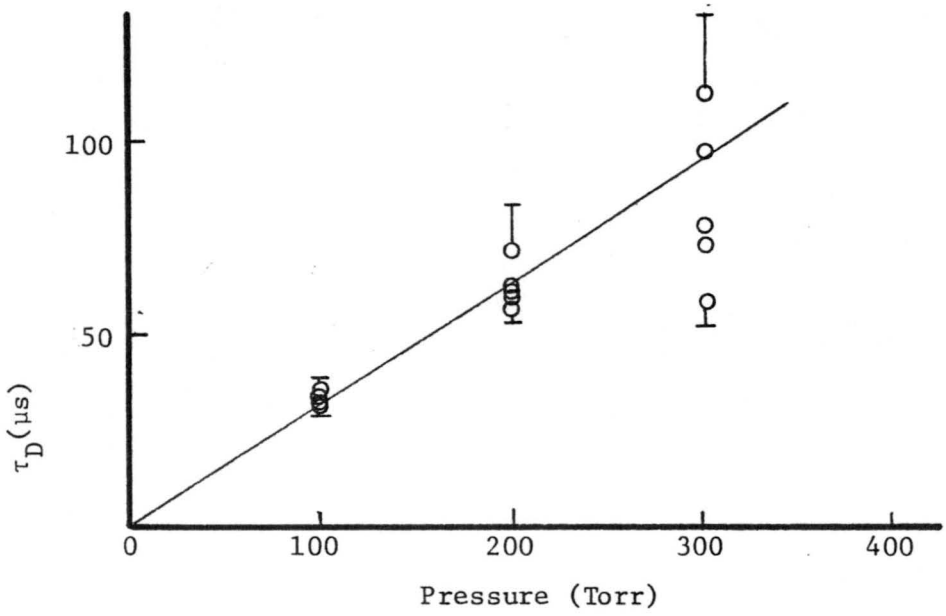

Fig. IV-13(a). Graph of τ_D vs. p for Na+He, taken 2/17/81.

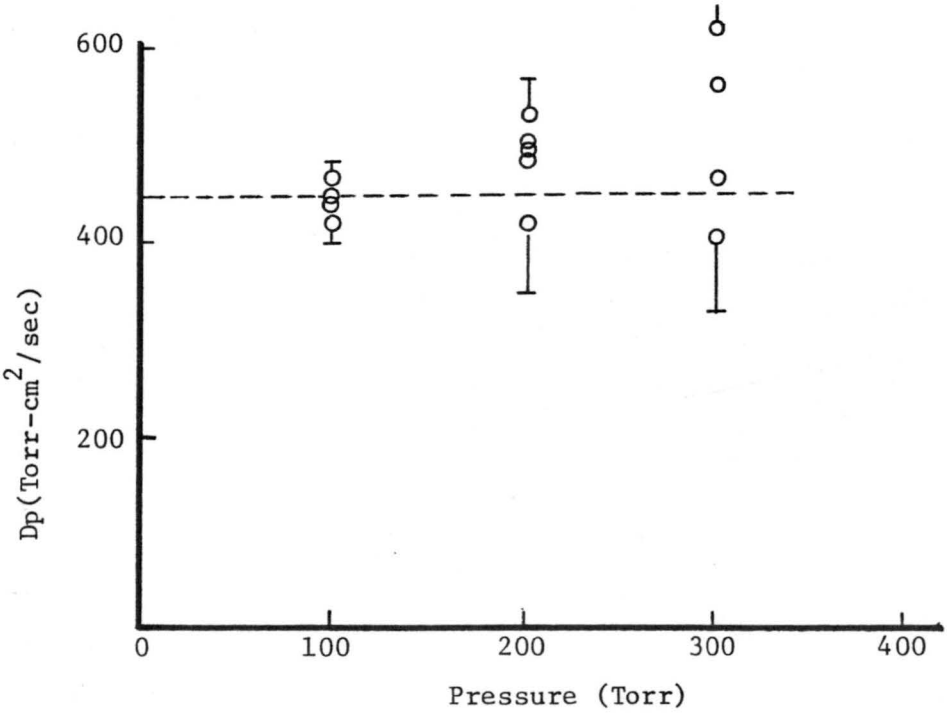

Fig. IV-13(b). Graph of Dp vs. p for Na+He, taken 2/17/81.

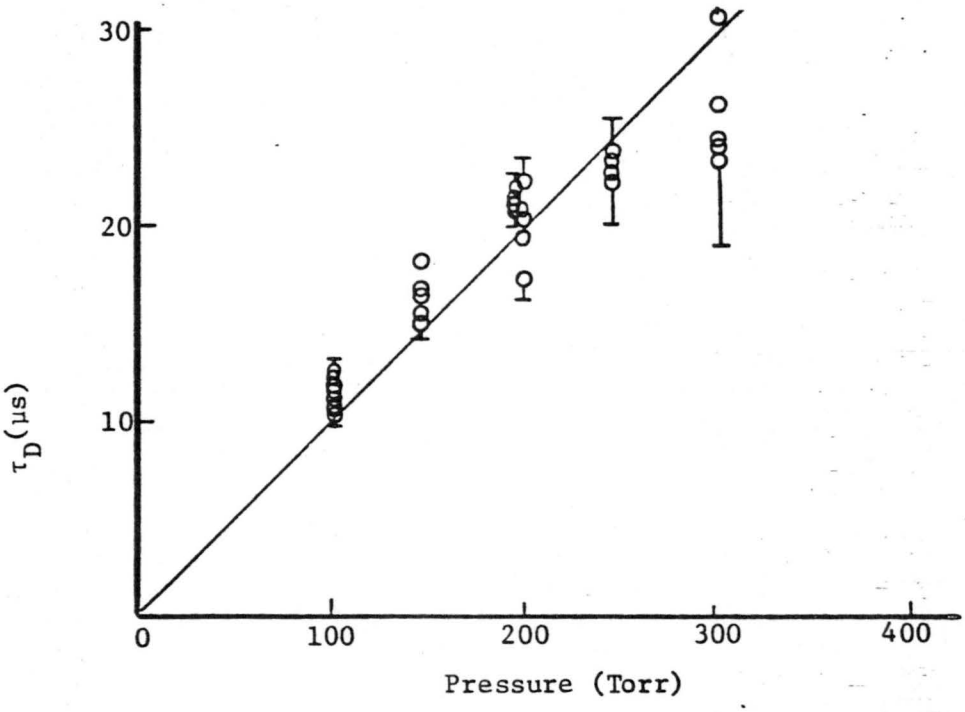

Fig. IV-14(a). Graph of τ_D vs. p for Na+He, taken 5/9/81.

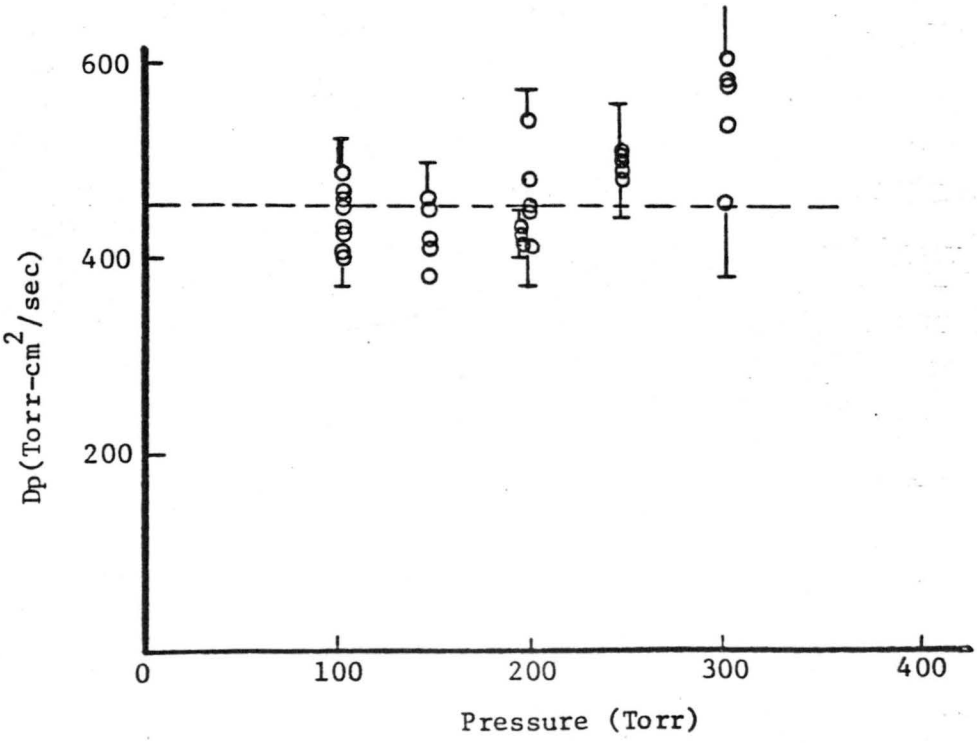

Fig. IV-14(b). Graph of Dp vs. p for Na+He, taken 5/9/81.

Table IV-4. Summary of diffusion data for the $Na(^2S_{1/2})$+Ne system.

Run #	Pressure (Torr)	τ_D (315°K) (μs)	w_L (cm)	Diffusion Constant (D) cm^2/sec	Dp $Torr\text{-}cm^2/sec$
90204A	102.0	8.43 ± .240	8.89×10^{-3}	2.294 ± .065	234.4 ± 6.6
90204B		7.64 ± .32		2.540 ± .105	259.1 ± 10.7
90205A		8.24 ± .28		2.346 ± .081	239.3 ± 8.3
90205B		8.30 ± .34		2.323 ± .096	236.9 ± 9.8
90206A		8.07 ± .28		2.382 ± .082	243.0 ± 8.4
90207A	147.0	10.01 ± .24		1.930 ± .046	283.7 ± 6.7
90207B		10.08 ± .23		1.914 ± .044	281.3 ± 6.5
90208A		10.08 ± .30		1.914 ± .058	281.3 ± 8.5
90208B		10.08 ± .32		1.914 ± .060	281.3 ± 8.8
90209A		9.90 ± .38		1.939 ± .073	285.0 ± 10.8
90210A	195.0	13.00 ± .43		1.474 ± .049	287.5 ± 9.5
90210B		12.96 ± .37		1.493 ± .043	291.2 ± 8.3
90211A		12.65 ± .49		1.518 ± .059	296.1 ± 11.5
90211B		12.33 ± .40		1.563 ± .051	304.7 ± 10.0
90212A		13.18 ± .54		1.455 ± .060	283.7 ± 11.7
90213A	240.0	14.24 ± .60		1.362 ± .058	326.9 ± 13.8
90213B		13.66 ± .37		1.424 ± .039	341.7 ± 9.3
90214A		15.01 ± .65		1.295 ± .056	310.9 ± 13.5
90214B		14.61 ± .58		1.326 ± .053	318.3 ± 12.6
90215B	290.0	21.71 ± 1.80		.889 ± .073	257.8 ± 21.4
90216A		18.38 ± 1.04		1.051 ± .060	304.7 ± 17.3
90216B		16.67 ± 1.00		1.157 ± .069	335.6 ± 20.1
90217A		17.92 ± 1.23		1.072 ± .074	310.9 ± 21.4
90217B		14.65 ± 1.51		1.319 ± .136	382.4 ± 39.4
90218B	340.0	21.11 ± .72		.914 ± .031	310.9 ± 10.6
90219A		21.03 ± 1.20		.918 ± .052	312.1 ± 17.8
90219B		21.46 ± 1.43		.900 ± .060	306.0 ± 20.4
90220A		23.57 ± 1.33		.820 ± .046	278.8 ± 15.7
90317A	390.	23.73 ± .94		.810 ± .032	315.8 ± 12.5
90317B		24.94 ± .73		.772 ± .023	301.0 ± 8.8
90318A		21.71 ± .95		.889 ± .039	346.7 ± 15.2
90318B		23.90 ± 1.04		.806 ± .035	314.6 ± 13.7
21501A	111.	3.347 ± .426	6.60×10^{-3}	3.254 ± .414	361.2 ± 46.0
21501B		3.683 ± .958		2.956 ± .769	328.1 ± 85.3
21502A		3.090 ± .266		3.675 ± .330	408.0 ± 36.6
21502B		5.012 ± .370		3.524 ± .422	391.2 ± 46.8
21512A	153.	3.250 ± .616	6.60×10^{-3}	2.172 ± .267	332.4 ± 40.8
21512B		5.912 ± .500		3.351 ± .515	513.7 ± 78.9
21513A		4.350 ± .874		1.842 ± .272	281.8 ± 41.6
21513B		5.974 ± .634		2.503 ± .365	383.0 ± 55.8
21503A		5.235 ± .719		1.823 ± .219	364.6 ± 43.8
21503B		7.377 ± .653		2.080 ± .259	416.0 ± 51.9

Table IV-4. Continued

21504A		7.377 ± 1.066	1.476 ± .213	295.2 ± 42.7
21504B		4.943 ± .793	2.203 ± .353	440.6 ± 70.6
21509A	244.	7.892 ± .893	1.380 ± .156	336.7 ± 38.1
21509B		7.293 ± .976	1.493 ± .200	364.3 ± 48.7
21510A		6.973 ± .869	1.562 ± .195	381.1 ± 47.4
21510B		6.143 ± .704	1.773 ± .203	432.6 ± 49.6
21505A	293.	7.481 ± 1.152	1.456 ± .224	426.5 ± 65.7
21505B		7.046 ± 1.053	1.546 ± .231	452.8 ± 67.7
21506A		8.148 ± 1.129	1.337 ± .185	391.6 ± 54.3
21506B		8.404 ± .973	1.296 ± .150	379.7 ± 44.0
21507A	338.0	9.193 ± 1.010	1.185 ± .130	400.4 ± 44.0
21507B		8.123 ± 1.082	1.340 ± .178	453.1 ± 60.3
21508A		10.950 ± 1.177	.995 ± .107	336.1 ± 36.1
21508B		9.716 ± 1.403	1.121 ± .162	378.8 ± 54.7

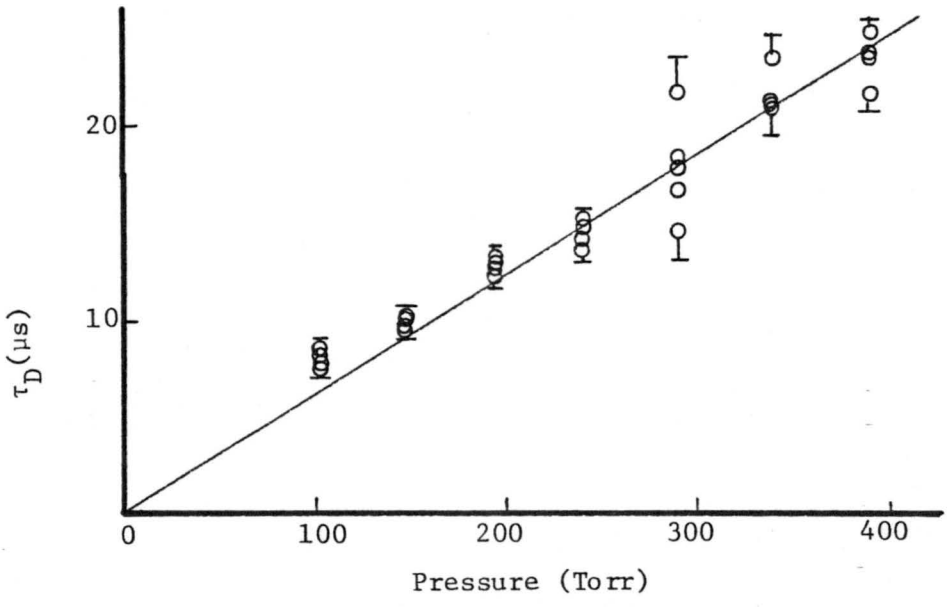

Fig. IV-15(a). Graph of τ_D vs. p for Na+Ne, taken 9/2/79.

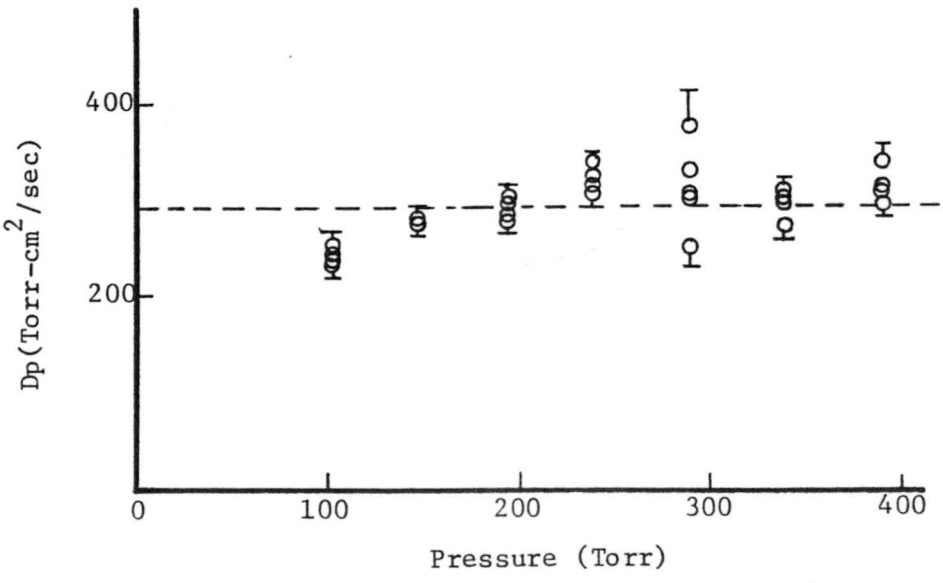

Fig. IV-15(b). Graph of Dp vs. p for Na+Ne, taken 9/2/79.

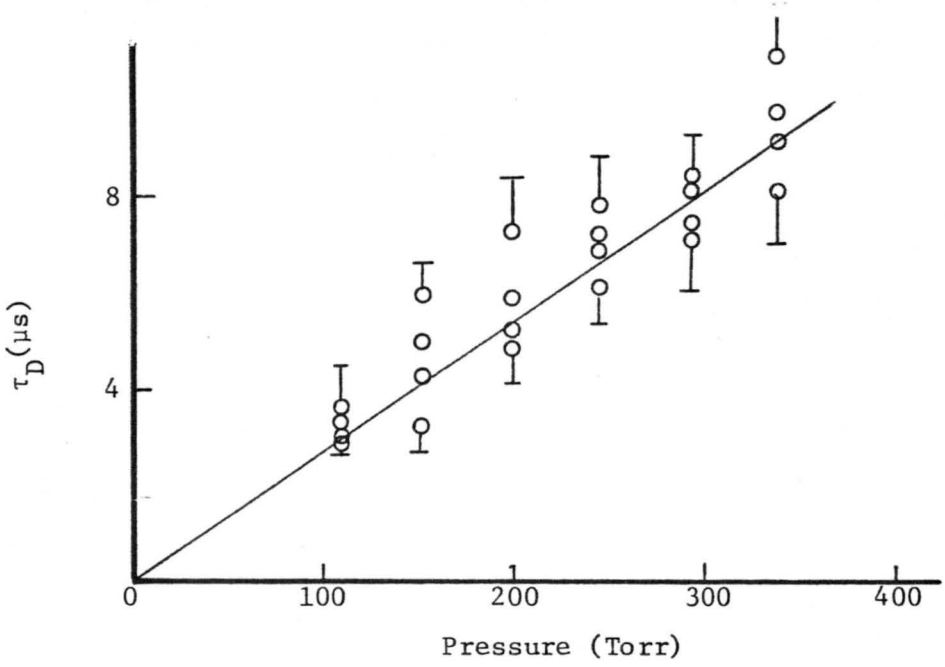

Fig. IV-16(a). Graph of τ_D vs. p for Na+Ne, taken 2/15/80.

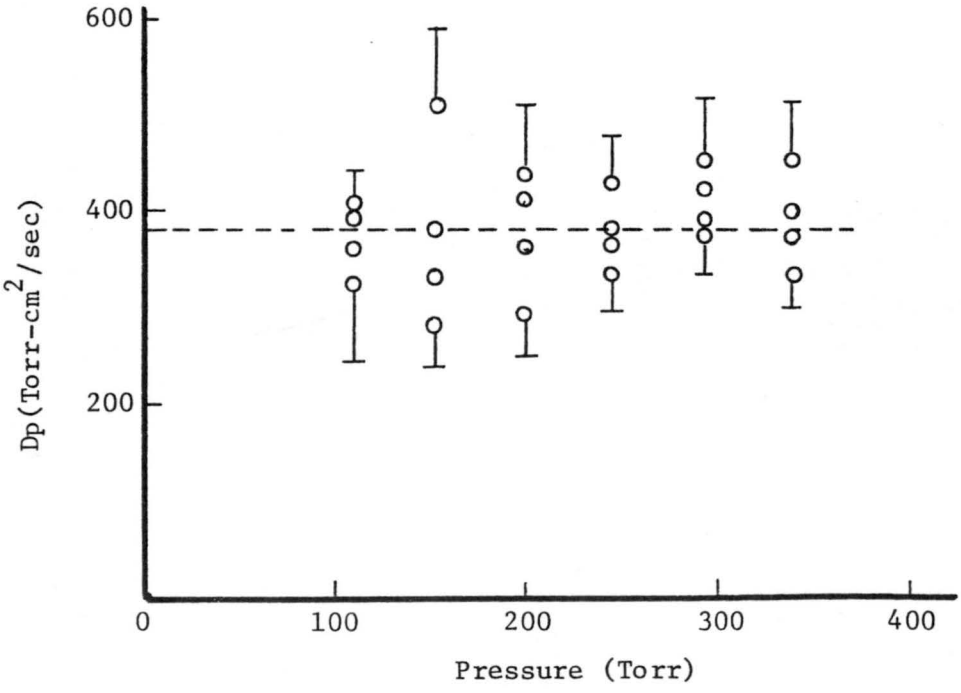

Fig. IV-16(b). Graph of Dp vs. p for Na+Ne, taken 2/15/80.

Table IV-5. Summary of diffusion data for the $Na(^2S_{1/2})+Ar$ system.

Run #	Pressure (Torr)	τ_D (315°K) (μs)	w_L (cm)	Diffusion Constant (D) (cm^2/sec)	Dp (Torr-cm^2/sec)
90303A	101.	9.04 ± .42	8.80×10^{-3}	2.142 ± .100	216.3 ± 10.1
90303B		9.24 ± .44		2.095 ± .101	211.6 ± 10.2
90304A		10.68 ± .66		1.813 ± .123	183.1 ± 11.4
90304B		10.65 ± .72		1.818 ± .123	183.6 ± 12.4
90305B	149.	16.68 ± 1.35		1.160 ± .094	172.9 ± 14.0
90306A		13.07 ± .82		1.480 ± .093	220.7 ± 13.8
90306B		22.47 ± 2.03		.862 ± .078	128.4 ± 11.6
90307A		24.79 ± 1.98		.781 ± .062	116.4 ± 9.3
90308A	193.	18.58 ± 1.26		1.042 ± .070	201.1 ± 13.6
90308B		16.27 ± .98		1.190 ± .072	229.7 ± 13.9
90309A		17.00 ± 1.21		1.139 ± .081	219.8 ± 15.6
90309B		17.00 ± 1.24		1.139 ± .083	219.8 ± 16.0
90310B	243	20.60 ± 1.82		.940 ± .083	228.4 ± 20.2
90311A		22.98 ± 2.34		.842 ± .086	204.7 ± 20.8
90311B		24.55 ± 2.92		.789 ± .094	191.7 ± 22.8
90312A		21.54 ± 2.38		.899 ± .099	218.4 ± 24.1
90313A	285	24.11 ± 2.37		.803 ± .079	228.8 ± 22.5
90313B		22.80 ± 2.04		.849 ± .076	242.0 ± 21.6
90314A		26.95 ± 2.75		.719 ± .073	204.8 ± 20.9
90314B		30.38 ± 2.91		.637 ± .061	181.6 ± 17.4
21401A	101.	4.05 ± .85	6.60×10^{-3}	2.689 ± .562	271.6 ± 56.7
21401B		4.60 ± .96		2.367 ± .494	239.1 ± 49.9
21402A		4.88 ± .45		2.231 ± .205	225.4 ± 20.7
21402B		4.45 ± .47		2.447 ± .259	247.2 ± 26.2
21409A	148.	6.43 ± .66		1.693 ± .175	250.7 ± 26.0
21409B		6.41 ± .53		1.699 ± .139	251.4 ± 20.6
21410A		6.23 ± .72		1.748 ± .201	258.7 ± 29.7
21410B		5.14 ± .47		1.833 ± .145	271.3 ± 21.4
21403A	195.	5.98 ± 1.30		1.821 ± .397	355.1 ± 77.4
21403B		7.78 ± 1.90		1.400 ± .341	272.9 ± 66.6
21404A		8.40 ± .99		1.296 ± .153	252.8 ± 29.9
21404B		5.25 ± .57		2.074 ± .227	404.5 ± 44.3
21407A	237.	11.42 ± 1.85		.949 ± .154	225.0 ± 36.5
21407B		13.23 ± 2.17		.823 ± .134	195.1 ± 31.9
21408A		9.65 ± 1.11		1.128 ± .130	267.5 ± 30.7
21408B		9.65 ± 1.02		1.128 ± .119	267.5 ± 28.2
21405A	287.	12.71 ± 2.31	6.60×10^{-3}	.867 ± .158	245.9 ± 44.7
21405B		13.07 ± 2.32		.833 ± .148	239.1 ± 42.4
21406A		14.47 ± 2.40		.756 ± .125	216.0 ± 35.8
21406B		15.32 ± 2.20		.711 ± .102	204.0 ± 29.2

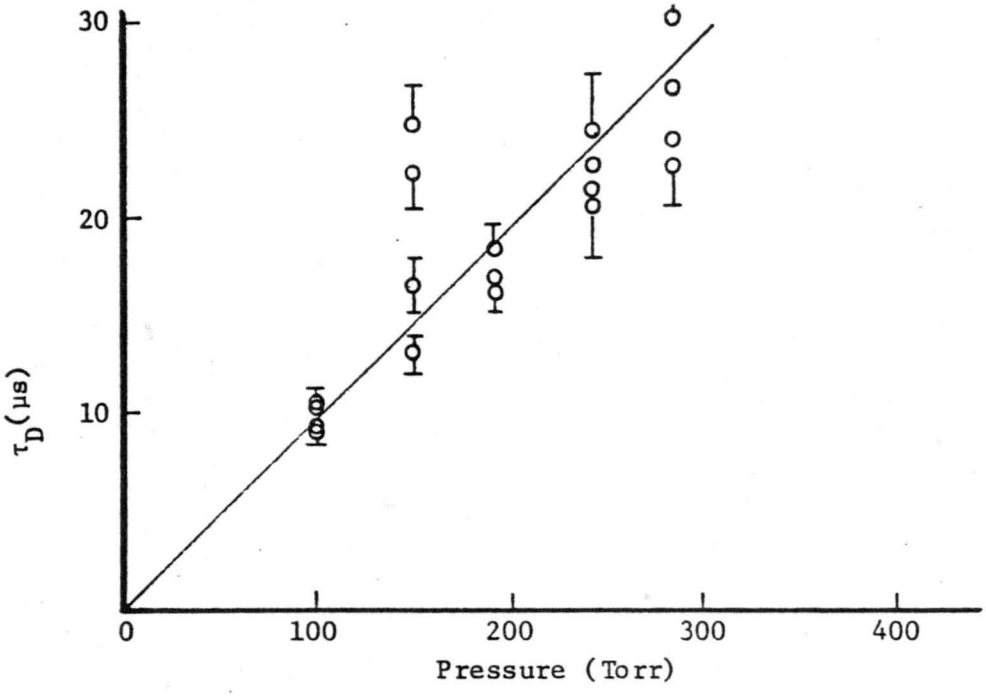

Fig. IV-17(a). Graph of τ_D vs. p for Na+Ar, taken 9/3/79.

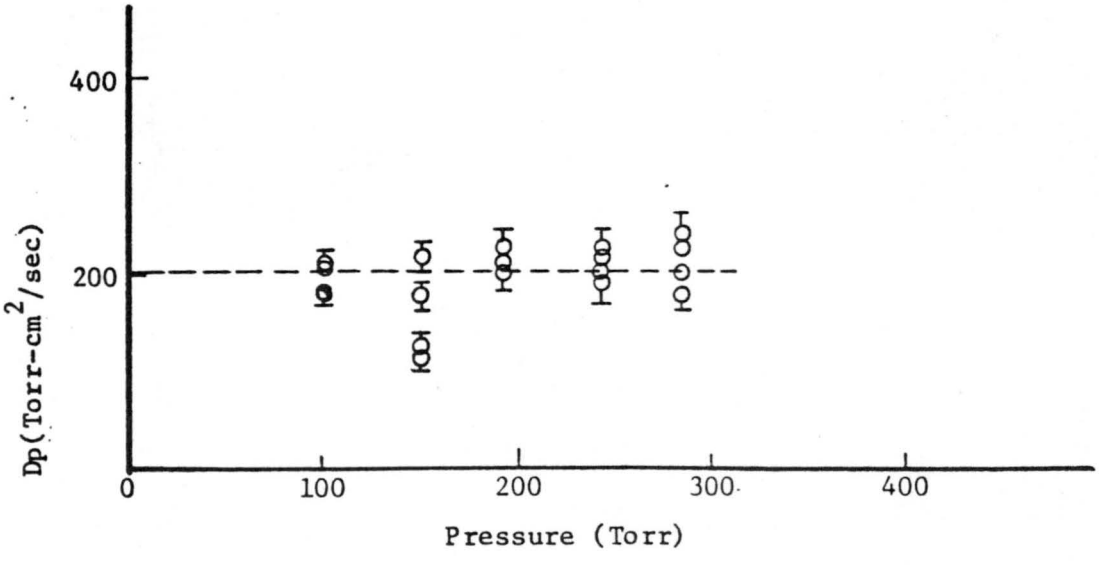

Fig. IV-17(b). Graph of Dp vs. p for Na+Ar, taken 9/3/79.

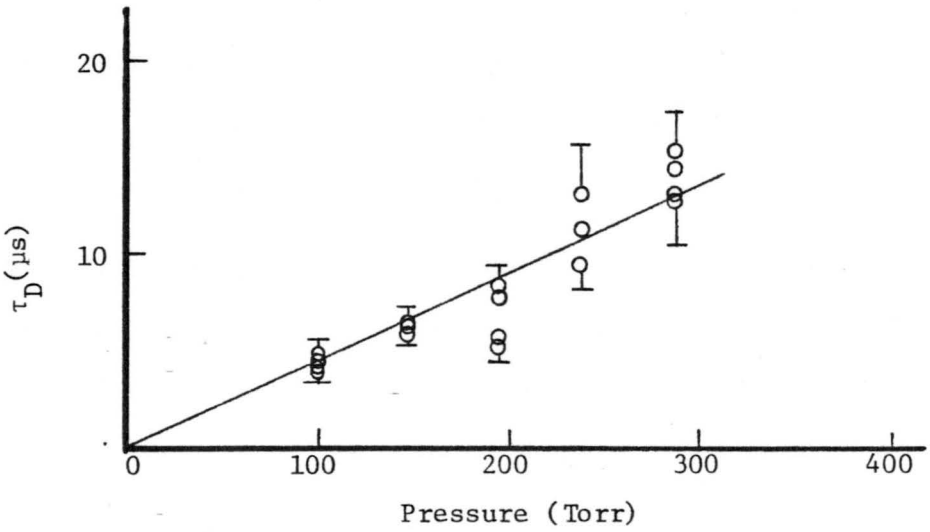

Fig. IV-18(a). Graph of τ_D vs. p for Na+Ar, taken 2/14/80.

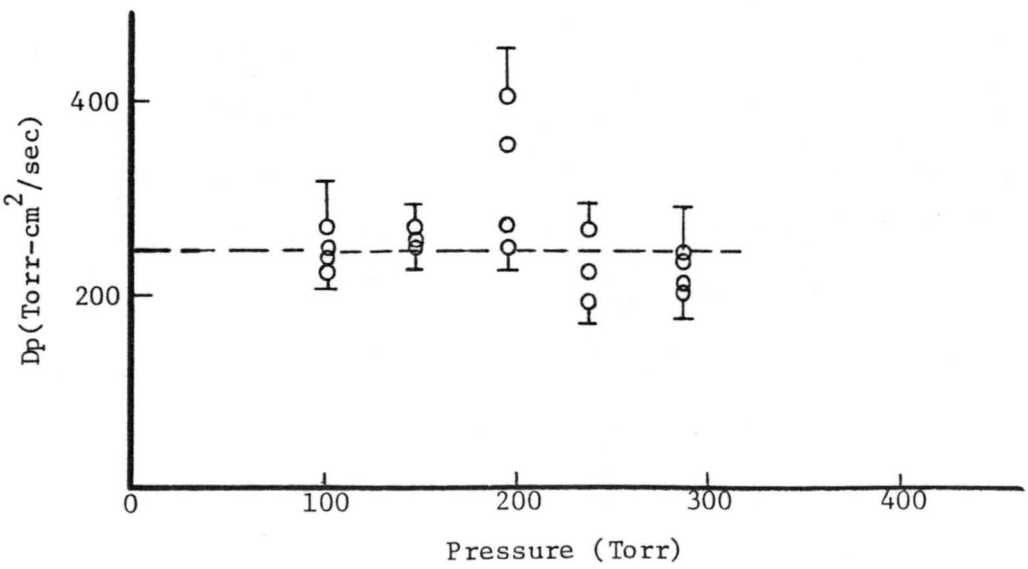

Fig. IV-18(b). Graph of Dp vs. p for Na+Ar, taken 2/14/80.

dimension of the elliptical laser beam (designated as w_ℓ) to which the computer fits were made, the corresponding diffusion constants (D) and the products, Dp (the diffusion constant times the system pressure). The errors given for τ_D, D and Dp were calculated by the computer fitting routine and represent the predicted standard deviations for τ_D (the fitting parameter). Where no errors are given, the computer did not give a prediction. The value of D was generated using Eq. (II-35b) and τ_D, then the product Dp was found from the value of D. The column under the heading "Run #" is just an identifier attached to each of the corresponding autocorrelation functions representing the day on which the data was taken. Each graph represents a plot of τ_D vs. p (graph "a") and Dp vs. p (graph "b") for data taken on a given day and with a particular background gas.

The data taken on the Na($^2S_{1/2}$) + He system is given in Table IV-3 and in Figs. IV-10 through IV-14. Table IV-4 and Figs. IV-15 and 16 give the corresponding information for the Na($^2S_{1/2}$) + Ne system and the Na($^2S_{1/2}$) + Ar data is presented in Fig. IV-17 and 18 and Table IV-5. In the figures, the lines that were drawn were the "best" fit visually, i.e., no regression analysis was done. (Since no information was to be extracted from the lines themselves, no regression fit was deemed necessary. A weighted average for all the data sets for a given system was carried out.) Both lines are predicted to be straight lines by the theory presented in Chapter II. One can immediately see that there is quite a bit of scatter within each data set, the scattering generally becoming worse at the higher pressures. The reason for this rather large scatter is not yet known. As we look at the plots of τ_D vs. p, we can see that values are not the same from graph to graph for a particular

pressure and background gas. The reason for this is that τ_D depends on the laser beam waist which changes from graph to graph (see the tables for the values of w associated with each graph). The line on the Dp vs. p graph should be at the same height for all graphs for a particular gas; as can be seen this generally is not the case.

The diffusion constant (or alternatively the product Dp) is the important information to be distilled from the experimental data. A weighted average was performed on the product, Dp, for each of the three systems with the value of the weights being inversely proportional to the standard deviation. The values that were obtained were as follows: $Na(^2S_{1/2})$ + He, $D_{He}p$ = 427.32 ± 2.27 Torr cm^2/sec; $Na(^2S_{1/2})$ + Ne, Dp = 286.88 ± 1.83 Torr cm^2/sec; $Na(^2S_{1/2})$ + Ar, $D_{Ar}p$ = 200.04 ± 2.88 Torr cm^2/sec. The errors given for these values are the weighted standard deviations of the mean. The above value for the $Na(^2S_{1/2})$ + Ne system must be modified, however, because the Ne gas cylinder actually contained a mixture of 90% Ne and 10% He. Using Eq. (II-65) with D_{grd} and D_{exc} being replaced by D_{He} and D_{Ne}, f_1 = 0.1 and f_2 = 0.9, and multiplying by 1/p and solving for $D_{Ne}p$

$$D_{Ne}p = f_2 \frac{(Dp)(D_{He}p)}{D_{He}p - f_1(Dp)} \qquad (1)$$

where the quantity Dp is that which was determined by the weighted average above. This expression gives a value for $D_{Ne}p$ of 276.77 ± 3.27 Torr cm^2/sec. This value for $D_{Ne}p$, along with the values for $D_{He}p$ and $D_{Ar}p$ given above, are also given in Table IV-6. The errors quoted in the table for these values are three times the weighted standard deviation of the mean. This error limit, however, is valid only if the errors

Table IV-6. Summary of diffusion results.

	Dp (Torr-cm^2/sec)			
	Na+He	Na*+He	Na+Ne	Na+Ar
Theoretical				
Baylis[1]	304	603	129	125
Havey[2]	377	447	---	---
York[3]	---	---	---	428
Ahmad-Bitar[4]	---	---	171	---
Experimental				
Anderson[5]	686 ± 206	---	343 ± 117	---
Gozzini[6]	1413	---	---	---
Are'Yev[7]	448	---	250	---
Coolen[8]	---	---	286 65	---
This Work	427 ± 7	598 ± 85	277 ± 10	200 ± 9

(1) Ref. (19)
(2) Ref. (20)
(3) Ref. (21)
(4) Ref. (22)
(5) Ref. (23)
(6) Ref. (24)
(7) Ref. (25)
(8) Ref. (26)

given in Tables IV-3 through IV-5 are truly indicative of the standard deviation for the associated number. If this is not true, then an error of 20% should be included in our reported results given in Table IV-6 to account for the uncertainty in w^2 (the beam waist, squared).

Table IV-6 contains the values of Dp (for the three systems mentioned above) given by or calculated from, other experiments or theoretical values. The first four authors have calculated the interatomic potential parameters from which the diffusions constant could be determined from Eq. (II-72) (using the appropriate potential form). The second four authors presented experimentally measured diffusion constants at various conditions with respect to temperature and pressure. All results presented in Table 6 have been normalized to or calculated at 315 K and 760 Torr. Upon studying this table, we can easily see that no clear consensus can be made concerning the values from the literature. Our values are closest to the three found in Ref. (25) (once their values are normalized to our pressure and temperature). Coolen's value[26] for the Na+Ne system is also very close to the value we determined. In all cases the theoretical values are quite a bit different.

IV-2.2. Results From the Experiments Involving Na($^2P_{3/2}$) and He. Along with determining the value of the diffusion constant for the sodium ground state interaction with helium, we also determined the diffusion constant for the Na($^2P_{3/2}$)+He system from our autocorrelation functions. This is the first experiment to our knowledge that attempts to provide a measurement of this quantity. The procedure followed to collect the data and to analyze this data was described in Chapter IV. The results are presented in Fig. IV-19.

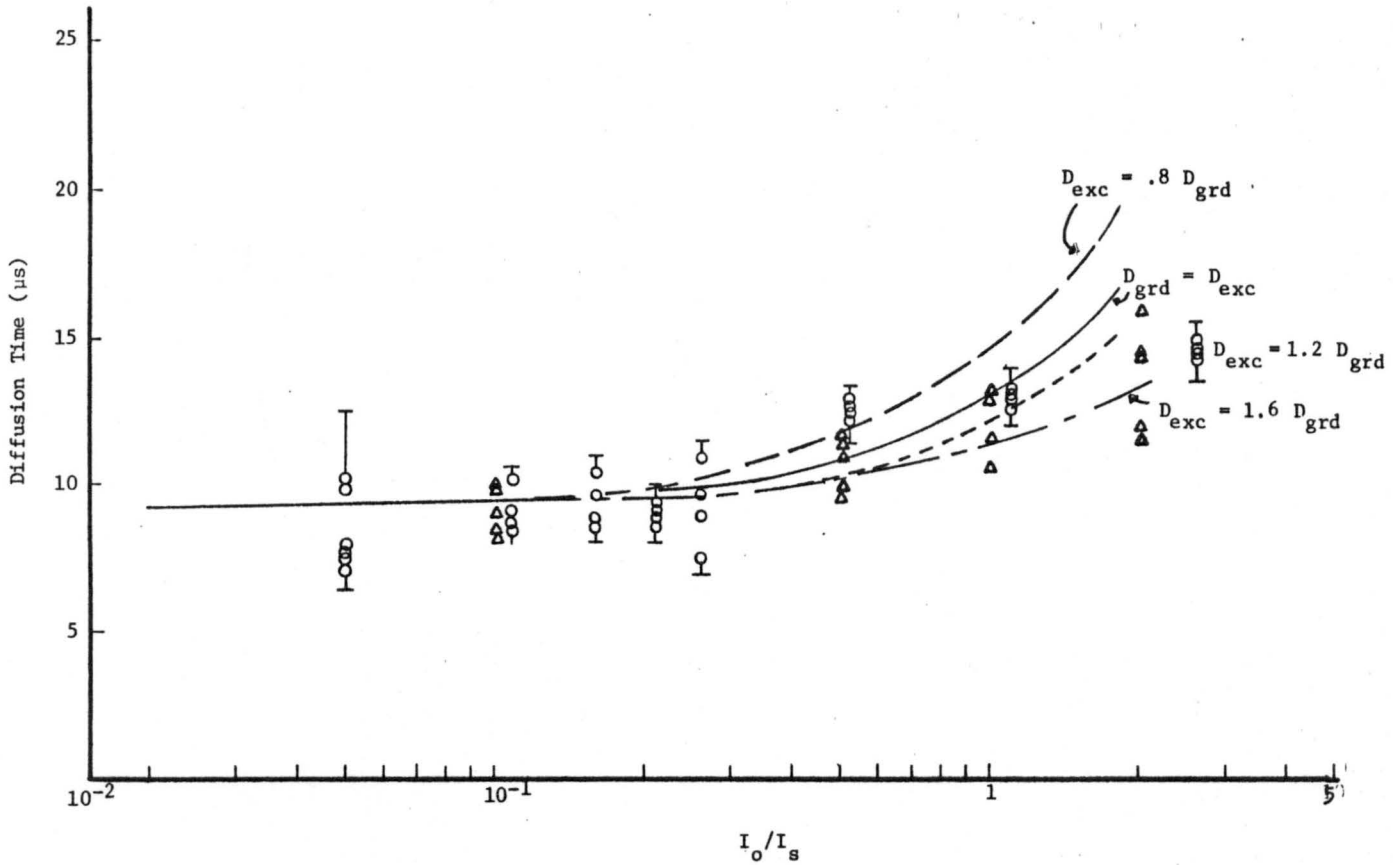

Fig. IV-19. Graph of τ_D vs. I_o/I_s for Na+He and theoretical curves for D_{exc}/D_{grd} = 0.8, 1.0, 1.2, 1.6.

The experimentally determined points are given by the circles and triangles. The family of curves (τ_D as a function of I_o/I_s for various values of D_{exc}/D_{grd}) generated by using Eq. (II-70) are shown by the lines. Upon examining this graph we find that the curves generated for values of D_{exc}/D_{grd}=0.8 to 1.0 seem to be too high compared to the experimental values. However, the curves representing values of 1.2 to 1.6 seem to straddle the data points. Based on this observation by simple averaging, we predict a value of $1.4\pm.2$ for D_{exc}/D_{grd}. Using the previously given ground state value for $D_{He}p$, the above prediction gives approximately 598 ± 85 Torr cm^2/sec for the $Na(^2P_{3/2})$+He system.

Two possible problems exist with respect to the determination of the excited state diffusion constant. The first concerns the theoretically generated form for the expected correlation function, Eq.(II-70). Actually the quadruple integral expression Eq.(II-69) should be used to generate the theoretical correlation function, but limitations on computer access made the reduction to II-70 necessary. The second problem lies in the computer fitting of the experimental data. Fitting functions, Eqs. III-17 and 18 represent only the dominant term in the series given by Eq. II-49 for the correlation function. But for high intensities ($.5\lesssim I_o/I_s<1.$) more terms of II-49 would be needed to adequately represent the correlation function. For $I_o/I_s>1.$, the expansion of the autocorrelation in powere of I_o/I_s is not valid. In either intensity regime, neither Eq. III-17 nor 18 should be used as the fitting function, but Eq. II-69 should be used. Nevertheless, the calculated value of Dp for the excited state system does follow the general trends predicted by Baylis[19] and Havey[20] in that it is larger than the corresponding value for the ground state interaction.

V. CONCLUSIONS

Using the technique of Fluorescence Correlation Spectroscopy (FCS), we have demonstrated that the motions of atoms can be measured. We have shown that from the signal generated by a single atom, its flow velocity can be found (we have been able to determine flow velocities up to 10 m/sec in this manner using a single, low power cw dye laser). Using two laser beams, we have not yet determined the velocities of single atoms but by averaging over a small number ($\sim 10^5$) of atoms (corresponding to an observation time of 1 second), flow velocities up to 88 m/sec were successfully measured. These results represent the first such measurements of atoms to be made using laser induced fluorescence.

Another type of motion that we were able to characterize, using FCS, is that involved in the diffusion process. We have measured the diffusion constants for sodium atoms in background gases of helium, argon and neon. The results for the product of the diffusion constant and the buffer gas pressure for these cases are 427 ± 7 Torr cm^2/sec, 200 ± 9 Torr cm^2/sec and 277 Torr cm^2/sec, respectively. (See Chapter IV for an explanation of the errors given here.) We have also been able to determine the diffusion constant for the excited state sodium [$Na(^2P_{3/2})$] in a helium buffer gas with the associated value of Dp of 598 ± 80 Torr cm^2/sec. Although further investigations and analyses can be made to better evaluate the connection between theory and experiment, this measured value is in qualitative agreement with recent theoretical predictions.

This represents the first "direct" experimental determination of diffusion constant of an atom in the excited state, to our knowledge.

One of the major factors limiting our ability to see a clear signal from one atom was the low total detection efficiency of our collection system. The primary cause of this was found to be due to the deterioration of our photomultiplier tube. If we used the original value for the quantum efficiency of this tube (15% at 1500 V and 29% at 1800 V[12]), the total efficiency of our system would have been between 8.5% and 16%. At this level of detection ability, for an atom moving through the center of the laser beam (w = 300 μm and I_o/I_s = 1.91) at 10 m/sec, we could expect to detect between 100 and 200 photons (depending on the voltage applied to the PMT). If this signal is spread over ten channels in our correlator, the resulting average signal counts per channel would be between ten and twenty, while the noise would only be between 4.5 and 9 counts per channel. Although the noise is still high, this signal could have readily been seen (signal to noise ratio between 4.8 and 6.7). An even better improvement of the single atom signal would result if we could reduce the stray light contribution to the noise to be much under the level of the Rayleigh scattering. At this noise level, thermal velocities of sodium atoms in vacuum could be measured. If we use a beam with w = .5 cm and I_o/I_s = 1.91, then for an atom traveling at 5.7×10^4 cm/sec (average thermal velocity at 300°K) through the center of the beam, we would detect ∿40 photons. If this signal is spread out over eight correlator sample times, then the average number of signal counts per channel would be five. The average number of noise counts would only be .2 (the total noise was assumed to equal the Rayleigh contribution at 200 Torr of He). This signal could be seen

very clearly (for the above vacuum calculations we have assumed that the ellipsoidal collector would not limit the number of photons detected because of its focusing characteristics.)

It would also be of interest to automate the acquisition of data from the single atom experiments (both for one laser beam and two laser beams). Such a system would have the benefit of more stable conditions during the collection of data, since the data would be acquired faster. Automation of the data collection procedure would also eliminate any bias that might be introduced by the experimenter. A microprocessor was programmed to acquire this data as per the procedure outlined in Chapter III. Unfortunately, inadequate quantum efficiency of the photomultiplier tube and a very high background level precluded it from being used.

For the diffusion measurements that we made, lack of quantum efficiency or high background signal were not thought to be a problem. However, we do not know at this time the reasons for the large scatter in the individual diffusion data sets. Two possible factors might be variations in the beam waist from one experimental run to the next and a possible interference due to an imposed flow or turbulence in the viewing volume. The effect of the second possibility can be reduced by running the diffusion experiments using a sealed cell, that is, close off the input flow tube and exhaust tube. A different method of getting sodium into the laser beam must also be devised if a sealed cell is used. Perhaps sodium metal could be placed on the cell and after filling it with the appropriate gas to the desired pressure, the whole cell could be heated. After equilibrium has been reached, the diffusion measurements could start. Of course, if the main contribution to the

scatter is the variation of the laser beam, then this procedure should have little effect on the magnitude of the scatter in the measured diffusion times.

One other facet of diffusion studies that still needs to be pursued concerns the analysis of the sodium excited state diffusion data. At the present time, there appears to be two, perhaps related, problems. The first problem involves the computer program used to generate the theoretical diffusion autocorrelation function [it numerically integrates Eq. (II-70)]. The values of the characteristic diffusion time predicted by this program appear to be much larger than the experimentally determined diffusion times, at values of $I_o/I_s > 2$. The reason(s) for this need to be determined. Another possible problem that needs to be investigated is the use of Eq. (II-70) to analyze the experimental data directly. (Currently we have used the same fitting functions to analyze both the experimental data and the theoretically predicted correlation function.) If the data could be analyzed directly by Eq. (II-70) then τ_D as a function of I_o/I_s can be determined, from which a value of D_{exc}/D_{grd} could be obtained. The present difficulty in this procedure relates to the feasibility of using Eq. (II-70) as a fitting function in one of the standard non-linear regression routines available. Perhaps a non-linear routine could be written specifically for this case.

Even though more work could be done concerning both velocity measurements and the diffusion constant determinations, we can see that our original objectives have been accomplished. We have used the techniques of FCS to measure atomic velocities and if the improvements discussed earlier can be implemented, it would appear that this

technique can be used to measure flows in high speed wind tunnels (the thermal velocities mentioned earlier are about Mach 1.7). This method has the advantage of being unobtrusive and only requires seeding the flow with an appropriate atomic species. Also the capability of being able to measure gaseous diffusion constants, relatively quickly and potentially quite accurately, using FCS will enable more extensive range of systems to be studied. The procedure and the results presented in this thesis represent an important stage in the accomplishment of both the preceding goals.

APPENDIX A

Derivation of fitting function for laser beam waist measurements.

The method for measuring the laser beam waist consisted of measing the power (through a 30 m aperature) at many points within the laser beam. In order to have a function to fit this data to, an expression must be derived that gives the power through a finite aperature as a function of distance from the center of the beam. This expression can be found from the intensity distribution of the laser beam.

If the laser beam intensity distribution, perpendicular to its direction of propagation, is assumed to be an elliptical TEM_{oo} mode (the major and minor axes coinciding with the x and y axes) then

$$I(x,y) = I_o EXP\left[-2(x^2/w_x{}^2 + y^2/w_y{}^2)\right] \quad . \qquad (A\text{-}1)$$

The total power in such a beam is just the integral over the xy plane and is given by

$$P_T = \int_{-\infty}^{+\infty} dx \int_{-\infty}^{+\infty} dy \; I_o EXP\left[-2(x^2/w_x{}^2 + y^2/w_y{}^2)\right]$$

$$= \frac{\pi w_x w_y}{2} I_o \quad . \qquad (A\text{-}2)$$

Our problem is to find the power, P, through an aperature of known dimensions, as a function of the aperature's position. If we have a

square aperture of area $4a^2$ (i.e., length 2a) centered at a position (x_o, y_o) then the power measured at that point would be

$$P(x_o,y_o) = \int_{x_o-a}^{x_o+a} dx \int_{y_o-a}^{y_o+a} dy \; I_o \mathrm{EXP}[-2(x^2/w_x^2 + y^2/w_y^2)]. \tag{A-3}$$

These integrals can be evaluated analytically[40] with the result

$$P(x_o,y_o) = \frac{w_x y_x I_o}{8} \left\{ \mathrm{erf}\left[\frac{\sqrt{2}}{w_x}(x_o+a)\right] - \mathrm{erf}\left[\frac{\sqrt{2}}{w_x}(x_o-a)\right] \right\} * \left\{ \mathrm{erf}\left[\frac{\sqrt{2}}{w_y}(y_o+a)\right] - \mathrm{erf}\left[\frac{\sqrt{2}}{w_y}(y_o-a)\right] \right\} \tag{A-4}$$

where erf(z) is the error function and is given by

$$\mathrm{erf}(z) = \frac{2}{\sqrt{\pi}} \int_o^z e^{-t^2} dt \tag{A-5}$$

The expression in (A-4) can also be modified to account for uncertainty in the location of the center of the beam. In order to do this, the x and y in (A-1) are replaced by $x-x_c$ and $y-y_c$ where the beam is now centered at (x_c,y_c). Working through (A-3) with the above modifications, one finds that

$$P(x_o,y_o) = \frac{w_x w_y I_o}{8} \left\{ \mathrm{erf}\left[\frac{\sqrt{2}}{w_x}(x_o-x_c+a)\right] - \mathrm{erf}\left[\frac{\sqrt{2}}{w_x}(x_o-x_c-a)\right] \right\} * \left\{ \mathrm{erf}\left[\frac{\sqrt{2}}{w_y}(y_o-y_c+a)\right] - \mathrm{erf}\left[\frac{\sqrt{2}}{w_y}(y_o-y_c-a)\right] \right\} \tag{A-6}$$

Since our fits were to only one direction at a time and assumed the other direction was at the center of its range (i.e., $x_o = x_c$ or $y_o = y_c$),

(A-6) reduces to

$$P(x,y_c) = \left\{\frac{\pi w_y I_o}{4}\,\mathrm{erf}\left(\frac{\sqrt{2}}{w_y}\,a\right)\right\} w_x \left\{\mathrm{erf}\left[\frac{\sqrt{2}}{w_x}\,(x-x_c+a)\right] - \mathrm{erf}\left[\frac{\sqrt{2}}{w_x}\,(x-x_c-a)\right]\right\} \qquad \text{(A-7a)}$$

$$P(x_c,y) = \left\{\frac{\pi w_x I_o}{4}\,\mathrm{erf}\left(\frac{\sqrt{2}}{w_x}\,a\right)\right\} w_y \left\{\mathrm{erf}\left[\frac{\sqrt{2}}{w_y}\,(y-y_c+a)\right] - \mathrm{erf}\left[\frac{\sqrt{2}}{w_y}\,(y-y_c-a)\right]\right\} \qquad \text{(A-7b)}$$

Both (A-7a) and (A-7b) have three parameters that are unknown. The quantity in the first set of brackets in each equation is treated as a parameter, and then w_x and x_c for (A-7a) and w_y and y_c for (A-7b) are treated as parameters.

The quantity, a, in the above equations is determined by the aperture that was used. For our case, this aperture was circular with a diameter of 30 μm. In order to exactly calculate P(x,y), one would have to modify the integrals to take into account the fact that a circular aperture is used. This modification, however, leads to integrals which cannot be solved analytically. For this reason we chose to use a square aperture, whose area is the same as the circular one used, in order to evaluate the integrals. Therefore, since $4a^2 = \pi\,\frac{(30)^2}{4}$, for our case a = 13.3 μm.

APPENDIX B

Nonlinear Least Squares Fitting Routines

Most of the common nonlinear least squares regression routines used today follow the same general procedure.[41-43] The function to which the data is to be fitted is first approximated by a Taylor series expression (in the parameters). This series is truncated at the first term which is linear in the fitting parameters. Working with an initial guess for the parameters, the computer evaluates the derivatives of the fitting function with respect to the parameters at the point corresponding to the initial guess. Using these derivatives, a direction toward a minimum is found and the parameters are incremented in that direction. The magnitude of the increments are checked by calculating the sum of the squares of the differences between the data points and the fitting function. If this sum decreases, then the corresponding magnitude of the increments was correct, if not then the increment would be decreased. Once a new set of parameters is found which as reduces the sum of the squares, the process starts over again and continues until some convergence criteria is reached.

The programs used to analyze the data presented in this thesis were BMD07R and BMDP3R. Both of these programs are from the Biomedical Statistical Library developed by the Department of Biomathematics, UCLA. Several other nonlinear fitting routines were also tried. A program taken from the Statistical Package for the Social Sciences (SPSS) failed

to give reasonable results (the interation process did not converge). Two other routines (written by the author and modeled after BMDP3R and Ref. 44) gave results that were similar to those generated by BMDP3R and BMD07R, but generally took longer to execute and therefore were not extensively used. The procedure followed by BMDP3R (BMDP3R is the successor to BMD07R) is described below.

Basically, the fitting problem reduces to finding a set of parameters $\{P_i\}$, i = 1,2,...k, that give the "best" fit to a function of the form $y = f(\vec{x},\vec{P})$ where $\vec{x} = (x_1,x_2,x_3...)$ is a vector made from the independent variables $\{x_i\}$, and $\vec{P}$ is the parameter vector $(P_1,P_2...P_k)$. (Here, "best" is used in the sense of least squares, to be explained below.) Corresponding to each data point, we have a set of numbers $(\vec{x}_n,y)$ where $\vec{x}_n = (x_{n1},x_{n2}...)$ and n can take on values 1,2,...N. The number N is the total number of data points available. For these N data points we wish to find the vector $\vec{P}_f$ which minimizes $\theta(\vec{P})$, where

$$\theta(\vec{P}) = \sum_{n=1}^{N}\left[[y_n - f(\vec{x}_n,\vec{P})]^2\right] \quad . \qquad \text{(B-1)}$$

To accomplish this minimization, $f(\vec{x}_n,\vec{P}_f)$ is expanded in a Taylor series (as mentioned above). The expression for $f(\vec{x}_n,\vec{P}_f)$ is

$$f(\vec{x}_n,\vec{P}_f) \overset{\sim}{=} f(\vec{x}_n,\vec{P}_o) + \sum_{i=1}^{k} \frac{d}{dP_i} f(\vec{x}_n,\vec{P}_o)\Delta P_i \qquad \text{(B-2)}$$

where $\vec{P}_o$ is the vector corresponding to the initial guesses for the parameters, and $\Delta P_i = P_{fi} - P_{oi}$. The function $f(\vec{x}_n,\vec{P}_f)$ is now replaced by y_n and (B-2) can then be rewritten as

$$y_n - f(\vec{y}_n,\vec{P}_o) = \sum_{i=1}^{k} \frac{d}{dP_i} f(\vec{x}_n,P_o)\Delta P_i \qquad \text{(B-3)}$$

for each of the N data points. Equation (B-3) is a linear equation with respect to the parameters and the parameter increments can be solved for using standard linear regression techniques. A new parameter vector $\vec{P}_1 = \vec{P}_o+\Delta\vec{P}$ is created and $\theta(\vec{P}_1)$ is calculated and checked with its previous value. If $\theta(\vec{P}_1)$ is less than $\theta(\vec{P}_o)$ then the process continues until the convergence criteria is reached. If $\theta(\vec{P}_1)$ is greater than $\theta(\vec{P}_o)$, then the vector $\Delta\vec{P}$ is modified in magnitude and θ is again calculated. If no values of $\theta(\vec{P}_1)$ are less than $\theta(\vec{P}_o)$ the process terminates.

A general problem in the nonlinear fitting routines is that there can be "local minimums" in the parameter space. In order to find out if the arrived at final parameter vector is the "best", for several test cases the initial values of the parameters were changed by up to a factor of ten. BMDP3R seemed to always converge to the same final set of parameter values. We therefore assumed that for the fitting functions we used and the data that was fitted, there was no "local minimum" problem.

APPENDIX C

Tabulation of $f(x) = \sqrt{x} \int_{-\infty}^{\infty} \frac{du}{e^{u^2} + x}$

x	f(x)
0	0
.1	.5238
.2	.6962
.3	.8050
.4	.8810
.5	.9369
.6	.9790
.7	1.0115
.8	1.0368
.9	1.0566
1.0	1.0723
1.1	1.0844
1.2	1.0939
1.3	1.1013
1.4	1.1069
1.5	1.1110
1.6	1.1140
1.7	1.1159
1.8	1.1170
1.9	1.1173
2.0	1.1171
2.1	1.1163
2.2	1.1151
2.3	1.1136
2.4	1.1117
2.5	1.1096
2.6	1.1072
2.7	1.1046
2.8	1.1019
2.9	1.0990
3.0	1.0960
3.5	1.0799
4.0	1.0627
4.5	1.0454
5.0	1.0283
5.5	1.0117

Appendix C (continued)

x	f(x)
6.0	.9958
6.5	.9804
7.0	.9658
7.5	.9517
8.0	.9383
10.0	.8902
20.0	.7340
50.0	.5411
100.0	.4190
200.0	.3198
500.0	.2202
1000.0	.1646
2000.0	.1223
10000.0	.0604

BIBLIOGRAPHY

1. W. M. Fairbank, Jr., T. W. Hänch, and A. L. Schawlow, J. Opt. Soc. Amer. 65, 199 (1975).

2. G. S. Hurst, M. H. Nayfeh, and J. P. Young, Applied Phys. Lett. 30, 229 (1977).

3. G. I. Bekov, V. S. Letokhov, O. I. Matveev and V. I. Mishin, Opt. Lett. 3, 159 (1978).

4. J. A. Gelbwachs, C. F. Klein and J. E. Wessel, Appl. Phys. Lett. 30, 489 (1977).

5. G. W. Greenlees, D. L. Clark, S. L. Kaufman, D. A. Lewis, J. F. Tonn and J. H. Broadhurst, Opt. Comm. 23, 236 (1977).

6. V. I. Balykin, V. S. Letokov, V. I. Mishin and V. A. Semchishen, JEPT Lett. 26, 357 (1977).

7. W. M. Fairbank, Jr. and C. Y. She, Optics News, Spring 1979.

8. C. Y. She, W. M. Fairbank, Jr. and K. W. Billman, Optics Lett. 2, 30 (1978).

9. E. L. Elson and D. Magde, Biopolymers 13 1 (1974).

10. D. Magde, E. L. Elson and W. W. Webb, Biopolymers 13, 29 (1974).

11. D. Magde, W. W. Webb and E. L. Elson, Biopolymers 17 361 (1978).

12. C. L. Pan, Ph.D. Dissertation, Colorado State University (1979).

13. T. R. Marrero and E. A. Mason, J. Phys. Chem. Ref. Data, Vol. 1, 3 (1972).

14. J. V. Hirschfelder, C. F. Curtiss and R. B. Bird, Molecular Theory of Gases and Liquids, Wiley, New York (1954).

15. R. B. Bird, J. O. Hirschfelder and C. F. Curtiss, "The Equation of State and Transport Properties of Gases and Liquids," Handbook of Physics, 2nd Ed., E. U. Condon and H. Odiskaw, eds., McGraw-Hill, New York (1967).

Bibliography (continued)

16. K.G. Bartlett and C.Y. She, Opt. Lett. 1, 175 (1977).

17. F. J. Smith and R. J. Munn, J. Chem. Physics 41, 3560 (1965).

18. L. Monchich, The Physics of Fluids 2, 695 (1959).

19. W. E. Baylis, J. Chem. Physics 51, 2665 (1969).

20. M. D. Havey, S. E. Frolking and J. J. Wright, Phys. Rev. Lett. 45, 1783 (1980).

21. G. York, R. Scheps and A. Gallagher, J. Chem. Phys. 63, 1052 (1975).

22. R. Ahmed-Bitar, W. Lapatovich and D. Pritchard, Phys. Rev. Lett.39, 1657 (1977).

23. L. W. Anderson and A. Ramsey, Phys. Rev. 132, 712 (1963).

24. A. Gozzini, N. Ioli and F. Strumia, Il Nuovo Cimento 49B, 185 (1967).

25. K. M. Aref'yev, V. M. Borishanshiy, L. A. Vorontsova, T. V. Zablotskaya, N. I. Ivashchenko, I. I. Palayev and B. M. Khomchenko, Heat Transfer-Soviet Research 6, 66 (1974).

26. F. C. M. Coolen and H. L. Hagedorn, Physica 79C, 402 (1975).

27. J. E. A. Jean, Gas Dynamics, Allyn and Bacon, Boston (1969).

28. S. Pai, Fluid Dynamics of Jets, D. van Nostrand Co., New York (1954).

29. C. J. Oliver, "Correlation Techniques," in Photon Correlation and Light Beating Spectroscopy, H. Z. Cummins and E. R. Pike, eds., Plenum Press, London (1974).

30. V. Degiorgio, "Photon Correlation Techniques," in Photon Correlation and Light Beating Spectroscopy, H. Z. Cummins and E. R. Pike, eds., Plenum Press, London (1974).

31. E. Jakeman, E.R. Pike and Swain, J. Physics A: Gen. Phys. 4, 517 (1971).

32. D. Koppel, Phys. Rev. A.10, 1938 (1974).

33. J. D. Jackson, Classical Electrodynamics, 2nd Ed., John Wiley & Sons, New York (1975).

34. M. Kerker, The Scattering of Light and Other Electromagnetic Radiation, Academic Press, New York (1969)

Bibliography (continued)

35. Electromagnetic and Acoustic Scattering by Simple Shapes, J. J. Bowman, T.B.A. Senior and P.L.E. Uslenghi, eds., John Wiley & Sons, New York (1969).

36. R. R. Rudder and D. R. Bach, J. Opt. Soc. Amer. 58, 1260 (1968).

37. D. Hsu (personal communication).

38. M. J. Zacrow and J. D. Hoffman, Gas Dynamics, John Wiley & Sons, New York (1976).

39. R. V. Southwell and G. Vaisey, Phil. Trans. of the Royal Society 240, 117-161 (1945).

40. "Error Function and Frisnel Integrals," from Handbook of Mathematical Functions, M. Abramowitz and I. Stegum, eds., Dover Publications, New York (1972).

41. D. W. Marquardt, J. Soc. Indust. Appl. Math. 11, 431-441 (June 1963).

42. R. I. Jennrich and P. F. Sampson, Technometrics 10, 63-72 (Feb. 1968).

43. H. O. Hartley, Technometrics 3, 269-280 (May 1961).

44. D. J. Wilde and C. S. Brightler, Foundations of Optimization, Prentice-Hall, Englewood Cliffs, N.J., 203-242 (1967).